THE RADIO AND ELECTRONIC ENGINEER

The Journal of the Institution of Electronic and Radio Engineers

FOUNDED 1925 INCORPORATED BY ROYAL CHARTER 1961

"To promote the advancement of radio, electronics and kindred subjects by the exchange of information in these branches of engineering."

VOLUME 30 DECEMBER 1965 NUMBER 6

LOCAL AND INTERNATIONAL MEMBERSHIP

THE desire on the part of the graduate engineer to secure membership of a professional body is mostly prompted by self-interest *in gaining recognition of academic and professional ability* and *obtaining access to information of professional value.*

From the editorial chair it often seems that the first consideration exercises a more powerful influence than the second. Perhaps this is because in most countries, including Great Britain, the requirements of professional recognition are, generally speaking, an essential preliminary to achievement of the second.

There are, of course, many societies or institutions throughout the world which, whilst not requiring compliance with academic and professional ability for membership, are nevertheless performing a most useful function in disseminating, and even promoting knowledge. In general, however, such organizations command only local interest or limited national support.

The backing of a nationally recognized body is essential in order to secure international attention to the value of contributions to engineering literature as well as confirming the professional competence of the individual. Moreover, in this century, the ability of the individual to add to existing knowledge in science or technology is largely dependent upon his specialized training, and his 'suitability' is backed by university and technical college training, kept up to date, in large measure, by the 'learned society' activities and membership requirements of the professional institutions. In this way new developments in science and technology, whether achieved by government research or industrial enterprise, are reflected in the training of engineers seeking qualifications.

Thus, membership of an institution, such as the I.E.R.E., is a means by which it is possible authoritatively to disseminate and constructively to discuss new ideas which will advance engineering practice. Indeed, the Institution also provides a forum for promoting both pure and applied research, by examining the deficiencies of new techniques.

Even the numerically smallest Section of the Institution can contribute to the objects of promoting and disseminating new ideas. The attendance of qualified radio and electronic engineers at a local meeting makes worthwhile the preparation and presentation of a paper and the subsequent discussion on the efficiency of the particular project. Moreover, problems, as well as ideas, may from the local centre highlight the need for national discussion of the project and associated technology and provide the basis of a paper for *The Radio and Electronic Engineer;* from such activity may even spring the need for international conference in order both to give information and receive ideas on the broadest possible basis.

The I.E.R.E. through its Sections and National Divisional activities provides the opportunity for the individual engineer to participate in local, national and international discussion on matters affecting his profession. The success of the Institution depends ultimately upon the help and support given by every member, irrespective of whether his local Section is in Great Britain, Canada, India, or wherever the Institution has an active Section.

In short, the Institution provides wide opportunities which can be used more fully, with advantage to the individual and to the profession as a whole.

G. D. C.

INSTITUTION NOTICES

Reception for Overseas Engineers

Members of the Institution who are especially concerned with space research and communications, including Mr. L. H. Bedford (Past President) and Mr. I. Maddock (Vice President), entertained a number of overseas engineers at an informal reception at 9 Bedford Square on 25th November last. The engineers, several of them members of the Institution, were taking part in a course on satellite communications sponsored by the British Council and organized by the Post Office. During the course visits were made to telecommunications engineering organizations and a week was spent at the Goonhilly earth station.

Most of the course members belonged to telecommunications administrations, but several were from universities; countries represented on the course were: Chile, Denmark, Ethiopia, Greece, Hong Kong, Irish Republic, Israel, Italy, Jordan, Kuwait, Netherlands, Nigeria, Norway, Poland, Sierra Leone, Sweden and the United States of America.

Conference on Networks

A Conference on Electrical Network Theory and Design, organized jointly by the University of Newcastle-upon-Tyne, the Ministry of Technology, the I.E.E. and the I.E.R.E. (North Eastern Sections), will take place during the week commencing 11th September 1966 at the University of Newcastle-upon-Tyne. Lectures will be given in the Electrical Engineering Department and accommodation provided in one of the University Halls of Residence.

Topics to be discussed include:

Analysis and Synthesis of Linear Passive Networks; and of Linear Active Networks;

Non-linear and Time Variant Networks;

The Place of Network Theory in the Design of Integrated Circuits;

Applications of Computers to Network Design.

Offers of papers, as soon as possible, on the above subjects will be welcomed. Details of papers and requests for further information should be sent to Dr. A. G. J. Holt, Electrical Engineering Department, Merz Court, The University, Newcastle-upon-Tyne 1.

Reprints of Papers

Reprints of any paper published in *The Radio and Electronic Engineer* may be obtained on application to the Publications Department, I.E.R.E. The usual cost of reprints is 3s. 6d. per copy (postage included) and orders should be accompanied by a remittance.

In this issue is published the final instalment of the paper "Dielectric Loaded Waveguides—A Review of Theoretical Solutions" by S. K. Chatterjee and Mrs. R. Chatterjee (see page 353). A collected reprint of all four sections of this monograph may be obtained at the special price of 10s. 6d. per copy. It is believed that many will wish to have the parts of this paper collected together for convenience.

Statistically-minded readers may be interested to note that this paper was the 1000th to be published in the Institution's *Journal* since the start of the new series in 1939. Over 500 have been published in the past six years.

London Meeting on Colour Television

The I.E.R.E. Television Group Committee has arranged a Symposium of four short contributions on "Television Receivers for the PAL Colour System". It will take place at the London School of Hygiene and Tropical Medicine, Gower Street W.C.1, on Wednesday, 16th January next at 6 p.m.

The contributions will deal with general receiver design, simple and 'de luxe' decoders and delay lines. Further information will be available from the I.E.R.E. on request during January.

Institution Participation in the Paris Components Show

This year the Salon International des Composants Electroniques will be held in Paris from 3rd to 8th February 1966. An Exhibition of Electro-Acoustic Equipment will take place concurrently.

The Institution will again be taking part in the Salon as a publisher; information on *The Radio and Electronic Engineer* and other publications will be available at the I.E.R.E. stand in the section devoted to the Technical Press.

Members of the Institution residing in France and any of members visiting the Salon are invited to call at the Institution's stand. The French Section, which was established during last year, will hold a meeting during the course of the Salon, and details of the meeting will be sent to members in France shortly.

I.E.R.E. Offices Overseas

CANADA: 504 Royal Trust Building, Albert Street, Ottowa, Ontario. Telephone: 234-5513.

INDIA: 7 Nandidrug Road, Bangalore 6. Telephone: Bangalore 29640.

Index to Volume 30

This issue completes Volume 30 of *The Radio and Electronic Engineer* which covers the period July–December 1965. An Index to the volume will be included with the February 1966 issue.

U.D.C. 621.396.677

A Comparison of the Detection and Resolution Performance of Multiplicative and Additive Aerial Arrays in the Presence of Noise

By

E. SHAW, Ph.D.†

Summary: This paper discusses the effect of receiver noise on a multiplicative receiving array. A comparison is made between the low signal/noise performance of an array using multiplicative signal processing and the same array using square-law detection of its signal outputs.

A theoretical analysis of the detection performance of a multiplicative array in terms of probability distributions is presented. It is shown that the detection performance of a multiplicative array is identical to a signal processing scheme proposed by Marcum. This scheme involved the subtraction of a square-law detected noise-only pulse from every possible signal and noise square-law detected pulse. The loss in radar detection performance of a multiplicative array compared to an array using square-law detection is found to be quite small for radars that have few pulses per target available for video integration. For a radar that integrates as many as 100 pulses per target the loss in effective input signal/noise ratio is of the order of 1 dB.

An experimental X-band array and associated circuitry to perform either multiplicative or square-law processing are briefly described and some photographed video responses to both single and double targets are presented. Limited experimental results showing the probability density functions of the output of the multiplier and square-law detector are plotted. An experimental comparison of resolution performance at low signal/noise ratios of the two types of signal processing is also made.

The environments where a multiplicative radar system may prove advantageous are suggested.

List of Principal Symbols

$D_M(p)$	Directional pattern of multiplicative array
$D_A(p)$	Directional pattern of additive array
$D_S(p)$	Directional pattern of square-law detected array
R	Signal to noise ratio
A, B	Voltage vector outputs from left and right halves of array
C, D	Sum and difference voltage outputs from array
S	Signal voltage vector
$\mathbf{x}_1, \mathbf{x}_2, \mathbf{y}_1, \mathbf{y}_2$ $\mathbf{g} = \mathbf{x}_1 + \mathbf{x}_2$ $\mathbf{z} = \mathbf{x}_1 - \mathbf{x}_2$	Noise voltage vectors
X	Amplitude of low-pass filtered output of multiplier
$P(X)$	Probability density function of X
$\phi(t)$	Characteristic function of $P(X)$

† Formerly in the Department of Electronic and Electrical Engineering, Birmingham University; now with the Admiralty Surface Weapons Establishment.

1. Introduction

Multiplicative signal processing is an alternative method of demodulating the signal outputs of a directional receiving array. The output signals are grouped into two or more summations which are then multiplied together and sent through a low-pass filter. The process is similar to synchronous demodulation in that the resulting video output may have either negative or positive polarity.

The earliest application of this technique to radar appears to be in a scheme of aerial signal processing,[1] reported in 1946, which involved a similarity to multiplicative processing. The outputs from two halves of an array were processed to form both the additive and split beam directional patterns. These were demodulated and subtracted from each other. If square-law detectors were used for demodulation then the output would be proportional to the product of the two halves of the array. This can be seen from the following identity:

$$(A+B)^2-(A-B)^2 = 4AB \qquad \ldots\ldots(1)$$

where A and B correspond to the outputs from the two halves of the array. This is a convenient way to look upon some aspects of multiplicative processing and will be utilized later.

Apart from this early example, multiplicative processing appears to have been pursued in reception systems, such as radio-astronomy[2,3] and passive sonar.[4,5] Several theoretical papers pertaining to multiplicative processing in an active sonar or radar system appeared later.[6,7,8] An active sonar system was then demonstrated successfully[9] and recently several theoretical and experimental papers have appeared on this topic in the radar literature,[10,11,12]

2. Multiplicative Operation of an Array

Consider the processing scheme shown in Fig. 1; this involves an eight-element linear array whose summed outputs from the two halves of the array are multiplied together. The double-frequency component arising from the multiplier is removed by a low-pass filter. The low frequency component is at zero frequency (i.e. d.c.) and is a bipolar video output. Its magnitude is proportional to three quantities: the two amplitudes of the input sinusoids and the cosine of the phase difference between them. The directional pattern of a multiplicative array is therefore the product of three factors: the directional patterns of the two summed portions and the interferometer term arising from multiplying two sinusoids whose phase difference is proportional to the distance between the phase-centres of the two summed arrays.

In general, a multiplicative array's directional pattern can be expressed as:

$$D_M(p) = D_1(p).D_2(p).I(p) \qquad .....(2)$$

where

$$I(p) = \cos\left(\frac{2d_1}{d} \cdot p\right)$$

where d_1 is the separation of the two phase centres, and $D_1(p)$, $D_2(p)$ are the additive patterns of the two summed arrays. $p = \pi d/\lambda \sin\theta$, d = element spacing and λ = operating wavelength, θ = angle between array's normal and direction of incoming wave-front. For the particular case of the array shown in Fig. 1.

$$D_M(p) = \left(\frac{\sin 4p}{4\sin p}\right)^2 \cos 8p \qquad .....(3)$$

This output is at zero frequency and requires no further demodulation.

On the other hand, the additive output of the whole array would be

$$D_A(p) = \frac{\sin 8p}{8\sin p} \cdot \cos\omega t \qquad .....(4)$$

where ω can be the radio or intermediate frequency. When this waveform is demodulated the resulting directional pattern is affected by the detecting device. The so-called 'linear' rectifier produces the response $\left|\frac{\sin 8p}{8\sin p}\right|$ whereas a square-law detector produces an output, $D_S(p) = \left(\frac{\sin 8p}{8\sin p}\right)^2$. These directional patterns are drawn in Fig. 2. It should be noted that $D_S(p)$ is uni-polar and has very low side-lobes, whilst $D_M(p)$ is bipolar and has a narrower beam-width and a pair of large negative side-lobes.

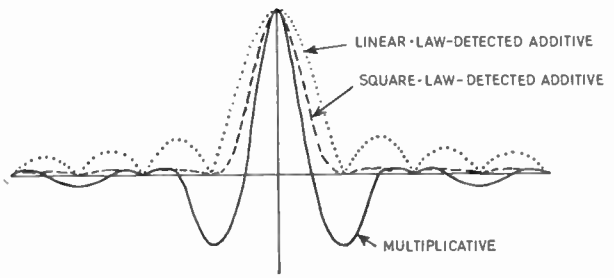

Fig. 2. Directional patterns.

The split-beam directional pattern of this array obtained by subtracting the outputs from the two halves, is given by:

$$\frac{\sin^2 4p}{4\sin p} \cdot \cos\omega t$$

If this output is square-law detected and subtracted from $D_S(p)$, it gives the multiplicative directional pattern, i.e.

$$\left(\frac{\sin 8p}{8\sin p}\right)^2 - \left(\frac{\sin^2 4p}{4\sin p}\right)^2 = \frac{\sin^2 4p}{16\sin^2 p}[\cos^2 4p - \sin^2 4p]$$

$$= \left(\frac{\sin 4p}{4\sin p}\right)^2 .\cos 8p = D_M(p)$$

A comparison of performance of the array types is made between the multiplicative arrangement of Fig. 1 and the output of this same array when the signals from the whole array are added together and then square-law detected. The choice of the square-

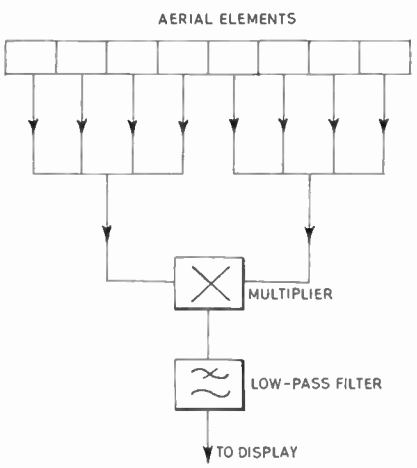

Fig. 1. A multiplicative array.

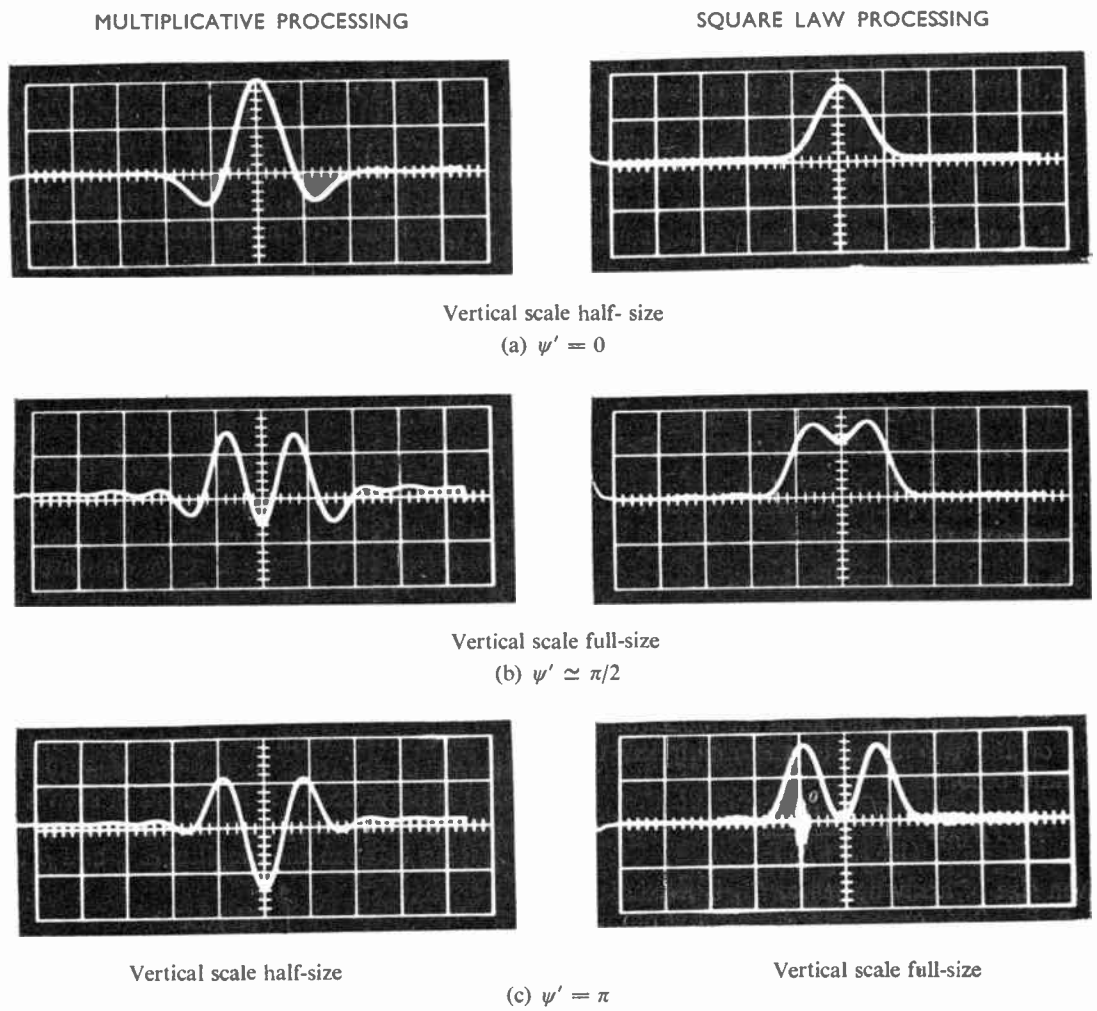

Fig. 3. Directional response to two equal strength targets separated by an additive beamwidth (2·4 deg).

law detected array output as a comparison standard is made for two reasons.

(1) Both array schemes possess square-law behaviour to the magnitudes of the received signal voltages. This means that they both discriminate between unequal strength targets as the squares of the respective voltages that these targets produce in the array.

(2) Square-law detection optimizes the video output signal/noise ratio at low input signal/noise ratios as opposed to other power laws of detection.

3. Resolution at High Signal/Noise Ratios

A former paper[10] has discussed the significance of the narrower multiplicative beamwidth in improving the resolution performance for two closely-spaced targets. Since a radar p.p.i. display is a peak detection system a resolution criterion was adopted whereby the angular output from a scanned array must possess two distinct 'peaks', and the height of the smaller peak must be greater than 3 dB above the height of the 'dip' separating the peaks. The analysis was pursued in terms of the directional patterns $D_S(p)$ and $D_M(p)$, which neglects the effect of noise but is valid for high signal/noise ratios. It was found that for equal strength targets the multiplicative array gave an improvement of 25% in resolution performance. The improvement in resolution performance is clearly seen in Fig. 3. These are experimental results of the array's response to two targets whilst undergoing electronic scanning at a rate of 1 kc/s. Resolution of the two targets depends on ψ', the relative phase difference between the returns from the two targets, but for a given situation multiplicative processing produces a larger 'dip' between the two target response than square-law processing. A more detailed discussion of the high signal/noise resolution performance has been given in a previous paper.[10]

4. Noise and Multiplicative Processing

The usual limitation on the detection of a weak target echo in a radar system is set by the noise that originates in the radar receiver. It will also be assumed that a low-pass filter permits only the difference frequency components from the detection process to be retained. Detection using a multiplicative radar is compared with a radar using square-law detection, which is the optimum detection system.[13] Narrow-band systems are assumed so that the same representation of signal and noise as adopted by Rice[14] may be used.

4.1. *Detection in Terms of R.M.S. Quantities*

It is convenient, but not rigorous, to discuss signal detection in terms of the input and output signal/noise ratios of the detector circuit. The video output signal/noise ratio is defined as:

$$\frac{\text{change in mean level on application of signal}}{\text{r.m.s. of a.c. noise components when signal present}} = R$$

Expressions for the video s/n ratio for a multiplier and square-law detector are presented in a paper by Tucker.[15] Defining R_1 and R_2 as the input voltage s/n ratios of the two arms to the multiplier, the video s/n ratio becomes

$$R_M = \frac{\sqrt{2}R_1 R_2}{(1+R_1^2+R_2^2)^{\frac{1}{2}}}$$

For a given size of array aperture, R_M is maximized when $R_1 = R_2$. This occurs when the array outputs are split into two equal parts. Under these conditions

$$R_M = \frac{\sqrt{2}R_1^2}{(1+2R_1^2)^{\frac{1}{2}}} \qquad \text{.....(5)}$$

Methods of splitting the outputs from the array aperture into two unequal parts, result in a worse s/n performance. These schemes involving unequal grouping of the array outputs are therefore not pursued in this work.

For the square-law detector, again with input s/n ratio of R_1,

$$R_A = \frac{R_1^2}{(1+2R_1^2)^{\frac{1}{2}}} \qquad \text{.....(6)}$$

This seems to imply that at low input s/n ratios the multiplier gives a video s/n output that is $\sqrt{2}$ greater for the same input s/n ratio. This improvement does exist and is not surprising when it is realized that the multiplier has uncorrelated noises at its two inputs, whereas the square-law detector must always involve a product of correlated noise. However, square-law processing of the outputs of an array involves summing all the n channels so that the input s/n ratio to the square law detector is $(\sqrt{n}).R_0$, where R_0 is the single-channel voltage s/n ratio. The multiplicative array sums into two groups so that the voltage s/n ratio is $(\sqrt{n/2}).R_0$. Therefore an input s/n ratio of R_1 for a multiplicative array must be compared with an input s/n ratio of $(\sqrt{2}).R_1$ for a square law detected array. Making the appropriate substitutions in eqns. (5) and (6) yields a video s/n ratio that is $\sqrt{2}$ greater for the square-law detected array. This seems to indicate that there is a degradation of detection performance for a multiplicative array. Although this analysis is correct, it is quite wrong to deduce that this corresponds to a $\sqrt{2}$ worsening in probability of detection. This can only be assessed by a rigorous study of the probability distributions of the signals and noise.

4.2. *Detection in Terms of Probability Density Functions*

The probability of an event is a measure of the likelihood of its occurrence. Given a waveform that adopts only discrete amplitude levels, a plot could be made of probability of amplitude against amplitude. This would show how frequently any of the discrete amplitude levels would be attained in a long sample of this waveform. However, for a continuous process such as the waveform of signal and noise from a detecting device the probability density function (p.d.f.) is introduced. It is defined in such a manner that if $P(X)$ is an amplitude p.d.f. then the probability of X lying between the amplitudes α and β is

$$\int_{\beta}^{\alpha} P(X)\,\mathrm{d}X$$

When the probability density functions of the output amplitude from a detection device are known for various input s/n ratios, the Neyman-Pearson detection criterion can be used. An amplitude threshold is chosen which gives a probability of false alarm that can be tolerated. This false alarm probability is determined by the area of the p.d.f. for the case of noise only that exceeds the chosen threshold. The probability of detection for a given s/n ratio is then the area of this signal and noise p.d.f. that exceeds the threshold. These two parameters indicate the detection performance. It is usual to derive a further graph from these p.d.f.'s depicting the probability of detection against s/n ratio for a fixed probability of false alarm. It is thought that an observer watching a p.p.i. display makes his decisions in a similar manner and, of course, the analysis is pertinent to an automatic peak detection system.

4.3. *The Probability Density Function of the Output of a Multiplier*

Cooper[16] has produced the probability density distributions of the output amplitude of a multiplier

and low-pass filter. His analysis is quite general, but as a special case he considers the p.d.f.'s produced when the multiplier is fed with correlated sinusoidal signals and uncorrelated noises at its input, i.e. the situation that prevails for multiplicative processing of the signal outputs of an array. His method of analysis is briefly presented below.

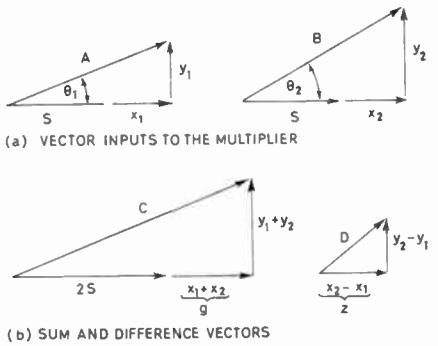

Fig. 4. Vector representation of noise and signal.

Adopting the approach of Rice[13] the vectors representing the signal and narrow-band noise components for the two halves of the array are drawn in Fig. 4(a). The noise vectors $\mathbf{x}_1$, $\mathbf{x}_2$, $\mathbf{y}_1$, $\mathbf{y}_2$ are independent normally distributed variables with zero means and all have a variance, σ^2. The low-pass filtered output of the multiplier is the product, $AB\cos(\theta_2-\theta_1) = X$.

$$X = \mathbf{S}^2+\mathbf{S}(\mathbf{x}_1+\mathbf{x}_2)+\mathbf{x}_1\mathbf{x}_2+\mathbf{y}_1\mathbf{y}_2 \quad \text{.....(7)}$$

If $P(X)$ is a p.d.f. its characteristic function is defined as

$$\phi(t) = \int_{-\infty}^{+\infty} P(X)\exp(jtX).\mathrm{d}X \quad \text{.....(8)}$$

but

$$\int_{-\infty}^{\infty} P(X)F(X)\,\mathrm{d}X = \text{av. } F(X)$$

Therefore

$$\phi(t) = \text{av. } \exp(jtX)$$

Substituting for X from eqn. (7) and averaging by integrating with respect to the four variables $\mathbf{x}_1$, $\mathbf{x}_2$, $\mathbf{y}_1$, $\mathbf{y}_2$ yields:

$$\phi(t) = \frac{\exp(-2R_1^2)}{1+t^2}\cdot\exp\left[\frac{2R_1^2}{1-jt}\right] \quad \text{.....(9)}$$

where $R_1 = S/\sqrt{2}\sigma$ is the voltage s/n ratio at each input to the multiplier.

Taking the inverse fourier transform of $\phi(t)$ to obtain the p.d.f.'s is laborious but has been computed for various values of the power s/n ratio, R_1^2. The resulting probability distributions are shown in Fig. 5(b).

The p.d.f.'s of the output amplitude of square-law detected signal with narrow-band noise has been performed by Marcum.[13] Graphs of the p.d.f.'s obtained for various input s/n ratios are shown in Fig. 5(a). A comparison of the detection performance of a multiplicative array and a square-law detected array is deferred until Section 4.6.

Marcum also analysed a composite detection scheme[13] in which a square-law detected noise-only pulse was subtracted from every possible signal and noise pulse that was square-law detected by the

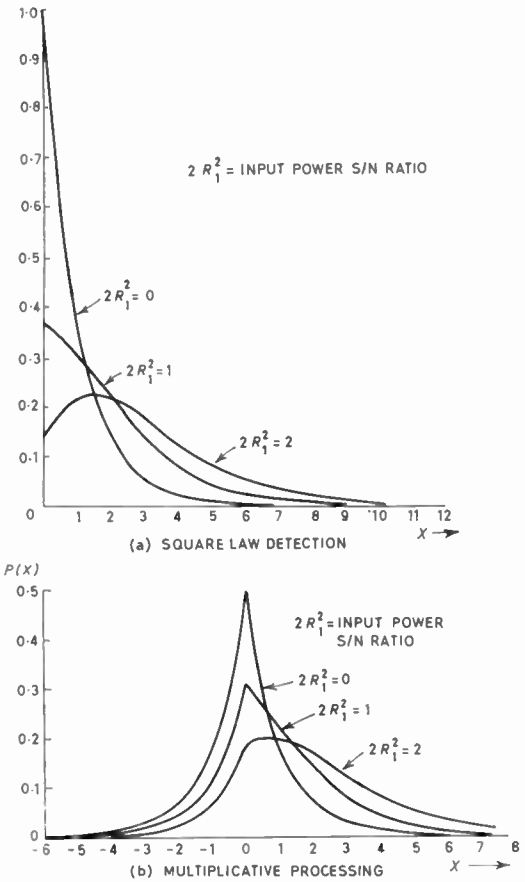

Fig. 5. Probability density functions.

receiver. The characteristic function he derived from this analysis is found to be identical to that above in eqn. (9), and consequently the p.d.f.'s he obtained are the same as those of Fig. 5(b). This may seem a surprising result, consequently the relationship between the composite scheme and multiplicative processing is studied in the next section.

4.4. *Alternative Method of Obtaining the Probability Density Functions of the Multiplier Output*

The key to the relationship between the two processing schemes lies in the identity given in eqn. (1):

$$(A+B)^2-(A-B)^2 = 4AB$$

Forming the sum and difference of the vector quantities from the two halves of the array (Fig. 4(a)) results in the vector quantities displayed in Fig. 4(b). The sum quantity, **C**, is merely the straight vector addition of the signal output of the array so that the s/n of this quantity is the same as if the whole array output was subjected to square-law detection. The difference quantity, **D**, consists of noise components only. Since the sum and difference quantities are squared before subtraction, it is seen that multiplicative processing is similar to Marcum's composite scheme. The p.d.f.'s of square-law detected signal and noise, and noise only, together with their associated characteristic functions are well known; but the characteristic function approach to determine the p.d.f. of the subtraction (or addition) of two variables of known p.d.f.'s can only be used when the variables are statistically independent. In Marcum's scheme this is necessarily the case as the noise-only pulse is taken from a different range interval than the possible signal and noise pulse. However, in the multiplicative scheme, the sum and difference quantities involve the same noise vectors, and it is not obvious that these quantities are independent.

Consider only the **x** components; the variables $\mathbf{x}_1$ and $\mathbf{x}_2$ are independent and have the following Gaussian p.d.f.'s

$$p(\mathbf{x}_1) = \frac{1}{\sqrt{2}\pi\sigma}\exp\left[-\frac{\mathbf{x}_1^2}{2\sigma^2}\right];$$

$$p(\mathbf{x}_2) = \frac{1}{\sqrt{2}\pi\sigma}\exp\left[-\frac{\mathbf{x}_2^2}{2\sigma^2}\right] \qquad \text{.....(10)}$$

The quantities $\mathbf{g} = \mathbf{x}_1+\mathbf{x}_2$ and $\mathbf{z} = \mathbf{x}_1-\mathbf{x}_2$ are formed in Fig. 4(b). Since $\mathbf{x}_1$ and $\mathbf{x}_2$ are independent it can easily be shown by the use of characteristic functions that $p(\mathbf{g})$ and $p(\mathbf{z})$ are themselves Gaussian with zero mean and variance $2\sigma^2$. It is shown in Appendix 1 that **g** and **z** are independent. It therefore follows that the sum and difference quantities shown in Fig. 4(b) are independent. The characteristic function of the multiplied output is now readily obtained.

The p.d.f. of square-law detected signal and noise is:

$$P(\mathbf{C}) = \exp\left[-(2R_1^2+)\mathbf{C}\right].I_0(2R_1\sqrt{2}\mathbf{C}) \qquad \text{.....(11)}$$

where $2R_1^2$ is the power s/n ratio of the summed quantities, i.e. of the whole array.

For noise alone this reduces to

$$p(\mathbf{D}) = \exp(-\mathbf{D}) \qquad \text{.....(12)}$$

The characteristic function of $\mathbf{C}-\mathbf{D}$ is required; this can be written as $\mathbf{C}+(-\mathbf{D})$. The characteristic functions of **C** and $(-\mathbf{D})$ are:

$$\phi_1(t) = \int_0^\infty p(\mathbf{C})\exp(\mathrm{j}t\mathbf{C})\,\mathrm{d}\mathbf{C}$$

$$= \frac{\exp(-2R_1^2)}{1-\mathrm{j}t}.\exp\left[\frac{2R_1^2}{1-\mathrm{j}t}\right] \qquad \text{.....(13)}$$

$$\phi_2(t) = \int_{-\infty}^0 p(-\mathbf{D})\exp(\mathrm{j}t\mathbf{D})\,\mathrm{d}\mathbf{D}$$

$$= \frac{1}{1+\mathrm{j}t} \qquad \text{.....(14)}$$

Therefore the characteristic function of $\mathbf{C}-\mathbf{D}$ is

$$\phi(t) = \phi_1(t).\phi_2(t)$$

$$= \frac{\exp(-2R_1^2)}{1+t^2}\exp\left[\frac{2R_1^2}{1-\mathrm{j}t}\right] \qquad \text{.....(15)}$$

This is identical to the characteristic function obtained by the previous method of analysis and confirms the relationship between Marcum's composite detection scheme and multiplicative processing. It also shows that not only can the multiplicative directional pattern be obtained from a consideration of the normal additive and split-beam patterns (as performed in Section 2) but that the detection performance is also obtained.

4.5. *The Effect of Integration on the Probability Density Function*

The graphs shown in Figs. 5(a) and 5(b) are the p.d.f.'s for a single pulse. If linear integration of k independent pulses is assumed to take place in the receive system then these p.d.f.'s alter. Their characteristic function can easily be found by raising the appropriate characteristic function for a single pulse to the kth power. The result of integrating several square-law detected noise pulses is to cause the mean value of the p.d.f. to increase in magnitude. Thus for a fixed threshold of detection, the probability of false alarm will vary depending on the number of pulses integrated. It was to avoid resetting the threshold for differing numbers of pulse integrated that Marcum introduced the scheme of subtraction of a square-law detected noise-only pulse from every possible signal and noise pulse detected by the receiver. This results in a p.d.f. for noise only that always has zero mean level irrespective of the number of pulses integrated.

4.6. *Comparison of Detection Performance of a Multiplicative and Square-Law Detected Array*

Marcum[13] has made a fairly extensive comparison between his noise subtraction scheme and normal square-law processing of signals and noise in terms

of detection performance. It has been shown that multiplicative processing of the two halves of an array is equivalent to his noise subtraction scheme applied to the same array. Therefore the results of his comparison are valid when considering the detection performances of a multiplicatively processed or square-law detected array. A graph of the

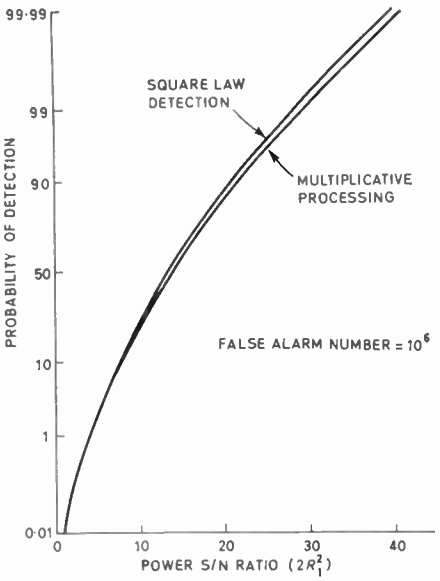

Fig. 6. Comparison of probabilities of detection.

probability of detection for a single pulse against s/n ratio for a fixed false alarm number of 10^6, taken from his work, is shown in Fig. 6. This shows that there is very little difference in detection performance of a single pulse between an array processed multiplicatively or square-law detected.

Marcum has compared his subtraction scheme with conventional square-law detection for various numbers of pulses integrated. He concludes that there is no appreciable difference in probability of detection for integrating from between 1 to 10 pulses. When integrating between 100 to 1000 pulses there is a loss in detection performance which amounts to a 1 dB lowering of the effective input s/n ratio. Therefore in comparing multiplicative processing versus square-law detection of an array's outputs the former is only marginally inferior for small numbers of integration of pulses and is only inferior to the extent of 1 dB in the effective input s/n ratio when hundreds of pulses are integrated.

4.7. *Some Advantages of Multiplicative Processing*

(*a*) For the case of noise only at the input of the multiplier the p.d.f. is symmetrical with zero mean. Integration of any number of noise pulses always results in a distribution with zero mean. Therefore the probability of false alarm is relatively insensitive to the number of pulses integrated.

(*b*) There are regions in the directional output of a multiplicative array which have negative polarity. Consider the case of the large negative side-lobe in the response of a single target. The p.d.f. of this situation is obtained by inverting the negative and positive positions of the p.d.f. whose characteristics are determined by the s/n of the signals producing this negative lobe. For a given threshold of detection (which is still a positive value) the probability of a false alarm is less than that produced by noise only. The side-lobe response of a square-law detected array will always increase the probability of false alarm in the side-lobe region. The video output from a multiplicative array that is scanning a lightly populated target environment produces a well-contrasted p.p.i. display. The bright target indications are surrounded by a darker area due to the negative side-lobes. If, however, it is hoped to detect a target that is situated in the negative side-lobe of another target then this effect is a disadvantage.

4.8. *Signal/noise Ratio and Resolution*

When the peak detection criterion postulated for resolution of two targets is employed then the preceding analysis is applicable. The p.d.f.'s of the multiplier output must be determined at the two 'peaks' and 'dip' of the two target output. For any of these positions the signal vector at the input to the multiplier is the vector addition of the signals from the two targets. The noise components are, of course, the same as in the single target case. In general, the resulting signal vectors at the two inputs to the multiplier are not in phase so that the p.d.f.'s produced are somewhat different to those produced in Fig. 5(b).

When the detection threshold and the p.d.f.'s for these three angular positions of the array are known, then an estimation of the resolution performance can be made. The probability of the video output exceeding the threshold at these three positions can be found by integration of the appropriate p.d.f.'s. Then a parameter such as:

$$\gamma = \frac{\text{probability of output exceeding threshold at position of weaker target}}{\text{" " " " " " mean position between targets}}$$

may be defined. When γ is high, resolution is certainly obtained, but when γ is near unity then resolution is unlikely. This procedure could be repeated for the square-law detected array to obtain a comparison of resolution performance. The labour involved in producing values for γ is very great and no theoretical assessment has been made, but some experimental results are reported in Section 6.2.

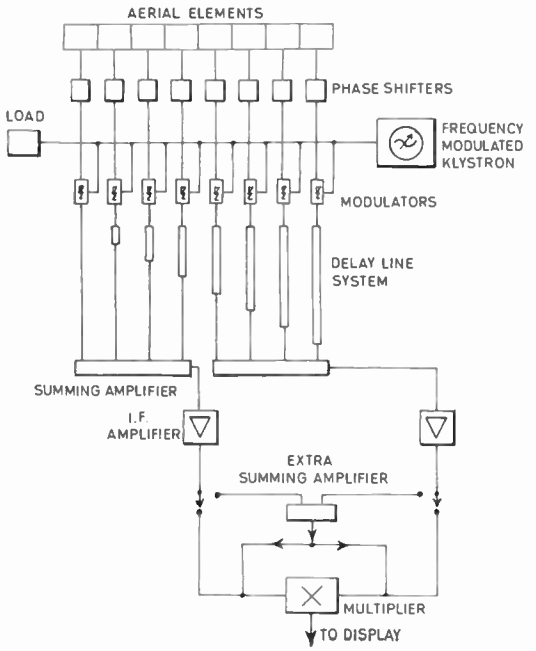

Fig. 7. (a) Electronically-scanned receiving system.

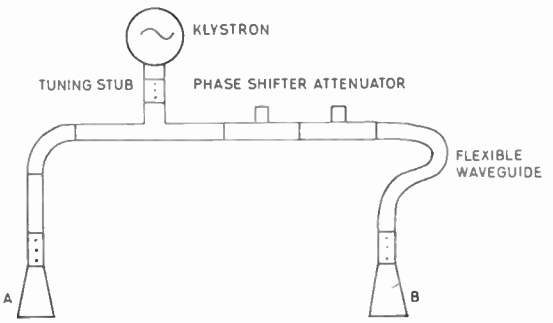

Fig. 7. (b) Simulation of two targets.

5. The Experimental Apparatus

5.1. *The Receiving Array and Transmitter*

A block diagram of the receiving array and processing circuitry is shown in Fig. 7(a). The microwave circuitry has been described in a previous paper[10] and will be only briefly reviewed. It is an X-band linear array radiating at 9415 Mc/s, having an aperture composed of 8 square horns of side 2·63 λ, making its overall length equal to 22·6 λ. This gives a multiplicative beamwidth of 1·2 deg, and when using square-law detection a beamwidth of 1·6 deg. The beamwidths are based on the separation of the 3-dB points of the video voltage, directional patterns for a single point target.

A point target was simulated by a small horn transmitting directly at the array. In the case of the resolution studies, two such horns fed from the same klystorn were directed towards the array. The feeder network to these horns allowed adjustments to be made to the relative strengths and phase-difference of their outputs. A diagram of this feeder arrangement is shown in Fig. 7(b).

5.2. *Method of Electronic Scanning*

The signal outputs of the array are electronically scanned by means of a frequency-modulated local oscillator and delay line system. The length of delay cable per channel increases uniformly from left to right in arithmetic progression. Hence to each instantaneous frequency at the outputs of the mixers, the delay lines will set up a linear phase taper across the array. As the frequency is varied so will this linear phase taper alter in magnitude so that the diffraction pattern of the array is scanned. The pattern of each horn element comprising the array is, of course, not scanned. This constitutes a difference between an electronically-scanned array pattern and a mechanically-scanned array pattern.

5.3. *The Summing Amplifier*

The outputs from the left half and right half aerial elements of the array are fed to independent summing amplifiers. These summing amplifiers have individual grid circuits for each pentode valve but have a common anode load. The circuit diagram is shown in Fig. 8.

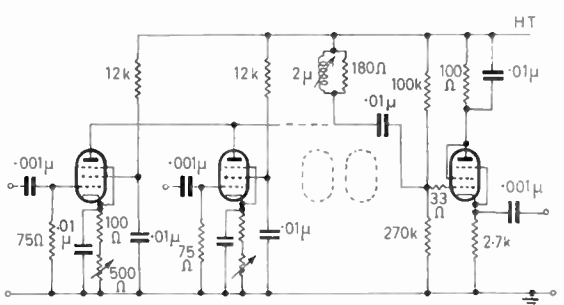

Fig. 8. Summing amplifier.

Since the pentodes are essentially constant-current generators, variations in anode voltage due to a signal input on one valve do not affect the operating conditions of the other valves. Intermodulation distortion is therefore minimized. A cathode follower delivers the output to the i.f. amplifier. Then depending on the signal processing required, the amplified outputs of the two halves of the array are either multiplied together, or added in a further summing amplifier and then square-law detected.

5.4. *The Multiplier*

The crystal diode ring multiplier described by Wilcox[17] was used. The circuit (Fig. 9) is similar to a conventional ring modulator except that there is an interchange of input and output functions. The output is taken from across the positions where the switching signal is normally applied and both input signals are fed across the diodes by means of transformer

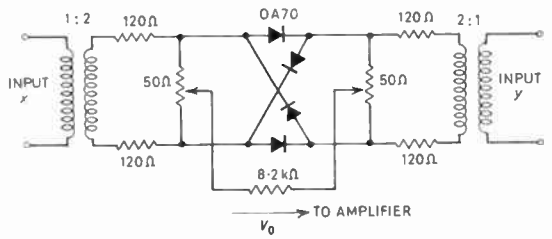

Fig. 9. Multiplier circuit.

coupling. The characteristics of the multiplier are given in Fig. 10. The two inputs are plotted on a log–log scale for constant output values. It can be seen that the circuit operates correctly as a multiplier for equal input signals over a range of about 24 dB. A limitation of this multiplier is that it only possesses this correct behaviour for low signal levels and would need some form of automatic gain control to keep it within these limits.

For multiplicative processing of the array signal outputs, the summed signal outputs from the two halves of the array are fed to the multiplier inputs. When square-law detection of the array outputs is required again the multiplier circuit is used. The signal outputs of the two halves of the array are summed together and then split into two identical inputs which are fed to the multiplier. The advantage

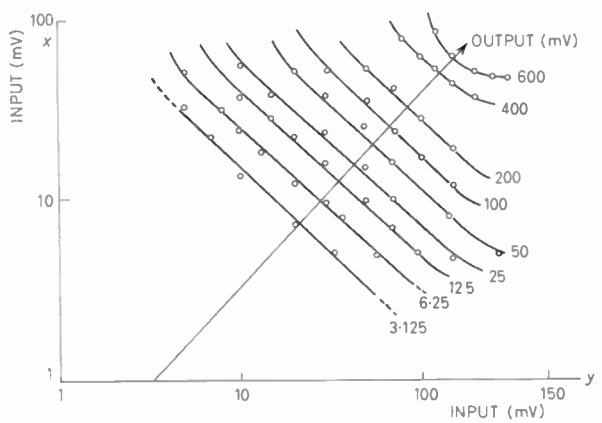

Fig. 10. Multiplier characteristics.

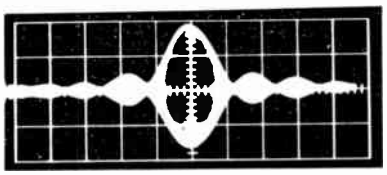

(a) Additive i.f. output.

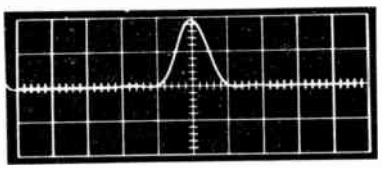

(b) Square-law detected.

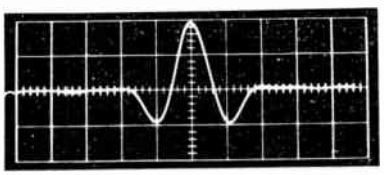

(c) Multiplicative.

Fig. 11. Electronically scanned directional patterns.

of using the same circuit to perform both processing operations is that any deviations from true multiplier action is now present for both forms of signal processing.

6. Results

To demonstrate the versatility of the experimental apparatus as a research tool, the electronically scanned directional patterns of the array are shown in Fig. 11. The additive voltage output of the whole array prior to demodulation is shown in Fig. 11(a). The directional response using square-law detection of this output is given in Fig. 11(b), whilst Fig. 11(c) is the directional pattern obtained by multiplicatively processing the outputs of the two halves of the array. These results were taken at an electronic scanning rate of 1 kc/s. The scanning rate was chosen for practical convenience, this method of scanning has previously been used on the apparatus to investigate very fast scanning rates.[18]

The directional responses shown in Fig. 11 are taken at a high s/n ratio. At low s/n ratios it is difficult to make a quantitative estimation from photographed directional responses of the suitability of either form of signal processing for the detection of a single target against the background receiver noise. Since this problem has been discussed theoretically in statistical terms some experimental probability density functions were obtained.

6.1. *Measurement of Probability Density Functions*

It is possible to measure the probability density function of the amplitude of any voltage waveform using an oscilloscope, a tube mask that possesses a slit, and a photo-electric cell. The mask is fitted to the oscilloscope tube and the slit only allows light from a narrow horizontal strip of the waveform to fall on the photo-electric detector. The slit therefore acts as an amplitude selector. The amount of time that the waveform spends in the region selected by the slit is on the average proportional to the value of the p.d.f. of the waveform at this amplitude (see Appendix 2). The amount of light falling on the photocell and hence the current produced in the photocell's circuit is therefore related to the p.d.f. Since the slit cannot be infinitely thin, then a 'smoothed' p.d.f. is obtained. The intensity of the oscilloscope tube must be kept fairly low as the photocell's characteristic of intensity against current is only linear for low intensities.

The portion of the waveform that is selected by the slit is varied by adding a measured d.c. bias to the waveform and using the d.c. input to the oscilloscope. Therefore, the p.d.f. is obtained by plotting the current in the photocell circuit against the values of the d.c. bias voltage added to the waveform.

In this manner the p.d.f. of the output of the multiplier with uncorrelated noises at its inputs was obtained and is plotted in Fig. 12(a). Below it, in Fig. 12(b), is shown the output of the multiplier to correlated noise at its inputs, i.e. square-law detected noise.

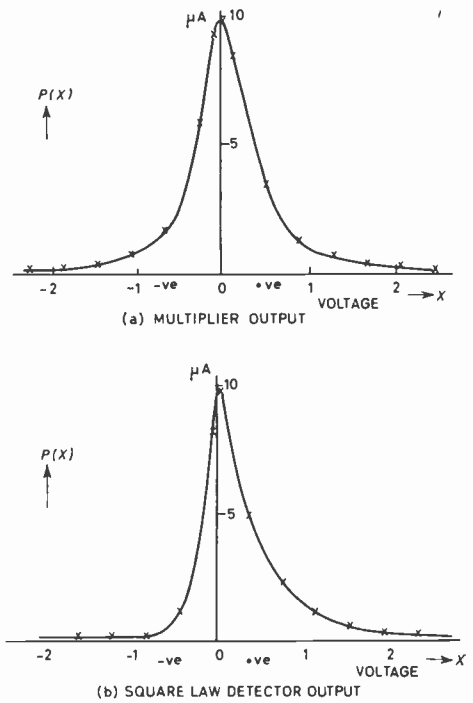

Fig. 12. Noise only probability density functions.

The bipolar nature of the noise output of the multiplier is clearly indicated. The unipolar nature of the squared noise output is apparent but it also shows up the limitation of a finite slit width in taking these p.d.f. measurements. The cut-off on the left-hand side of Fig. 12(b) is not very sharp. This may also be due to the absence of d.c. amplification after the multiplier so that some of the low frequency components are removed. The bandwidth of the post-multiplier amplifier was sufficient to encompass all the different frequency intermodulation products of the multiplier output. Bearing in mind these differences in the experimental arrangement and the theoretical situation analysed there is reasonable agreement between the results shown in Fig. 12 and the theoretical curves for noise alone ($2R_1^2 = 0$) plotted in Fig. 5.

6.2. *Resolution in the Presence of Noise*

At high s/n ratios multiplicative processing is clearly superior to square-law detection in resolving two equal strength targets as discussed in Section 3. Some experimental tests were performed to attempt to assess the resolution performance of either processing system as the target strengths become masked by the noise in the receiver circuits.

The target situation yielding the processed outputs shown in Fig. 3(b) was chosen. In order to make a more realistic model of the normal radar method of p.p.i. display, the video waveform was applied to the intensity modulation control of the oscilloscope tube. The intensity control was adjusted so that at high s/n ratio, the electronically-scanned output appeared as two distinct light patches on the tube. The mask and photocell arrangement was mounted on the tube so that the slit was vertical. Now by operating the X-shift control on the oscilloscope, the various dark and light patches of the intensity modulated time-base scan would be placed near the slit. The light output was measured at the two bright positions corresponding to the target positions and the mean value of the two current readings recorded. The minimum photocell current at a position between the two target responses was then recorded. This was never zero because of the slight glow on the tube and also due to light from the bright target indications passing through the slit. The ratio of these two recorded readings was determined. It can correspond in a loose manner to the parameter, γ, introduced in Section 4.8, and is some measure of the probability of resolution in the presence of noise. When the current ratio is large the probability of resolution is high, when this ratio approaches unity it is very

unlikely that resolution of the two targets would be obtained. This current ratio was determined for both forms of processing of the array outputs and at various s/n ratios.

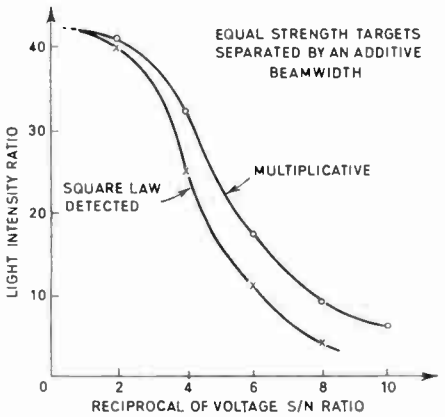

Fig. 13. Resolution performance in the presence of noise.

The results are plotted in Fig. 13 as a graph of current ratio against the reciprocal of the voltage s/n ratio. The curves should be treated with caution as far as quantitative information is concerned. The current intensity ratio is a function of the intensity control-grid voltage so that different results would be obtained for varying settings of this control. Also the effective input s/n ratio was much greater than the input values quoted because of the integration occurring on the oscilloscope tube. Nevertheless these results remain valid as a comparison and show that for the resolution of two equal targets multiplicative processing is superior at high s/n ratios and that the deterioration of resolution performance at lower s/n ratios proceeds no faster than that of square-law detection.

7. Possible Applications of Multiplicative Processing

Multiplicative processing can be applied to any receiving system where it is possible to split the output of the receiving aerial into two parts. It is best suited to a situation where a constant false alarm rate is required and the number of pulses obtained per target scan is varying but does not exceed about fifteen. For these small numbers of pulse integration the multiplicative system presents very little loss in detection performance compared to square-law detection. It is also useful in a situation where improved resolution is required. However, for certain separations of unequal strength targets the multiplicative array suffers from a strong-signal capture effect which partly nullifies this resolution improvement.

A practical difficulty of multiplicative processing is the need for two output feeders from the radar aerial. Since most radar aerials rotate continuously over 360 deg in azimuth, the two outputs need a double rotating joint. Multiplicative processing utilizes the phase relationships between the signals from the two halves of the array and these phases must be preserved by the joint. However, the design requirements of the joint can be considerably eased by producing the multiplicative processing in the manner indicated by eqn. (1). If the outputs from the two halves of the array are first combined in a hybrid coupler to produce sum and difference outputs no phase-shift restrictions need be made on the double rotating joint. The sum and difference outputs are then square-law detected and subtracted from each other to give the multiplicative response. The design of square-law detectors is no more stringent than the design of the multiplier as their functions are interchangeable.

A further difficulty arises when it is desired to use coherent moving target indication (m.t.i.) on a multiplicative radar system. Coherent m.t.i. usually involves synchronous demodulation of the incoming signal which translates it to a video frequency. Multiplicative processing compares the phase relationship of two signals and cannot operate on two video signals. It is either necessary to perform the coherent m.t.i. at an intermediate-frequency, using identical delay lines and subtraction circuits for each half of the array output to preserve the phase relationship; or use a network filter to provide some attenuation of the clutter frequency components prior to multiplication. Both schemes are not very satisfactory and it can be concluded that multiplicative processing is better suited to applications where coherent m.t.i. is not required.

Bearing in mind this limitation, multiplicative processing could find useful application in an airfield surface movement radar and has already been tried in an experimental harbour radar.[12] In these environments m.t.i. is not normally employed because the targets are stationary or moving very slowly; also there are many targets within a confined area so that high angular resolution is required. For these close-range radars the s/n ratio is high, but since it has been shown that detection and deterioration of angular resolution at low s/n is very similar to conventional radar processing, multiplicative processing could be applied to any radar system where the moderate increase in angular resolution it affords more than offsets the extra engineering difficulties in applying it.

8. Conclusions

Multiplicative processing of the signal output of an array has been compared with square-law detection

of the same output, when the signal level is confused by receiver noise. A previous paper[10] discussed multiplicative processing at high s/n ratios. It showed that for the resolution of two closely spaced targets, multiplicative processing proved superior to an extent of a 25% reduction in the target separation. Some experimental results in the paper have shown that even in the presence of receiver noise multiplicative processing appears to provide a superior resolution performance.

A theoretical analysis of the detection performance of a multiplicative array has been made in terms of probability density functions. It has been shown that multiplicative processing of an equally split array is identical to a subtraction processing scheme postulated by Marcum, whereby a square-law-detected noise pulse is subtracted from each possible square-law-detected signal and noise pulse. The similarity is shown by considering the sum and difference signals obtained from the two halves of the array.

On the basis of Marcum's comparisons, it can be concluded that there is little loss in detection performance in a radar system using multiplicative processing compared to square-law detection of the array output. In fact, when there are not many integrations of consecutive pulses this loss in performance is very small and for the case of integration of hundreds of pulses there is a loss of about 1 dB in the effective input s/n ratio.

A useful feature of multiplicative processing is that the mean level of the noise does not build up with integration of several noise pulses but remains always at zero. This prevents having to alter the detection threshold, in order to maintain a fixed false alarm probability, when the number of pulses that are integrated is varying. Also, the negative excursions of the video output of a multiplicative array undergoing scanning, will reduce the false alarm probability so that a lightly populated target situation is depicted with more contrast on the p.p.i. display. Each bright patch denoting the target is accompanied by a dark area due to the negative lobes. On the other hand, this can be deleterious in trying to resolve a denser target situation where small targets may be positioned in the negative side-lobe region of a larger target.

The performance of the two types of processing have been pursued in terms of voltage s/n, and this has indicated that the multiplicative array was inferior by a factor $\sqrt{2}$ in terms of the commonly used video s/n ratio. This ratio is defined using only the first and second moments of the probability density functions. The discrepancy in the results when the full p.d.f.'s are utilized illustrates the danger of specifying statistical processes by their first two moments.

A practical disadvantage of multiplicative processing is the need for two rotating joints, though phase restrictions on these joints can be relaxed if the r.f. aerial outputs are first combined in a hybrid junction. Also, it is difficult to perform coherent m.t.i. and multiplicative processing simultaneously. Nevertheless, multiplicative processing could usefully be employed in an airfield surface movement radar or harbour radar, and can be considered an attractive alternative method of detecting the signal outputs of a radar aerial.

9. Acknowledgments

The author wishes to thank Professor D. G. Tucker for suggesting this project and for providing research facilities in the Department of Electronic and Electrical Engineering, University of Birmingham. Thanks are also due to Dr. D. E. N. Davies and Dr. D. C. Cooper for many useful discussions on this topic.

10. References

1. D. Taylor and C. H. Westcott, "Divided broadside aerials with applications to 200 Mc/s ground radiolocation systems", *Proc. Instn Elect. Engrs*, **93**, Part IIIA, No. 3, p. 588, 1946.
2. M. Ryle, "A new radio interferometer and its application to the observation of weak radio stars", *Proc. Royal Soc.*, A, **211**, p. 351, 1952.
3. B. Y. Mills and A. G. Little, "A high resolution aerial system of a new type", *Aust. J. Phys.*, **6**, p. 272, 1953.
4. J. J. Faran and R. Hills, "The Application of Correlation Techniques to Acoustic Receiving Systems", Acoustic Research Labs. Harvard University, Tech. Memo. No. 28, November 1952.
5. A. Berman and C. S. Clay, "Theory of time-averaged product arrays", *J. Acoust. Soc. Amer.*, **29**, p. 806, 1957.
6. V. G. Welsby and D. G. Tucker, "Multiplicative receiving arrays", *J. Brit. I.R.E.*, **19**, p. 369, June 1959.
7. I. W. Linder, "Application of Correlation Techniques to Antenna Systems", University of California, Electronics Research Lab. Report, Series No. 60, Issue 267, January 1960.
8. M. E. Pedinoff and A. A. Ksienski, "Multiple target response of data processing systems", *Trans. Inst. Radio Engrs on Antennas and Propagation*, **AP-10**, No. 2, p. 112, March 1962.

   Also discussion on above paper by R. H. Macphie, *loc. cit.*, No. 5, p. 642, September 1962.
9. V. G. Welsby, "Multiplicative receiving arrays—the angular resolution of targets in a sonar system with electronic scanning", *J. Brit. I.R.E.*, **22**, No. 1, p. 5, July 1961.
10. E. Shaw and D. E. N. Davies, "Theoretical and experimental studies of the resolution performance of multiplicative and additive aerial arrays", *The Radio and Electronic Engineer*, **28**, No. 4, p. 279, October 1964.
11. A. A. Ksienski, "Multiplicative processing antenna systems for radar applications", *The Radio and Electronic Engineer*, **29**, No. 1, p. 53, January 1965.
12. R. Blommendaal, "A note on multiplicative receiving systems for radar", *The Radio and Electronic Engineer*, **28**, No. 5, p. 317, November 1964.

13. J. I. Marcum, "A statistical theory of target detection by pulsed radar", *Trans. Inst. Radio Engrs on Information Theory*, **IT-6**, No. 2, p. 59, April 1960.

14. S. O. Rice, "Mathematical analysis of random noise", *Bell Syst. Tech. J.*, **23**, p. 282, July 1944, and **24**, p. 46, January 1945.

15. D. G. Tucker, "Signal/noise performance of multiplier (or correlation) and addition (or integration) types of detector", *Proc. Instn Elect. Engrs*, **102**, p. 181, 1955.

16. D. C. Cooper, "The Probability Density Distribution at the Output of a Correlator with Band-Pass Input Waveforms". Memo. 202, Electronic and Electrical Engineering Dept. University of Birmingham.

17. R. H. Wilcox, "Use of a diode ring circuit as a four quadrant multiplier", *Rev. Sci. Instrum.*, **30**, No. 11, p. 1009, 1959.

18. D. E. N. Davies, "A fast electronically scanned radar receiving system", *J. Brit. I.R.E.*, **19**, p. 369, June 1959.

11. Appendix 1
Statistical independence of g and z

Consider $p(g)$ and $p(z)$ where $g = x_1+x_2$ and $z = x_1-x_2$ and

$$p(x_1) = \frac{1}{\sqrt{2\pi}\sigma}\exp\left[-\frac{x_1^2}{2\sigma^2}\right]$$

and

$$p(x_2) = \frac{1}{\sqrt{2\pi}\sigma}\exp\left[-\frac{x_2^2}{2\sigma^2}\right] \qquad \text{.....(16)}$$

The quantities x_1 and x_2 represent the noises originating in the separate receiving sections of the two halves of the array and are independent. Therefore it is quite easy to use the characteristic functions of $p(x_1)$ and $p(x_2)$ to form:

$$p(g) = \frac{1}{\sqrt{2\pi}\sqrt{2}\sigma}\exp\left[\frac{-g^2}{4\sigma^2}\right] \qquad \text{.....(17)}$$

and

$$p(z) = \frac{1}{\sqrt{2\pi}\sqrt{2}\sigma}\exp\left[\frac{-z^2}{4\sigma^2}\right] \qquad \text{.....(18)}$$

Hence $p(g)$ and $p(z)$ are normal distributions with zero mean values and both have a variance of $2\sigma^2$.

The bivariate distribution of two normally distributed variables g, z can be written as:

$$p(g,z) = \frac{1}{2\pi A}\exp\left\{-\frac{1}{2A^2}[\mu_{02}g^2-2\mu_{11}gz+\mu_{20}z^2]\right\} \qquad \text{.....(19)}$$

where

$$A^2 = \mu_{02}\mu_{20}-\mu_{11}^2 \quad \text{and} \quad \mu_{02} = \mu_{20} = 2\sigma^2$$

The covariance of g and z is μ_{11}. But

$$\mu_{11} = \overline{gz} = \overline{(x_1+x_2)(x_1-x_2)} = \overline{x_1^2-x_2^2} \qquad \text{.....(20)}$$

$$= \overline{\overline{x_1^2}-\overline{x_2^2}} = 0 \qquad \text{.....(21)}$$

Since

$$\overline{x_1^2} = \overline{x_2^2} = \sigma^2 \qquad \text{.....(22)}$$

The bar denotes that the quantities are averaged. Substituting $\mu_{11} = 0$ into $p(g, z)$

$$p(g,z) = \frac{1}{2\pi 2\sigma^2}\exp\left\{-\left[\frac{g^2}{4\sigma^2}+\frac{z^2}{4\sigma^2}\right]\right\} \qquad \text{.....(23)}$$

$$= \frac{1}{\sqrt{2\pi}\sqrt{2}\sigma}\exp\left[-\frac{g^2}{4\sigma^2}\right]\cdot \frac{1}{\sqrt{2\pi}\sqrt{2}\sigma}\exp\left[-\frac{z^2}{4\sigma^2}\right] \qquad \text{.....(24)}$$

$$= p(g).p(z) \qquad \text{.....(25)}$$

The fact that $p(g, z)$ can be written as the product of the individual distribution is a necessary and sufficient condition for the statistical independence of g and z.

12. Appendix 2
Theory of p.d.f. measurement

The slit allows the light from a finite portion of the random waveform to fall on the photocell. The relative frequency at which the waveform passes through the amplitude interval selected by the slit, determines the reading of the meter in the photocell's circuit. This reading is a measure of the probability of the waveform lying in this amplitude interval.

Let the slit of width $\delta X'$ cover the amplitude interval X' to $X'+\delta X'$.

Then the measured probability is proportional to

$$\int_{X'}^{X'+\delta X'} P(X)\,dX = C(X'+\delta X')-C(X')$$

where

$$C(X) = \int_{-\infty}^{X} P(X)\,dX$$

is known as the cumulative probability distribution But

$$\lim_{\delta X'\to 0}\frac{C(X'+\delta X')-C(X')}{\delta X'} = \frac{dC(X')}{dX'} = P(X')$$

Therefore, for small $\delta X'$

$$C(X'+\delta X')-C(X') \simeq P(X').\delta X'$$

Since a constant $\delta X'$ is used for all meter readings, a plot of the meter reading versus the mean position of the slit gives an approximation to the p.d.f. of the amplitude X'.

Manuscript first received by the Institution on 2nd April 1965 and in final form on 10th August 1965. (Paper No. 1010/RN.446.)

I.E.C. Meeting in Tokyo*

For the second time in its 60 years' history, the International Electro-technical Commission met in Asia (in October 1965), the previous meeting 'East of Suez' having been the New Delhi meeting in 1960.

The Tokyo meeting attracted some 400 delegates from almost 30 countries, the host-country itself contributing a further 200. The U.K. delegation—headed by Mr. S. E. Goodall, chairman of the British National Committee of I.E.C.—comprised over 70 representatives drawn from 37 firms and organizations.†

During the course of two weeks, meetings were held of 36 technical committees and sub-committees and of the I.E.C. Committee of Action (the executive committee of the Council for technical matters).

Delegates were welcomed by Mr. I. Ishikawa, president of the Japanese Industrial Standards Committee, and by Mr. T. Miki, Minister for International Trade and Industry. In his reply, the president of I.E.C., Professor R. Radulet (Rumania), traced the growth of the Commission during the past 15 years—a period in which the number of member countries had increased from 23 to 40.

Committee of Action

The president welcomed Sir Jehangir Ghandy, president of I.S.O., who emphasized the need for ever-closer liaison between their two organizations. It was becoming more and more difficult, he said, to draw a line between what is and what is not a predominantly *electrical* subject, since 'electrics' (and 'electronics') were becoming an integral part of so many industrial equipments and processes.

An important step taken by the Committee of Action was the setting up, subject to confirmation by the National Committees, of a new technical committee to deal with the safety requirements of domestic electrical appliances. This will work closely with the existing committee dealing with standard methods of testing the performance of domestic appliances. Another new technical committee set up by the Committee of Action will deal with electronic instruments.

A new working group will look into the practicability of eliminating some of the differences existing in the national wiring regulations, some aspects of which affect the design of electrical equipment and may therefore constitute a barrier to international trade. It was realized that there might be considerable difficulty in getting the various countries to alter installation practices and rules which had developed as a result of experience over many years. Consequently, before setting up a technical committee to unify these aspects of the various national rules, the Committee of Action desired to be given guidance on the terms of reference that might be given such a committee with some real hope that they could be implemented.

Meetings of Technical Committees

The progress made by the 36 technical committees and subcommittees was regarded by all concerned as being very satisfactory, due in many cases to the excellent preparatory work done by working groups. A measure of the results achieved is shown by the number of documents completed to the stage where they are ready for circulation to the National Committees for approval under the so-called 'Six Months' Rule. Exactly 100 documents were so completed. Some of these, of special interest to electronic and radio engineers, can be grouped under the following subject-headings.

Methods of measurement on radio receivers.
Methods of measurement for radio transmitters.
Input arrangements for magnetic aerials.
Rules of behaviour with respect to possible hazards when dealing with electronic equipment.
Standard sheets for various electronic valve bases.
Methods of measurement for electronic valves.
Capacitors for electronic equipment.
Resistors for electronic equipment.
Revision of Publication 63, *Preferred number series for resistors and capacitors.*
Measurement of partial discharge on h.v. apparatus.
Terms and definitions for thyristors.
Letter-symbols for thyristors.
Terms and definitions for micro-electronics.
Ratings and characteristics for various types of semiconductor devices.
Methods of measurement for semiconductor devices.
Basic principles of mechanical standardization of integrated electronic circuit devices.
Micro-electronic outline drawings.
Methods for environmental testing of electronic components and equipment.
Specification sheets for various types of copper-clad laminated sheets for printed circuits.
Terms and definitions relating to the reliability of electronic parts and equipments.
Guidance for the assessment of reliability.

J. F. STANLEY

Mr. Stanley was deputy technical director (electrical) of B.S.I. prior to his retirement at the end of 1965

---

* Based on an article to appear in *B.S.I. News.*

† Government departments (7); Central Electrictity Generating Board (4); Electricity Area Boards (3); British Railways (1); Electrical Research Association (1); Manufacturers (47); Others (11).

U.D.C. 621.373.421.11

The Prediction of Performance of Tetrode and Pentode Harmonic Generators

By

S. M. ALI, B.Sc., Ph.D.†

Summary: The paper describes a new method for predicting the performance of harmonic generators which use tetrodes or pentodes. The inaccuracy of the method is of the order of $\pm 3\%$ whereas the errors in previous methods can be of the order of $\pm 20\%$. The present method has, basically, an analytical approach making use of the anode voltage current characteristics.

Tables from which design graphs can be plotted are given in the paper and with the aid of these tables the performance of harmonic generators can quickly be predicted.

1. Introduction

In a harmonic generator the anode circuit is tuned to a frequency which is an integral multiple of the frequency at the control grid, i.e. the anode circuit is tuned to the first, second, third or *n*th harmonic of the frequency of the excitation voltage applied at the control grid.

Figure 1 represents a typical harmonic generator, shown as a frequency doubler using a tetrode valve. The control grid is biased negatively so that the anode current flows for less than half of the excitation cycle. The anode–cathode and the grid–cathode circuits have a parallel tuned circuit each and direct voltage supplies. The alternating voltages developed across these circuits are of sinusoidal wave form. In the grid circuit the alternating voltage is superimposed on the direct bias voltage supply, and in the anode circuit the alternating voltage is superimposed on the direct anode voltage supply. Figure 1 shows the direct and instantaneous voltages throughout one radio frequency cycle on the control grid. These applied voltages cause anode, control-grid, and screen-grid currents to flow somewhat in the shapes indicated. The anode current flows as a result of the combined action of the instantaneous control-grid voltage, v_g, and the direct voltage applied at the screen grid, E_s. The anode current in screen-grid valves may be assumed to be independent of the anode voltage variation in all practical designs.

The total instantaneous space or cathode current i_k may be represented by the following expression, which is based on the Child-Langmuir formula:

$$i_k = K\left(v_g + \frac{E_s}{\mu_{sg}} + \frac{v_a}{\mu}\right)^{\gamma} \qquad \text{.....(1)}$$

where K and γ are constants.

† National Electricity Administration, Baghdad; formerly at the Department of Light Electrical Engineering, The Queen's University of Belfast.

The instantaneous anode current i_a is less than the space or cathode current by the sum of the control and screen grid currents, and therefore it may be represented by the following expression:

$$i_a = P\left(v_g + \frac{E_s}{\mu_{sg}} + \frac{v_a}{\mu}\right)^{\alpha} \qquad \text{.....(2)}$$

where P and α are constants. As i_a may be assumed to be independent of v_a for all practical designs, then

$$i_a = P\left(v_g + \frac{E_s}{\mu_{sg}}\right)^{\alpha} \qquad \text{.....(3)}$$

From Fig. 1,

$$v_g = V_g \cos \omega t + E_c \qquad \text{.....(4)}$$

$$i_a = P\left[V_g \cos \omega t + E_c + \frac{E_s}{\mu_{sg}}\right]^{\alpha} \qquad \text{.....(5)}$$

or

$$i_a = P\,[\text{alternating voltage} + (\text{direct voltage})]^{\alpha}$$

In harmonic generators, E_c is negative and greater than E_s/μ_{sg}, and i_a flows only when the function between the square brackets is positive.

Note.—Capital letters representing alternating voltages and currents indicate peak values.

2. Previous Design Analysis Methods

A number of methods are in use to calculate the performance of harmonic generators. These methods may be classified into two categories—graphical and analytical. Both of these methods make use of the static characteristics of the valve.

The graphical methods make use of either the anode current/voltage characteristics or the constant anode current charts. The performance of the valve is calculated by a step-by-step analysis where the instantaneous anode currents corresponding to the instantaneous grid and anode voltages are determined from the characteristics at various points in the excitation cycle.[1,4,11,13,14] The accuracy of the

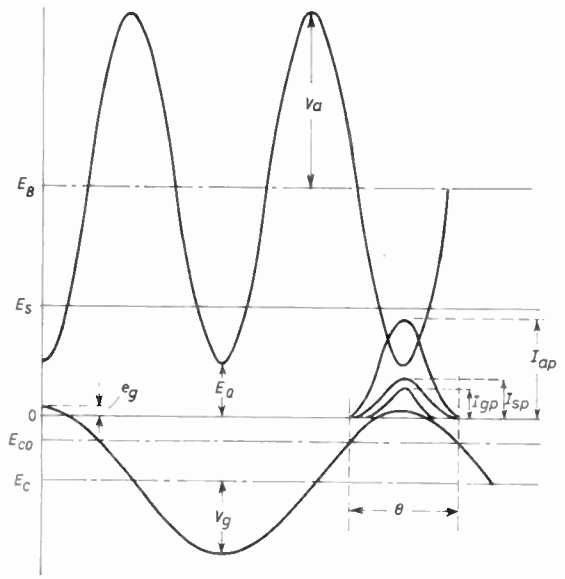

Fig. 1. Voltage-current relations in a valve used as a frequency doubler.

step-by-step graphical method is well established and also proved experimentally by the author. The performance figures obtained by this method are used as an accurate reference to which the corresponding figures obtained by the analytical methods are compared to determine the errors involved. The graphical calculation of the performance of harmonic generators is rather lengthy and laborious and a relatively accurate analytical approach is advantageous.

Two previous analytical methods are in use, namely Terman's 3/2 law method,[3,5,9,15] and the linear law method. Terman assumed γ in eqn. (1) to be equal to 3/2, i.e.

$$i_K = K\left(v_g + \frac{E_s}{\mu_{sg}} + \frac{v_a}{\mu}\right)^{3/2} \qquad \text{.....(6)}$$

The author has examined the validity of this method by applying it to a number of valves under various operating conditions and has found that the errors arising in it range from zero to +20% in the direct current component and from zero to +17% in the alternating current components.

The linear law method assumes that α in eqn. (3) is equal to unity,[6,12,16] i.e.

$$i_a = P\left(v_g + \frac{E_s}{\mu_{sg}}\right) \qquad \text{.....(7)}$$

The author has also examined the validity of this method and has found that the errors involved in it range from +7% to +32% in the direct current component and from nearly zero to +27% in the alternating current components.

3. The Author's Design Method

After examining the validity of the earlier analytical methods and finding that unpredictable errors of large magnitude may arise in computing the performance of harmonic generators, the causes which produce these large errors have been investigated. Referring to eqn. (3), which deals with the anode current flow in pentode and tetrode valves,

$$i_a = P\left(v_g + \frac{E_s}{\mu_{sg}}\right)^{\alpha}$$

and substituting

$$v_g = V_g \cos \omega t + E_c$$

and

$$\frac{E_s}{\mu_{sg}} = -(E_c + V_g \cos \theta/2)$$

the equation becomes

$$i_a = PV_g(\cos \omega t - \cos \theta/2)^{\alpha} \qquad \text{.....(8)}$$

Here i_a is a variable having different magnitudes at different values of ωt, between $t = 0$ and $t = \pm\theta/2$ and having a zero value for the rest of the cycle. $\theta/2$ is half the angle during which anode current flows and is arbitrarily chosen for any one design, so it is a constant. V_g is assumed constant and has a value which may be calculated.

It can be seen from eqn. (8) that for a particular valve under given operating conditions, the instantaneous anode current, i_a, varies with both ωt and the index α, i.e. α is not considered constant.

3.1. *Evaluation of the Index* α

From eqn. (8) when $\omega t = 0$

$$I_{ap} = PV_g(1 - \cos \theta/2)^{\alpha} \qquad \text{.....(9)}$$

Hence I_{ap} may be determined from the static characteristics and the chosen operating conditions.

From eqns. (8) and (9)

$$\frac{i_a}{I_{ap}} = \left(\frac{\cos \omega t - \cos \theta/2}{1 - \cos \theta/2}\right)^{\alpha} \qquad \text{.....(10)}$$

$$\alpha = \frac{\log I_{ap} - \log i_a}{\log(1 - \cos \theta/2) - \log(\cos \omega t - \cos \theta/2)} \qquad (11)$$

For a particular valve under assumed operating conditions E_B, E_s, θ, E_0, E_g and E_c are known. The anode tuned circuit is assumed to be tuned to the nth harmonic of the excitation frequency and to have a negligible impedance to all other harmonics. The instantaneous values of the anode and control grid voltages for any instant can be calculated, and the corresponding instantaneous anode currents can be determined from the static characteristics of the valve, following a point-by-point analysis. Knowing the

values of $\theta/2$, I_{ap}, ωt and i_a, the corresponding instantaneous values of α can be computed, using eqn. (11).

The author calculated the values of the instantaneous anode currents, using the principle of the point-by-point analysis, and the corresponding values of α for ωt from zero, in five degree steps to $\theta/2$. The instantaneous anode current and the corresponding figures of α are plotted as function of ωt. Typical graphs are shown in Fig. 2 for the Eimac tetrode valve type 4X150A used as a second harmonic generator, with

$E_B = 1000$ V $E_s = 300$ V
$V_a = 500$ V $e_g = +15$ V
$\theta = 100°$ $E_c = -228{\cdot}6$ V
$V_g = 243{\cdot}6$ V $I_{ap} = 1157$ mA

From these analyses it is found that the index α is not a constant, but varies with ωt. Its pattern of variation differs from one valve to another, and in the same valve from one set of operating conditions to another. Such irregular variations show that the value of α could not be established mathematically and yet cannot be considered as a constant.

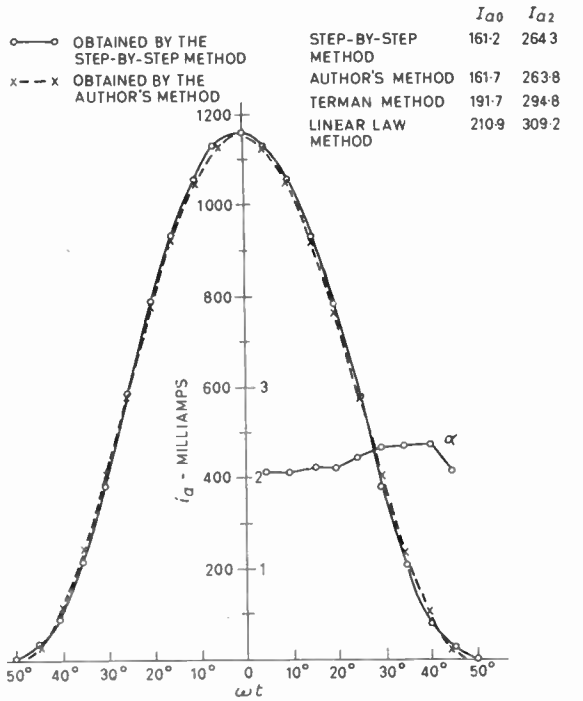

Fig. 2. Anode current and α as functions of ωt in an Eimac 4X150A valve used as a doubler.

The author has applied the above procedure to a number of designs, using various valves, and each valve under different operating conditions, and has found the performance figures obtained for the values of α corresponding to $\theta/4$ are nearly as accurate as the corresponding figures obtained by the step-by-step analysis.

In this method the optimum value of the index α is calculated for $\theta/4$ and assumed as a constant throughout the period of anode current flow, i.e. α is not a general constant for all valves under all operating conditions but a parameter, the value of which has to be determined for each design case from the following equation:

$$\alpha = \frac{(\log I_{ap} - \log i'_a)}{\log(1-\cos\theta/2) - \log(\cos\theta/4 - \cos\theta/2)} \quad (12)$$

where i'_a is the instantaneous anode current corresponding to $\omega t = \theta/4$.

In applying this method to a number of practical design examples, the author has found that the value of α ranges between approximately unity and 2·3 depending on the type of valve and its operating conditions. Therefore, the assumption taken by previous investigation that α is limited to a value between one and two is not correct.

3.2. *Simplification of the $\theta/4$ Method and the Procedure in its Application*

This method, like most other analytical methods of design, is not very convenient to apply unless design charts or graphs are available.

From eqn. (10) where

$$\frac{i_a}{I_{ap}} = \left(\frac{\cos\omega t - \cos\theta/2}{1-\cos\theta/2}\right)^{\alpha}$$

and by using graphical harmonic analysis,[17] the ratios I_{a0}/I_{ap} and I_{an}/I_{ap} are calculated for values of n from 1 to 5, θ from 40 deg to 140 deg inclusive in 10 deg steps. The value of α is assumed to be in turn 1, 1·3, 1·5, 1·7, 1·9, 2·0 and 2·3. The calculated ratios of I_{a0}/I_{ap} and I_{an}/I_{ap} are tabulated in the Appendix (Tables 2 to 8), corresponding to the various values of α. I_{a0} is the d.c. component of the anode current pulse and I_{an} is the peak value of the nth harmonic component of the anode current pulse. From these tables graphs may be plotted for the current ratios I_{a0}/I_{ap} and I_{an}/I_{ap} against θ, the angle of anode current flow. Graphs may also be plotted for these currents against α for the required values of n and θ.

The procedures in applying the $\theta/4$ method are in general the same as for those outlined in previous methods.[1,3,5,6,9,12,14–16] The only difference between this method and the other analytical methods is that the optimum value of α must be calculated for each design case.

For example, consider a tetrode valve to be used as an nth harmonic generator, with an anode voltage E_B and a screen grid voltage E_s, then the design procedure is as follows:

(1) Assume an angle of anode current flow, θ.

(2) Assume a maximum instantaneous positive control grid voltage e_g.

(3) Assume a minimum anode voltage, E_0.

(4) From the static characteristics determine I_{ap}, corresponding to E_0 and e_g.

(5) Calculate the peak value of the anode alternating voltage, V_a:

$$V_a = E_B - E_0$$

(6) Determine the effective negative bias voltage at the control grid for which anode current is cut off, E_{c0}.

(7) Calculate the necessary negative bias voltage, E_c:

$$E_c = -\frac{E_{c0} + e_g \cos\theta/2}{1 - \cos\theta/2}$$

(8) Calculate the required peak value of the excitation voltage, V_g:

$$V_g = e_g - E_c$$

(9) Calculate the instantaneous anode voltage v_a, and the instantaneous control grid voltage, v_g, corresponding to $\theta/4$:

$$v_a = E_B - V_a \cos n\theta/4$$

$$v_g = V_g \cos\theta/4 + E_c$$

(10) From the statio characteristic determine the value of i'_a corresponding to v_a and v_g in (9) above.

(11) From equation (12) calculate the value of α:

$$\alpha = \frac{\log I_{ap} - \log i'_a}{\log(1 - \cos\theta/2) - \log(\cos\theta/4 - \cos\theta/2)}$$

(12) Find the ratios I_{a0}/I_{ap} and I_{an}/I_{ap} corresponding to the value of α, from the appropriate graphs.

(13) Since I_{ap} is known, calculate the values of I_{a0} and I_{an}.

4. Experimental Verification of the Author's Method

The author has carried out practical experiments to verify the $\theta/4$ method. The valve chosen for these experiments is the S.T.C. Type 5B/254, which is a typical transmitting beam tetrode widely used in modern communication equipment. The static characteristics were accurately measured by the author, making use of the method of Macfadyen and Day.[18] The valve is used as a first, second and third

Table 1

Type of operation, with assumed (1) and derived (2) operating conditions for the S.T.C. 5B/254 valve (serial No. 1688BU) used as harmonic generator, with the corresponding current components predicted by the step-by-step method, and the author's method, and the corresponding measured current components

(1)		(1)	(1)	(2)	(2)	Step-by-step method		The author's method		Measured	
E_B volts	E_s volts	V_a volts	$\theta°$	E_c volts	V_g volts	I_{a0} mA	I_{an} mA	I_{a0} mA	I_{an} mA	I_{a0} mA	I_{an} mA
					FIRST HARMONIC:						
600	240	480	120	100·0	125	83·81	154·3	84·26	154·8	83·0	150·2
600	240	480	130	75·9	90·9	66·39	120·6	66·38	120·5	66·9	119·1
500	290	400	120	100·0	110·0	59·95	110·7	61·26	112·8	61·0	109·9
600	290	480	120	110·0	130·0	83·05	153·2	83·83	154·5	83·9	152·4
					SECOND HARMONIC:						
500	290	380	100	162·0	182·0	71·07	112·1	71·6	112·8	71·4	108·4
500	290	400	100	144·0	154·0	52·01	82·08	52·89	82·82	53·8	81·25
500	240	400	100	123·0	133·0	43·22	68·23	43·69	68·44	44·2	67·75
500	240	380	100	150·0	175·0	71·40	112·2	71·69	111·91	70·8	110·30
					THIRD HARMONIC:						
500	240	390	90	164·2	179·2	48·15	60·77	48·57	60·50	49·8	59·5
500	240	400	90	152·2	162·2	40·17	50·54	40·51	50·00	41·7	50·4
500	240	380	90	176·3	196·3	56·71	71·70	57·47	71·61	56·8	72·2
500	290	390	90	189·8	204·8	56·23	71·23	56·64	70·95	57·5	72·2

harmonic generator. The frequency of the excitation voltage at the control grid was 1·0 Mc/s. The values of e_g and E_0 were measured by specially designed slide-back voltmeters. The experimental results are given in Table 1 together with the corresponding calculated figures obtained by the step-by-step method and the author's method.

5. Conclusion

The author's method enables a designer to predict the performance of a harmonic generator with an error of less than 3% in cases of first, second and third harmonic order. The errors in the fourth harmonic case do not exceed ±5%.

The method is applicable to all beam tetrode and pentode valves and does not introduce any practical limitations.

Design tables, from which graphs may be plotted, are calculated for harmonic orders up to the fifth, and should enable designers seeking the generation of higher order harmonics to get an accurate prediction of valve performance simply and quickly.

This method has proved that the value of the index in the Child-Langmuir formula does not lie between unity and two as most investigators claim, but in some cases it has a value of 2·3.

As this is a semi-empirical analysis it might be thought that there could be a valve which would not obey the analysis. Consideration of the following will show that there would not be a tetrode or pentode which would not respond to the analysis.

In Terman's 3/2 method and the linear law method, the actual anode current pulse and the theoretical anode current pulse coincide at a minimum of the points, i.e. at the peak of the pulse and at its zero (corresponding to $\omega t = 0$ and $\omega t = \theta/2$ and between these two ordinates the theoretical pulse follows in most cases a shape far different from the shape of the actual pulse. In these two methods the theoretical pulse is assumed to follow a definite shape irrespective of the type of valve and its working conditions, whereas the actual pulse varies even in the same valve with varying working conditions.

In the $\theta/4$ method the theoretical pulse and the actual pulse coincide at the minimum of three points, instead of two, corresponding to the peak of the pulse at $\omega t = 0$, $\omega t = \theta/4$ and $\omega t = \theta/2$ and the discrepancy in the intermediate ordinates between these points in the actual and the theoretical pulse is rather negligible. Basically this method is the same as the other analytical methods, except that here the index α is considered as a parameter the magnitude of which must be evaluated for each individual design case whereas, in the other methods, this index is considered as a general constant for all types of tetrode and pentode valves.

6. Acknowledgment

The author is most grateful for the help and valuable advice received from Professor T. P. Allen throughout the research period and in preparing this paper.

7. References

1. D. C. Prince, "Vacuum tube as power amplifier", *Proc. Inst. Radio Engrs*, **11**, pp. 275, 332, 1923.
2. H. P. Thomas, "Determination of grid driving power in radio frequency amplifiers", *Proc. I.R.E.*, **21**, pp. 1134–41, August 1933.
3. F. E. Terman and J. H. Ferns, "Calculation of class C amplifier and harmonic generator performance of screen-grid and similar tubes", *Proc. I.R.E.*, **22**, p. 359, 373, March 1934.
4. I. E. Mouromtseff and H. N. Kozanowski, "Analysis of vacuum tubes as class C amplifiers", *Proc. I.R.E.*, **23**, pp. 752–78, July 1935.
5. F. E. Terman and W. C. Roake, "Calculation and design of class C amplifiers", *Proc. I.R.E.*, **24**, pp. 620–32, April 1936.
6. W. G. Wagener, "Simplified method for computing performance of transmitting tubes", *Proc. I.R.E.*, **25**, pp. 47, 77, January 1937.
7. H. J. Scott and L. J. Black, "Harmonic generation", *Proc. I.R.E.*, **26**, pp. 449, 468, April 1938.
8. W. L. Everitt and K. Spangenberg, "Grid-current flow as a factor in the design of vacuum-tube power amplifiers", *Proc. I.R.E.*, **26**, pp. 612–39, May 1938.
9. F. E. Terman, "Analysis and design of harmonic generators", *Trans. Amer. Inst. Elect. Engrs*, **57**, pp. 640–4, November 1938.
10. R. J. Sarbacher, "Power-tube performance in class C amplifiers and frequency multipliers as influenced by harmonic voltage", *Proc. I.R.E.*, **31**, pp. 607–25, November 1943.
11. R. H. Brown, "Harmonic-amplifier design", *Proc. I.R.E.*, **35**, pp. 771–7, August 1947.
12. R. J. Schwarz, "Low power frequency multipliers", *Proc. Natl Electronics Conf.*, **3**, pp. 220–39, 1947.
13. G. L. Edgecombe and J. G. Downes, "The application of the Radiotron type 807 valve as a frequency doubler", *A.W.A. Tech. Rev.*, **7**, No. 3, pp. 251–79, 1947.
14. R. S. Glasgow, "Principles of Radio Engineering", 1st edn. (McGraw-Hill, New York, 1936).
15. F. E. Terman, "Electronic and Radio Engineering", 4th edn., pp. 448–77 (McGraw-Hill, New York, 1955).
16. J. P. Heyboer and P. Zajlstra, "Transmitting Valves: The Use of Pentodes, Tetrodes and Triodes in Transmitting circuits". (Philips Technical Library, Eindhoven, 1951.)
17. H. V. Lowry and H. A. Hyden, "Advanced Mathematics for Technical Students", Part II, p. 324 (Longmans, Green, London, 1950).
18. K. A. Macfadyen and B. L. Day, "A dynamic valve test set", *J. Sci. Instrum.*, **16**, No. 10, pp. 324–31, 1939.
19. F. E. Terman and J. M. Pettit, "Electronic Measurements", 2nd edn. (McGraw-Hill, New York, 1952.)

8. Appendix

Table 2

I_{a0}/I_{ap} and I_{an}/I_{ap} (n = 1, 2, 3, 4, and 5) and the corresponding values of θ, for α = 1.

$\theta°$	$\frac{I_{a0}}{I_{ap}}$	$\frac{I_{a1}}{I_{ap}}$	$\frac{I_{a2}}{I_{ap}}$	$\frac{I_{a3}}{I_{ap}}$	$\frac{I_{a4}}{I_{ap}}$	$\frac{I_{a5}}{I_{ap}}$
40	0·0728	0·1439	0·1390	0·1311	0·1206	0·1079
50	0·0914	0·1795	0·1698	0·1545	0·1346	0·1117
60	0·1098	0·2139	0·1972	0·1715	0·1393	0·1042
70	0·1282	0·2471	0·2210	0·1817	0·1350	0·0872
80	0·1464	0·2791	0·2407	0·1851	0·1225	0·0636
90	0·1644	0·3095	0·2562	0·1818	0·1034	0·0369
100	0·1823	0·3383	0·2672	0·1724	0·0798	0·0108
110	0·2000	0·3654	0·2738	0·1576	0·0539	−0·0116
120	0·2176	0·3907	0·2760	0·1385	0·0279	−0·0279
130	0·2350	0·4140	0·2740	0·1162	0·0040	−0·0369
140	0·2522	0·4354	0·2681	0·0920	−0·0161	−0·0384

Table 3

I_{a0}/I_{ap} and I_{an}/I_{ap} (n = 1, 2, 3, 4, and 5) and the corresponding values of θ, for α = 1·3

$\theta°$	$\frac{I_{a0}}{I_{ap}}$	$\frac{I_{a1}}{I_{ap}}$	$\frac{I_{a2}}{I_{ap}}$	$\frac{I_{a3}}{I_{ap}}$	$\frac{I_{a4}}{I_{ap}}$	$\frac{I_{a5}}{I_{ap}}$
40	0·0679	0·1343	0·1301	0·1234	0·1143	0·1034
50	0·0849	0·1671	0·1589	0·1459	0·1290	0·1093
60	0·1019	0·1990	0·1850	0·1632	0·1358	0·1055
70	0·1188	0·2300	0·2080	0·1748	0·1349	0·0932
80	0·1356	0·2597	0·2276	0·1806	0·1267	0·0746
90	0·1521	0·2865	0·2426	0·1806	0·1135	0·0540
100	0·1686	0·3153	0·2559	0·1752	0·0938	0·0292
110	0·1849	0·3410	0·2644	0·1651	0·0723	0·0080
120	0·2010	0·3650	0·2692	0·1508	0·0498	−0·0092
130	0·2169	0·3876	0·2703	0·1333	0·0280	−0·0210
140	0·2325	0·4082	0·2680	0·1138	0·0086	−0·0271

Table 4

I_{a0}/I_{ap} and I_{an}/I_{ap} (n = 1, 2, 3, 4, and 5) and the corresponding values of θ, for α = 1·5

$\theta°$	$\frac{I_{a0}}{I_{ap}}$	$\frac{I_{a1}}{I_{ap}}$	$\frac{I_{a2}}{I_{ap}}$	$\frac{I_{a3}}{I_{ap}}$	$\frac{I_{a4}}{I_{ap}}$	$\frac{I_{a5}}{I_{ap}}$
40	0·0650	0·1288	0·1250	0·1188	0·1106	0·1007
50	0·0813	0·1601	0·1527	0·1409	0·1256	0·1077
60	0·0975	0·1906	0·1780	0·1583	0·1335	0·1059
70	0·1135	0·2202	0·2005	0·1706	0·1343	0·0961
80	0·1295	0·2487	0·2200	0·1775	0·1285	0·0802
90	0·1453	0·2762	0·2362	0·1793	0·1169	0·0604
100	0·1609	0·3023	0·2491	0·1760	0·1008	0·0391
110	0·1764	0·3271	0·2585	0·1682	0·0818	0·0189
120	0·1917	0·3505	0·2645	0·1566	0·0614	0·0016
130	0·2068	0·3725	0·2672	0·1417	0·0410	−0·0114
140	0·2216	0·3927	0·2668	0·1248	0·0227	−0·0195

Table 5

I_{a0}/I_{ap} and I_{an}/I_{ap} (n = 1, 2, 3, 4, and 5) and the corresponding values of θ, for α = 1·7

$\theta°$	$\frac{I_{a0}}{I_{ap}}$	$\frac{I_{a1}}{I_{ap}}$	$\frac{I_{a2}}{I_{ap}}$	$\frac{I_{a3}}{I_{ap}}$	$\frac{I_{a4}}{I_{ap}}$	$\frac{I_{a5}}{I_{ap}}$
40	0·0625	0·1238	0·1203	0·1147	0·1072	0·0981
50	0·0780	0·1538	0·1471	0·1364	0·1230	0·1061
60	0·0935	0·1831	0·1717	0·1538	0·1313	0·1059
70	0·1089	0·2116	0·1938	0·1667	0·1335	0·0983
80	0·1241	0·2390	0·2131	0·1746	0·1296	0·0846
90	0·1392	0·2655	0·2294	0·1777	0·1202	0·0670
100	0·1542	0·2907	0·2426	0·1760	0·1068	0·0474
110	0·1689	0·3148	0·2529	0·1704	0·0896	0·0283
120	0·1837	0·3379	0·2601	0·1610	0·0711	0·0111
130	0·1980	0·3590	0·2639	0·1483	0·0520	−0·0025
140	0·2121	0·3789	0·2649	0·1336	0·0341	−0·0120

Table 6

I_{a0}/I_{ap} and I_{an}/I_{ap} (n = 1, 2, 3, 4, and 5) and the corresponding values of θ, for α = 1·9

$\theta°$	$\frac{I_{a0}}{I_{ap}}$	$\frac{I_{a1}}{I_{ap}}$	$\frac{I_{a2}}{I_{ap}}$	$\frac{I_{a3}}{I_{ap}}$	$\frac{I_{a4}}{I_{ap}}$	$\frac{I_{a5}}{I_{ap}}$
40	0·0601	0·1192	0·1161	0·1110	0·1041	0·0958
50	0·0751	0·1481	0·1420	0·1323	0·1196	0·1046
60	0·0899	0·1763	0·1660	0·1497	0·1291	0·1058
70	0·1047	0·2038	0·1876	0·1651	0·1325	0·0999
80	0·1193	0·2303	0·2068	0·1716	0·1302	0·0883
90	0·1338	0·2559	0·2212	0·1759	0·1227	0·0725
100	0·1482	0·2805	0·2368	0·1758	0·1109	0·0546
110	0·1623	0·3039	0·2476	0·1717	0·0960	0·0364
120	0·1763	0·3255	0·2554	0·1641	0·0791	0·0197
130	0·1901	0·3469	0·2604	0·1535	0·0615	0·0057
140	0·2036	0·3667	0·2627	0·1406	0·0444	−0·0048

Table 7

I_{a0}/I_{ap} and I_{an}/I_{ap} (n = 1, 2, 3, 4, and 5) and the corresponding values of θ, for α = 2·0

$\theta°$	$\frac{I_{a0}}{I_{ap}}$	$\frac{I_{a1}}{I_{ap}}$	$\frac{I_{a2}}{I_{ap}}$	$\frac{I_{a3}}{I_{ap}}$	$\frac{I_{a4}}{I_{ap}}$	$\frac{I_{a5}}{I_{ap}}$
40	0·0591	0·1171	0·1141	0·1092	0·1027	0·0947
50	0·0737	0·1455	0·1397	0·1304	0·1182	0·1038
60	0·0883	0·1732	0·1633	0·1478	0·1280	0·1056
70	0·1028	0·2002	0·1848	0·1611	0·1320	0·1005
80	0·1171	0·2263	0·2038	0·1702	0·1304	0·0898
90	0·1313	0·2515	0·2203	0·1749	0·1237	0·0750
100	0·1454	0·2757	0·2340	0·1755	0·1128	0·0578
110	0·1593	0·2988	0·2450	0·1722	0·0987	0·0401
120	0·1730	0·3207	0·2532	0·1654	0·0827	0·0236
130	0·1865	0·3413	0·2586	0·1556	0·0657	0·0095
140	0·1998	0·3606	0·2614	0·1437	0·0491	−0·0013

Table 8

I_{a0}/I_{ap} and I_{an}/I_{ap} (n = 1, 2, 3, 4, and 5) and the corresponding values of θ, for α = 2·3

$\theta°$	$\frac{I_{a0}}{I_{ap}}$	$\frac{I_{a1}}{I_{ap}}$	$\frac{I_{a2}}{I_{ap}}$	$\frac{I_{a3}}{I_{ap}}$	$\frac{I_{a4}}{I_{ap}}$	$\frac{I_{a5}}{I_{ap}}$
40	0·0561	0·1114	0·1087	0·1044	0·0986	0·0916
50	0·0700	0·1383	0·1332	0·1250	0·1143	0·1015
60	0·0839	0·1647	0·1561	0·1424	0·1249	0·1049
70	0·0976	0·1905	0·1770	0·1561	0·1302	0·1019
80	0·1112	0·2155	0·1957	0·1660	0·1304	0·0936
90	0·1247	0·2396	0·2121	0·1720	0·1259	0·0811
100	0·1378	0·2627	0·2262	0·1742	0·1174	0·0660
110	0·1511	0·2849	0·2377	0·1728	0·1057	0·0499
120	0·1641	0·3065	0·2467	0·1682	0·0872	0·0342
130	0·1766	0·3258	0·2535	0·1611	0·0769	0·0199
140	0·1891	0·3424	0·2577	0·1514	0·0615	0·0082

Manuscript first received by the Institution on 17th March 1965 and in final form on 25th August 1965. (Paper No. 1011.)

U.D.C. 621.315.592.9 : 621.373

Some Aspects of Gunn Effect Oscillators

By

P. N. ROBSON, Ph.D.†

AND

S. M. MAHROUS, B.Sc.(Eng.)†

Reprinted from the Proceedings of the Joint I.E.R.E.-I.E.E. Symposium on "Microwave Applications of Semiconductors" held in London from 30th June to 2nd July 1965.

Summary: The general view is that the mechanism responsible for the Gunn effect must be similar to that proposed independently by Ridley and Watkins and by Hilsum several years ago. This theory is described and the experiments that have been reported to substantiate it indirectly are reviewed briefly.

A tentative theory to explain the wide tuning range observed when Gunn specimens are placed in a suitable cavity resonator (in some cases almost one octave) is advanced. Some experimental results, giving limited confirmation of the theory are presented.

1. Introduction

In 1963, J. B. Gunn reported[1] observing periodic fluctuations in the current passing through thin specimens of GaAs and InP when the applied voltage exceeded a certain critical threshold. These specimens were made with ohmic contacts and their current voltage characteristics were sensibly linear up to the threshold of oscillation. The particularly exciting feature of the oscillations was that their frequency could be made to lie in the microwave region of the spectrum by suitable choice of specimen thickness (usually a few thousandths of an inch), and peak power outputs of several watts could be obtained. Interest was very quickly aroused, particularly in the U.S.A., and as more results have become available, a clearer picture of the mechanism and its potentialities has emerged. The purpose of the first part of this paper is to review what is currently known about these instabilities and to explain the presently accepted mechanism for them.

Most experiments[2,3] have been performed with the specimen driven by a constant voltage source, and mounted in such a manner as to minimize spurious parasitic elements. By placing a resistor, much smaller than the low field resistance of the sample in series with it (Fig. 1), the current can be observed. The current is noted to be essentially proportional to the applied voltage up to a threshold V_T, when its value is I_T, say. When the threshold voltage is exceeded, the current drops rapidly to some lower value I_V, called the valley current, and remains at this value for a time before rising, usually more slowly than it fell, to its original threshold value I_T. There are deviations from this pattern and in some cases almost sinusoidal current waveforms have been reported.

† Department of Electronic and Electrical Engineering, University of Sheffield.

If the applied voltage is increased above the threshold voltage, the peak current is found in general to remain at the threshold value I_T, and the valley current I_V also remains constant. The period of oscillation τ is found to be proportional to the specimen length, the law for GaAs being about $(4\ \mathrm{Gc/s})^{-1}$ per thousandth inch for specimens a few thousandth of an inch and less. The period of oscillation is independent of applied voltage above the threshold and both period of oscillation and threshold electric field (deduced from threshold voltage and specimen length) are sensibly independent of resistivity in the range 0·1–10 ohm-cm.

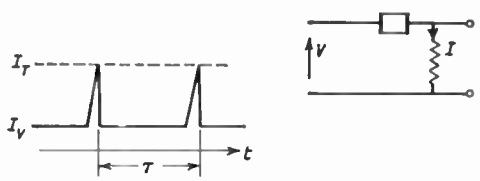

Fig. 1. Current waveform.

The currently favoured explanation, which fits all the observed effects to date, was suggested independently by Ridley and Watkins,[4] and by Hilsum,[5] as a possible means of obtaining bulk negative resistance effects in certain semiconductors with a suitable conduction band structure. Hilsum, in fact, suggested in his 1962 paper that GaAs should be a possible material to exhibit the effect.

2. Ridley-Watkins-Hilsum Transferred Electron Effect

The R-W-H model (for brevity) requires a semiconductor having two conduction bands separated by a small energy gap ΔE. The lower energy band has a smaller effective mass associated with it, and a

consequently larger mobility, than the upper band. The density of allowed states in the upper band is thus greater than that in the lower. GaAs has a suitable satellite band spaced 0·36 eV above the minimum of the principal conduction band.

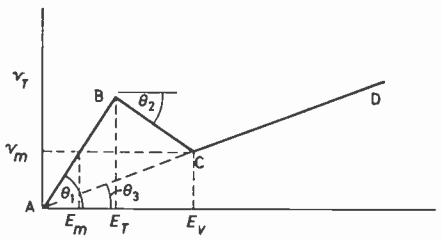

Fig. 2. Drift velocity/electric field.

Consider now Fig. 2, where, following Hilsum,[7] the electron drift velocity v is plotted as a function of electric field strength E. At low field strengths, the electrons are cool and near to the ambient lattice temperature T_0. Since for GaAs, at room temperature, $kT_0 \leqslant \Delta E$, it follows that most of the conduction electrons reside in the lower band where the mobility is μ_1, say. As the electric field is increased and carriers are accelerated more rapidly between collisions, they remain no longer in thermal equilibrium with the lattice but become heated to some temperature T, greater than T_0. As T increases, more electrons are able to transfer to the upper band and when $kT > \Delta E$ practically all the electrons are in the upper band as the availability of states is much greater in this band than in the lower band. Let the mobility of carriers in the upper band be μ_3, say. Thus at low field strengths the v/E characteristic will have gradient μ_1 and at high field strengths, gradient μ_3. These are portions AB and CD respectively of the curve in Fig. 2. There must be a transition from the line AB to CD and, if the rate of heating increases sufficiently with electric field strength then over this region the gradient of the characteristic may be negative. Hilsum showed that this was likely to be the case for GaAs, and recently[6] he has also suggested that many of the observed effects are consistent with a particularly simple characteristic, where the transition is also represented by a straight line, gradient $-\mu_2$. This is the line BC in Fig. 2.

The observed instabilities are considered to be caused by this region of negative mobility. Ridley[7] has shown that, in contrast to the tunnel diode, it is impossible to produce a stable working point along the negative mobility portion of the circuit, but rather domain formation is preferred in an attempt to minimize total entropy production in the sample. This has been found to be the case in practice and it has not been possible to inhibit oscillations by altering the circuit configuration. It is thus not possible to measure the v/E characteristic directly and the appropriate values for the valley field E_V, threshold field E_T, and mobilities μ_2 and μ_3 have to be measured by other means.

Hilsum[6] has suggested the following approximate values, based on the results of a number of workers, for the parameters relevant to GaAs.

$$\tan\theta_1 = \mu_1 \simeq 5000 \text{ cm}^2/\text{volt second}$$
$$\tan\theta_2 = -\mu_2 \simeq -200 \text{ cm}^2/\text{volt second}$$
$$\tan\theta_3 = \mu_3 \simeq 200 \text{ cm}^2/\text{volt second}$$
$$E_V \simeq 50\,000 \text{ volt/cm}$$
$$E_t \simeq 3600 \text{ volt/cm}$$

The low field mobility μ_1 is readily obtained by Hall type measurements. The threshold field E_T can be calculated by noting the voltage for onset of oscillation (the value for E_T quoted above is found in short specimens; it falls as the specimen length is increased however). The remaining quantities are obtained from measurements of the domain properties as described in the next section.

3. Domain Formation

In a series of very elegant measurements using a fine capacitively coupled electric probe placed close to the specimen and capable of being traversed along it, Gunn was able to observe the distribution of electric field with time and distance.[8]

Figure 3(a) shows the field distribution at a given time when the threshold voltage is exceeded. A narrow region of high electric field, normally referred to as the domain, was observed by Gunn to move along the specimen in the direction of electron flow (the specimens were all strongly n-type; the effect has not been observed in p-type material) with a constant drift velocity. During the period of domain transit, the current in the external circuit remained sensibly constant at the valley level I_V (see Fig. 1) and rose to the threshold level I_T as the domain moved into the anode contact. A new domain was then formed at the cathode, broke away, and the current once more returned to the valley level.

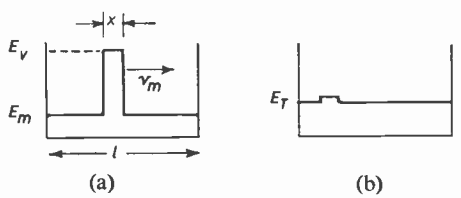

Fig. 3. Field distribution along sample.

The domain drift velocity, which remains constant, even when the applied voltage is increased above the threshold level, was measured to be some 10^7 volts/cm.

Since Gunn's results, further observations by a number of workers have put the domain field to be around 5×10^4 volts/cm. The domain width, which can be measured, not very accurately, with the probe technique, and can also be estimated by measuring the time the current takes to increase from the valley level I_V to the threshold I_T as the domain moves into the anode, is found to be about $\frac{1}{10}-\frac{1}{30}$ of the specimen length.

The domain is considered by Hilsum[6] to form in the following manner. Suppose the specimen is just biased initially, very slightly above the threshold voltage V_T so that the field is equal to E_T everywhere except over a very small region where some form of perturbation causes the field to be slightly greater than E_T. Suppose the field increases by a small amount ΔE_2 over the region of the perturbation length x, which is assumed small compared with the specimen length l. The bias source is assumed to be constant voltage, thus the field external to the perturbation must decrease by an amount ΔE_1 where $\Delta E_2 x = \Delta E_1(l-x)$. Reference to Fig. 2 then suggests that the drift velocity in the domain decreases by an amount $\Delta E_2\mu_2$, whilst external to the domain it decreases by $\Delta E_1\mu_1$. Now

$$\frac{\Delta E_2\mu_2}{\Delta E_1\mu_1}=\frac{(l-x)\mu_2}{x\mu_1}>1 \quad \text{if } x \text{ is small}$$

The current flow in the domain is therefore reduced below that external to the domain and charge must build up at the edges of the domain; positive charge at the anode end due to ionized donor sites and negative charge at the cathode end. This space charge accumulation further increases the field in the domain and decreases it outside. The amplitude of the field in the domain continues to grow in this manner until it reaches the value E_V, when the incremental mobility becomes positive again. More detailed considerations suggest that the domain stabilizes eventually with the field within it equal to E_V and external to it E_m (see Fig. 3(a)), since then the drift velocity of carriers both inside and outside it is the same (v_m in Fig. 2), and no further space charge accumulation takes place at the boundaries of the domain.† The domain thickness x must adjust itself to satisfy

$$E_V x+E_m(l-x)=V \qquad \text{.....(1)}$$

where V is the applied voltage. If V is just equal to the threshold field V_T where $V_T = E_T l$, then from eqn. (1) and Fig. 2, it can be readily shown that

$$\frac{x}{l}=\frac{\mu_2}{\mu_1+\mu_2}\simeq\frac{1}{25} \qquad \text{.....(2)}$$

with the values for μ_1 and μ_2 given previously. For any value of applied voltage $V_T+\Delta V$ above threshold, then

$$\frac{x}{l}=\frac{\mu_2}{\mu_1+\mu_2}\left(1+\frac{\mu_1(\mu_2+\mu_3)\Delta V}{\mu_2(\mu_1-\mu_3)V_T}\right)$$

$$\simeq\frac{\mu_2}{\mu_1+\mu_2}\left(1+\frac{2\Delta V}{V_T}\right) \qquad \text{.....(3)}$$

Thus from eqn. (2), the domain thickness is proportional to specimen length and, from (3), the application of voltages above threshold is absorbed by the domain widening, but its velocity remains constant at the value v_m.

This somewhat idealized picture, with an abrupt transition between fields inside and outside the domain, is unlikely to be correct in detail. For example, it implies vanishingly thin domain walls and Kroemer[9] has pointed out that the positive space charge density can never exceed the donor charge density, which particularly for high resistance specimens (low donor density) may mean a wall thickness comparable to x in order to support the discontinuity E_V-E_m in electric field. However, it does suggest that the current will oscillate between the values I_T and I_V ($J_T = Nev_T$, $J_V = Nev_m$, where N is the carrier density and J the current density), even when the applied voltage is increased above threshold, and also that the domain transit time $\tau = l/v_m$ will be independent of applied voltage, all of which are observed in practice.

The nature of the perturbation from which domain growth starts is not clearly understood; the point at which growth commences is usually called a nucleating centre. It appears that in order for coherent oscillations to be developed, one nucleating centre should be dominant. Since such a centre might be expected to occur wherever there is a change in crystal structure (for example a localized variation in donor concentration), it seems most likely for domains to nucleate near the cathode. Once the field starts to grow in one domain and thus suppresses the field external to it, no nucleation is possible elsewhere until this domain has reached the anode. The field then returns to the threshold value and the domain can form once more. In very many specimens the observed current fluctuations are not coherent but resemble band limited noise. It is thought that in such samples, several nucleating centres are perhaps present and the choice of centre, from cycle to cycle, is a random process.

† There is growing belief that this is not a correct description of conditions within the domain; but rather that the domain field might be considerably greater than the valley field (See J. E. Carroll, *Electronics Letters*, 1, p. 189, September 1965) which is possibly much less than the value 50 000 volt/cm, quoted in Section 2. (See P. Butcher, W. Fawcett, *Phys. Rev. Letters*, 17, p. 216, 1965).

It has been tacitly assumed so far that the domain builds up to its steady state amplitude in a time short compared to the transit time τ; otherwise it would grow as it drifted along the specimen. There is in fact some suggestion that this is the case in rather high resistance material. Field changes cannot take place in a time less than the dielectric relaxation time ε/σ, where ε is the permittivity and σ the conductivity. The low field dielectric relaxation time in 1 ohm-cm GaAs is about 10^{-12} s, and for 10 ohm-cm material, 10^{-11} s. However, for the region of negative mobility, BC in Fig. 2, we can define a negative relaxation time, which is to be interpreted as the characteristic high field build up time. Since the negative mobility appears to be some 25 times smaller than the low field value, the negative relaxation time is the slowest time-constant associated with the domain build-up. Thus for high resistivity material the domain build-up time can be a sensible fraction of the transit time, particularly for thin specimens designed to oscillate at microwave frequencies. There is evidence that domain formation can be inhibited completely in high resistivity material for the above reason.

Several other experiments have been performed which suggest that the R-W-H energy barrier mechanism is responsible for the observed instabilities. Briefly these are:

(*a*) The drift velocity at threshold and the domain drift velocity both increase as lattice temperature decreases.[11]

(*b*) The energy gap ΔE will change when the specimen is deformed by straining; thus the threshold field should also change. This has been observed by Hutson *et al.* who subjected specimens up to 28 kilobars hydrostatic pressure before oscillations were inhibited.[12]

4. Potentialities as a Microwave Source

If this instability is to form the basis for a useful microwave source then the following considerations are of interest:

(1) Possibility of c.w. operation

(2) Tunability

(3) Spectral purity

(4) Output power and efficiency

Taking these in turn:

(1) The earliest samples were operated with very short pulse lengths, typically 10–100 nanoseconds, to prevent failure due to excessive Joule heating. However, with improved encapsulation, several authors have reported c.w. operation.

(2) A very limited amount of information is available on tunability. At first sight it would appear that oscillations are limited to the natural domain transit time which appears to be only a function of temperature, and not of voltage. However, by mounting samples in a coaxial cavity, some degree of tunability has been observed. The second part of this paper is concerned with showing that a mode of oscillation exists when the specimen is placed in a cavity, and this mode can be tuned, in theory over at least one octave with suitable choice of cavity load conductance. High order modes of oscillation are also possible theoretically at what are thought to be lower efficiencies. Some results are presented for a sample tunable over the range 1·35 to 1·8 Gc/s by varying the cavity length.

(3) Hakki[10] has reported line widths of under 1 kc/s (his spectrum analyser was not able to resolve line widths less than this) at 2 Gc/s with specimens mounted in coaxial cavities. Operation was c.w.

(4) The most impressive results to date are probably those of the Bell Telephone Laboratories. Using material in the resistivity range 10–100 ohm-cm, they have constructed samples to oscillate over the range 1·2–8·5 Gc/s by altering the specimen thickness. Typical output powers in c.w. operation are around 10 mW, with corresponding efficiencies of about 2%. In pulsed operation 1·8 W at 4·9 Gc/s has been obtained.

The remainder of this paper is devoted to an aspect that has received to date very little attention, namely tunability. Firstly, some experimental results using a 0·003 in thick GaAs specimen mounted in a coaxial cavity are described and an attempt is made to explain them in terms of the rather idealized model of domain formation described in section 3.

5. Experimental

All the results reported here were obtained using a diode made in a manner similar to that described by Gunn. Tin contacts were alloyed to both sides of a slice 0·003 in thick GaAs with a nominal resistivity of 2·0 ohm-cm before alloying. The slice was encapsulated in epoxy resin and one edge was ground until the specimen resistance was increased to 100 ohms. The contacts were formed by springing tungsten wires on to the tin contacts and bonding these also with epoxy. A cross-sectional view of the diode is shown in Fig. 4.

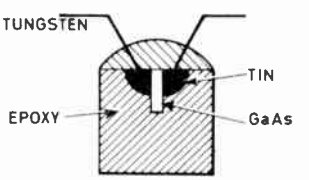

Fig. 4. Encapsulation of GaAs sample.

The diode was mounted in a coaxial cavity made from 50-ohm coaxial line as shown in Fig. 5. One end of the cavity was short circuited to r.f. by a 1000 pF coaxial by-pass capacitor. The diode was mounted in series with the inner conductor, as close to the by-pass capacitor as possible. The other end of the cavity was terminated in a moveable short

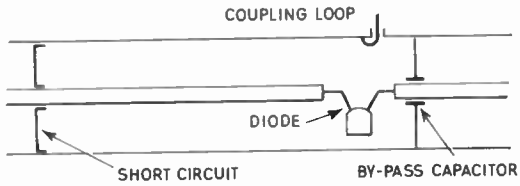

Fig. 5. Cavity configuration.

circuit. The bias voltage pulse was 1 μs long and the repetition frequency was 100 c/s. A lightly coupled loop was situated near to the by-pass capacitor to monitor the frequency; no attempt was made to optimize the loop for maximum output power in these experiments however.

The threshold voltage was 34 V. Figure 6 shows the output frequency as a function of short-circuit position for an applied voltage of 60 V. The output frequency is seen to be tunable from approximately 1·35 to 1·8 Gc/s. The curves (1) and (3) are limited at their extremes by the shortest and longest cavity lengths physically available. Curve (2) is the only one showing the complete tuning range. At any given frequency the curves are each separated by one half TEM wavelength, thus showing that they all represent the same electronic mode of oscillation. The behaviour when the characteristics (2) and (3) overlap near $z = 23$ cm (Fig. 6) is interesting. Two frequencies can be observed simultaneously, although the

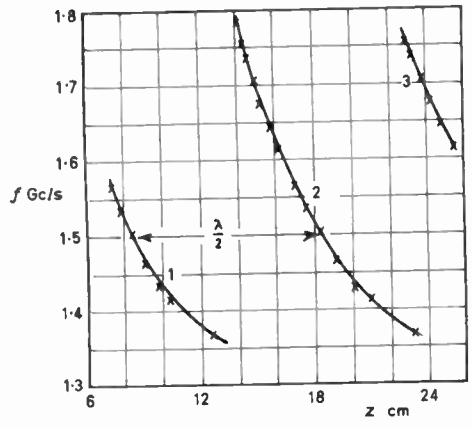

Fig. 6. Tuning characteristic.

output power at the lower frequency is very much less than that at the upper frequency.

By mounting the specimen in a low-Q resistive circuit, the current waveform was observed under conditions of constant voltage drive using a sampling oscilloscope. The natural transit time frequency was thus measured and found to be 1·85 Gc/s, independent of bias voltage. This is to be expected if the mechanism suggested in Section 3 is correct. This frequency is seen to be slightly higher than the maximum tunable frequency observed in Fig. 6.

The table below gives the maximum and minimum frequencies f_{max} and f_{min} respectively, of the tuning range, as the bias voltage is increased above threshold.

Table 1

V_{bias}	48	55	62	69	70	82	90
f_{max} Gc/s	1·8	1·78	1·77	1·73	1·69	1·67	1·65
f_{min} Gc/s	1·33	1·36	1·34	1·33	1·30	1·28	1·26

The tuning range Δf decreases slightly as the voltage is increased and both f_{max} and f_{min} decrease.

The natural, and simplest, equivalent circuit for the specimen is considered to be that shown in Fig. 7.

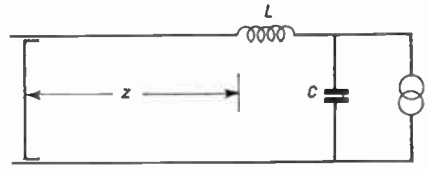

Fig. 7. Equivalent circuit of oscillator.

$$Z_0 \tan(\omega z/c) + \omega L - 1/\omega C = 0.$$

Here the diode is represented by a current source, of non-sinusoidal waveform, in parallel with the cold diode capacitance C. This parallel combination is in series with the lead inductance L and a length of line z, characteristic impedance Z_0. The resonant frequency f of this system is given by

$$Z_0 \tan\left(\frac{2\pi fz}{c}\right) + 2\pi fL - \frac{1}{2\pi fC} = 0$$

By plotting $f \tan 2\pi fz/c$ against f^2, a straight line should result with intercept $1/4\pi^2 LC$ on the f^2 axis and gradient $-2\pi L/Z_0$. Using the results given in Fig. 6, this curve is plotted in Fig. 8 and a good fit to a straight line is obtained. The corresponding values for L and C deduced from this curve are $L = 20$ nH, $C = 0{\cdot}655$ pF. Both values appear reasonable when the diode dimensions are considered.

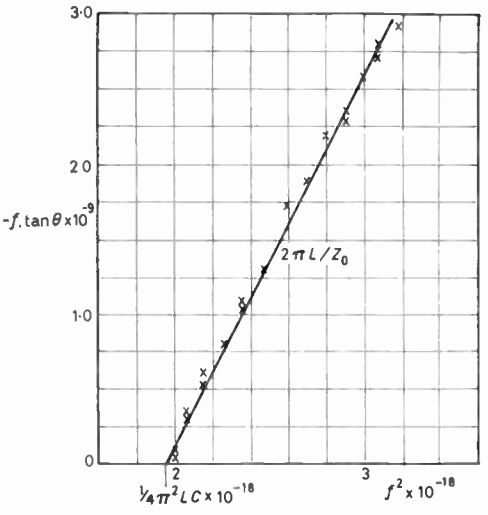

Fig. 8. $-f\tan\theta$ versus f^2.

6. Power Transfer to the Oscillating Field

We require to investigate the form of the current and voltage waveforms across the diode when placed in the resonant cavity. The diode current waveform is not likely to be sinusoidal but since the cavity formed by L, C and the transmission line has a reasonably high Q factor, we can assume that the alternating voltage appearing across the diode contacts is purely sinusoidal. The cavity, together with the lead inductance and capacitance can conveniently be represented, near resonance, by a parallel combination of susceptance and conductance R^{-1}.

Suppose now the specimen is biased just to the threshold voltage V_T. The total voltage across it is the sum of V_T and an a.c. component at the resonant frequency, amplitude V say. A domain will be launched just as the alternating voltage is zero and increasing. The current will fall, from the threshold level I_T to the valley level I_V and remain at this level for the domain transit time τ. At this instant, as the domain enters the anode, the current will revert to the threshold value only if the instantaneous voltage is greater than, or equal to, the threshold voltage. If the period of natural oscillation of the cavity $1/f$ is greater than τ, this is not the case and the specimen reverts to ohmic until the applied voltage once more increases above threshold. The current then drops to the valley level and the cycle begins once more. The current waveform under these conditions is shown in Fig. 9. Fourier analysis can readily be applied to this waveform. The fundamental in phase component I_p is given by

$$I_p = -\frac{2}{\pi}(I_T - I_V)\sin^2\frac{\omega\tau}{2} + \frac{V}{r}\left[\left(1 - \frac{\omega\tau}{2\pi}\right) + \frac{\sin 2\omega\tau}{4\pi}\right] \quad \ldots\ldots(4)$$

and quadrature component I_Q

$$I_Q = -\frac{1}{\pi}(I_T - I_V)\sin\omega\tau - \frac{V\sin^2\omega\tau}{2\pi r} \quad \ldots\ldots(5)$$

where r is the low field resistance of the specimen and ω is the angular frequency of oscillation. It has been assumed that the rise and fall times of the current pulse are negligible compared with a period. This is only true if the domain thickness x is much less than the sample length, which should be the case for low resistivity specimens. To include a finite rise-time at this stage makes eqns. (4) and (5) cumbersome.

This mechanism will only operate if $T \geqslant \tau \geqslant T/2$, where T is the period. If τ does not satisfy this inequality, the domain is re-triggered immediately after entering the anode and no tunability can result.

The steady state relationship between V, $\omega\tau$, specimen low field resistance r, and the cavity load resistance R can be obtained by noting that $V = -I_p R$ and then using eqn. (4) to eliminate I_p whence:

$$\frac{V}{r(I_T - I_V)} = \frac{\frac{2}{\pi}\sin^2\frac{\omega\tau}{2}}{\left(1 + \frac{r}{R}\right) - \frac{\omega\tau}{2\pi} + \frac{\sin 2\omega\tau}{4\pi}} \quad \ldots\ldots(6)$$

The output power (assuming R is due entirely to the load reflected into the cavity) is then given by $V^2/2R$.

If the voltage across the specimen, after the domain has been launched, falls to below the value $I_V r$, the domain is extinguished (see Figs. 2 and 3). The specimen then reverts to ohmic until the applied voltage increases above the threshold. Thus τ in Fig. 9 can be less than the natural transit time if this occurs.

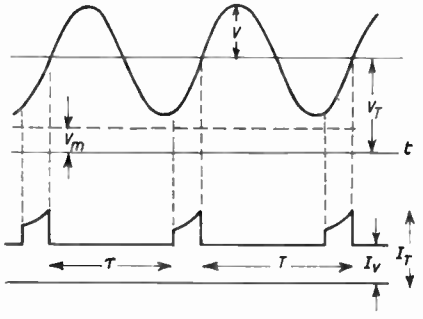

Fig. 9. Domain triggering.

When

$$I_T - I_V > \frac{V}{r} \quad \ldots\ldots(7)$$

the domain is not extinguished in transit. If this inequality is taken with eqn. (4), then it is

straightforward to show that I_p is always negative in the range $T \geqslant \tau \geqslant T/2$ and oscillations can be sustained. Thus a maximum tuning range of one octave, from $1/\tau$ to $1/2\tau$ is predicted theoretically for this particular mode of oscillation. There appear to be other tunable modes of oscillation where the domain transit time satisfies the inequality $nT \geqslant \tau \geqslant (n-\frac{1}{2})T$, where n is a positive integer. These modes appear attractive since they allow higher frequencies than the reciprocal of the transit time to be generated. The efficiency is likely to be very low however.

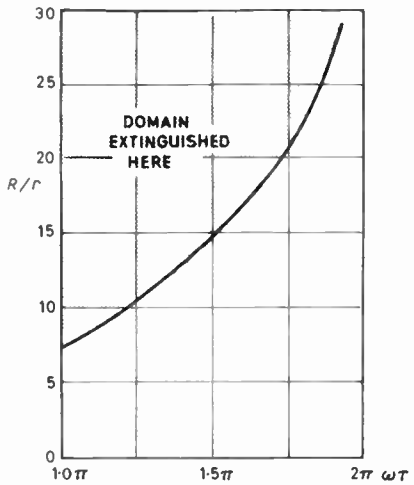

Fig. 10. Load resistance required to extinguish domain.

If inequality (7) is not satisfied then the time τ (Fig. 9) is determined by the following relationship rather than the domain transit time:

$$(I_T - I_V)r = -V \sin \omega\tau' \qquad \ldots\ldots(8)$$

since at this time the voltage across the specimen can only just support the domain. Here τ' has been used to differentiate between the natural domain transit time τ and the effective transit time τ' when the domain is suppressed.

It is interesting to note the values of R/r for which eqn. (6) is less than unity since, in this case, there is no possibility of extinguishing a domain. The range is shown in Fig. 10 as a function of $\omega\tau$. For values of $\omega\tau$ near 2π, the fundamental component of current is small and a high load resistance can be used; as $\omega\tau$ decreases the fundamental component increases, and in order to maintain the voltage swing across the load sufficiently small to prevent the domain being extinguished, R/r must decrease. If the load resistance is sufficiently large so that domain motion can be suppressed at some point in the r.f. cycle, then the period of oscillation T can be less than the natural transit time τ.

In Fig. 11, the quantity $\dfrac{V}{r(I_T - I_V)} \cdot \sqrt{\dfrac{r}{R}}$, which is proportional to the square root of the output power, is plotted as a function of $\omega\tau$ for various values of R/r, using eqn. (6). The two curves $R/r = 100$ and $R/r = 25$ are not continued much beyond $1/3\pi$ since these regions are not accessible, due to domain suppression. For $R/r < 10$ the tuning range is given by $2\pi \geqslant \omega\tau \geqslant \pi$ and the output power increases as the $\omega\tau$ product decreases. For $R/r > 10$, domain suppression allows $\omega\tau$ values greater than 2π since the effective transit time τ' is less than τ. In this case the output power remains sensibly constant over the tuning range.

7. Efficiency

The maximum output power occurs for $\omega\tau = \pi$, $R/r = 2$ as can be seen by differentiating eqn. (6), and from Fig. 11. The efficiency at this point is given by

$$\eta = 10\left(1 - \frac{I_V}{I_T}\right)\left(\frac{I_T}{I_V} - 1\right)\%$$

here the input power has been taken to be $I_T I_V r$, which is an underestimate, since the direct current will be greater than I_V. If I_T/I_V is taken to be 2, which is thought to be the correct order for GaAs, then a maximum efficiency of 5% is predicted. Efficiencies of up to 10% have been claimed but it is not clear if these values were observed at threshold bias or above.[10]

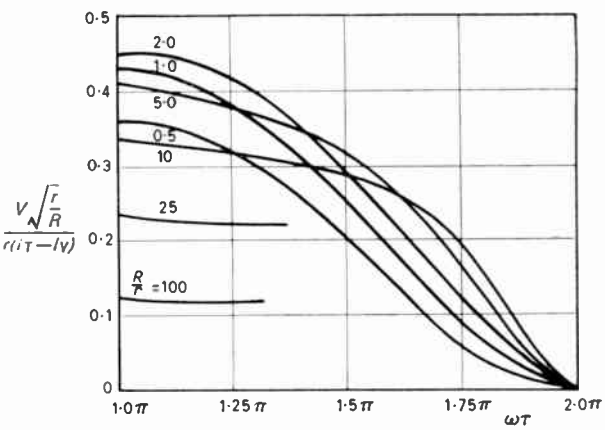

Fig. 11. $\dfrac{V}{r(I_T - I_V)} \cdot \sqrt{\dfrac{r}{R}}$ as a function of transit angle $\omega\tau$. The ordinate is proportional to (output power)$^{\frac{1}{2}}$. The curves are for varying R/r.

8. Comparison of Proposed Tuning Mechanism with Experimental Results

Much more experimental evidence is required before it can be claimed that the tunability reported here, and by other workers, is produced by a mechanism similar to that outlined in Sections 6 and 7 for an ideal specimen. However, the results presented in Section 5 are not inconsistent with the proposed mechanism. The natural domain transit time corresponds to a frequency of 1·85 Gc/s and this is the highest tunable frequency that should be observed if there is no domain suppression. The highest measured frequency is 1·8 Gc/s. The minimum frequency of oscillation should be about 0·93 Gc/s, whereas it is observed to be only 1·35 Gc/s. This restricted range cannot be understood at present and may be caused either by mode jumping, seen in Fig. 7 at the ends of the tuning range, or by departures from the idealized current waveform assumed in Section 6.

The appearance of the quadrature component of current, given by eqn. (5), implies that the oscillation frequency is not that suggested in section 5, but rather that a shunt susceptance I_Q/V must be added in parallel with the diode capacitance C. More detailed calculation shows that this is small compared with the diode capacitance in these experiments and consequently the straight line observed in Fig. 8 is to be expected.

We are not able to understand at present the tendency for the tuning range to move to lower frequencies as the bias voltage is increased. The preceding analysis is, however, being extended to cover this situation.

9. Conclusions

The Gunn effect and the currently accepted mechanisms to explain it have been described. A tentative theory has been advanced to explain the tuning range observed when specimens are placed in a resonant cavity. The efficiency at threshold bias is shown to be typically a few percent.

10. Acknowledgments

The authors are grateful to Dr. C. Hilsum for valuable discussions and to S.E.R.L. for some samples of GaAs.

11. References

1. J. B. Gunn, "Microwave oscillations of current in III–V semiconductors", *Solid State Communications*, **1**, p. 88, September 1963.
2. J. B. Gunn, "Instabilities of current in III–V semiconductors", *I.B.M. J. Res. Dev.*, **8**, p. 141, April 1964.
3. J. S. Heeks, A. D. Woode and C. P. Sandbank, "Coherent high field oscillations in long samples of GaAs", *Proc. Inst. Elect. Electronics Engrs*, **53**, p. 554, May 1965.
4. B. K. Ridley and T. B. Watkins, "The possibility of negative resistance in semiconductors", *Proc. Phys. Soc.*, **78**, p. 293, 1961.
5. C. Hilsum, "Transferred electron amplifiers and oscillators", *Proc. Inst. Radio Engrs*, **50**, p. 185, February 1962.
6. C. Hilsum, "A simple analysis of transferred electron oscillators", *Brit. J. Appl. Phys.*, **16**, p. 1401, September 1965.
7. B. K. Ridley, "Specific negative resistance in solids", *Proc. Phys. Soc.*, **82**, p. 954, 1963.
8. J. B. Gunn, "Instabilities of current and of potential distribution in GaAs and InP", I.B.M. Research Paper RC 1216, June 1964.
9. H. Kroemer, "Theory of the Gunn effect", *Proc. I.E.E.E.*, **52**, p. 1736, December 1964.
10. B. W. Hakki and J. C. Irvin, "C.W. microwave oscillations in GaAs", *Proc. I.E.E.E.*, **53**, p. 80, January 1965.
11. J. S. Heeks, A. D. Woode and C. P. Sandbank, "The mechanism and device applications of high field instabilities in GaAs", Proceedings of the Symposium on Microwave Applications of Semiconductors, London, June 1965, Paper No. 3. (Reprinted in *The Radio and Electronic Engineer*, **30**, No. 6, pp. 377–87, December 1965.)
12. A. R. Hutson *et al.*, "Mechanism of the Gunn effect from a pressure experiment", *Phys. Rev. Letters*, **14**, p. 639, April 1965.

Manuscript first received by the Institution on 14th July 1965 and in the revised form on 7th August 1965. (Paper No. 1012.)

U.D.C. 621.372.853.1

Dielectric Loaded Waveguides—A Review of Theoretical Solutions

Part III: The Impedance Approach to Dielectric Loaded Waveguides†

By

S. K. CHATTERJEE, M.Sc.‡

AND

(Mrs.) R. CHATTERJEE, Ph.D., M.S.E., M.Sc.‡

Summary: Surface impedance, transverse and longitudinal impedances are defined in analogy with the circuit theory definition. The concept of wave impedance and its relation to orthogonality of electric and magnetic fields is discussed. It is shown that in the case of multi-mode transmission, the wave impedance is not unique. Wave impedances of E and H modes in dielectric-filled waveguides and different impedance characteristics of a circular cylindrical waveguide containing two coaxial dielectrics and a coaxial guide containing two different dielectrics are discussed.

16. Definition of Impedance in Analogy with the Circuit Concept

An impedance description of electrical networks and transmission lines at low frequencies is made in terms of the ratio V/I, where V and I represent the magnitudes of alternating voltage and current respectively. This definition of impedance at low frequencies where we deal with lumped elements is unique as the voltage between any two points can be defined uniquely. In distributed circuits, however, the voltage is expressed as follows from the law of magnetic induction

$$\oint \mathbf{E}.\mathrm{ds} = -\frac{\partial \Phi}{\partial t} \qquad \text{.....(274)}$$

where Φ is the flux through the surface enclosed by the path of integration and $\mathbf{E}$ is the electric field. The definition of voltage as a line integral between two points loses, in most cases, its physical significance in the case of distributed circuits. As an illustration, let us consider a re-entrant cavity (Fig. 65), in which case, it is usual to speak of the alternating voltage across the gap AB. This voltage is equal to the negative rate of change of Φ threading the dotted curve, which runs along the inside walls and across the resonator gap as indicated by the arrows. Since in practice the line integral of field strength along the resonator wall is vanishingly small compared to that over the gap

$$\oint \mathbf{E}.\mathrm{ds} = \int_A^B \mathbf{E}.\mathrm{ds} \qquad \text{.....(275)}$$

So the voltage across the gap AB may be written as

$$V = -\int_A^B \mathbf{E}.\mathrm{ds} \qquad \text{.....(276)}$$

In distributed circuits, therefore, voltage is to be always understood in this sense. Thus the idea of voltage between any two arbitrary points C and D

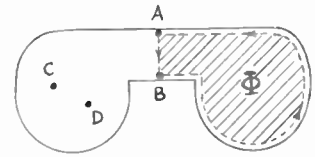

Fig. 65. The definition of voltage for a microwave cavity.

has no physical meaning in this context. Also, at high frequencies, curl $\mathbf{E}$ differs increasingly from zero and the voltage difference between any two points defined as the line integral of the electric field between the points ceases to be unique. In waveguide problems at microwave frequencies, the circuit theory definition of impedance breaks down in most of the cases. For example, in the case of a circular cylindrical guide excited by the circularly symmetric H_{01} mode which is characterized by a complete absence of longitudinal flow of current in the guide walls and voltage across any radius of the guide, the impedance defined by the V/I relation loses its meaning.

The impedance may be defined in several ways. The field vectors $\mathbf{E}$ and $\mathbf{H}$ are associated with V and I respectively and the impedance depends on the direction in which it is measured. This does not mean that impedance is a vector. The circuit theory definition of impedance may be applied in some cases to waveguides used as transmission lines. For example,

† Parts I and II of this paper were published in the September, October and November issues of *The Radio and Electronic Engineer* (30, Nos. 3, 4 and 5, pp. 145–60, 195–205 and 259–88).

‡ Department of Electrical Communication Engineering, Indian Institute of Science, Bangalore, India.

in the case of a circular cylindrical waveguide of radius a, the transverse voltage V between the axis chosen arbitrarily as a reference and the inner wall of the guide is defined by the following relation

$$V_t = \int_{r=0}^{a} E_r \, dr \qquad \text{.....(277)}$$

The longitudinal current along the guide walls is obtained by taking the line integral of the transverse component of $\mathbf{H}$ (H_θ) around the surface of the guide.

$$I = \oint_{r=a} H_\theta \, d\theta \qquad \text{.....(278)}$$

The transverse impedance is then defined as

$$Z_t = V_t/I \qquad \text{.....(279)}$$

It is obvious that Z_t is, in general, a function of r and θ as V_t and I may not involve the same function of r and θ. So Z_t is not uniquely defined.

The impedance depends also on the direction of power flow as it is associated with the total power flow in the following way

$$Z = \frac{V}{I}\frac{V^*}{V^*} = \frac{V^2}{2P^*} \qquad \text{.....(280)}$$

where the asterisk indicates the complex conjugate and V and I represent the peak values of voltage and current respectively. The field theory counterpart of the circuit theory definition of the complex power of $\frac{1}{2}VI^*$ is expressed by the following integral

$$P = \tfrac{1}{2}\mathrm{Re}\int_S \mathbf{E}\times\mathbf{H}.\mathbf{n}\,ds \qquad \text{.....(281)}$$

where $\mathbf{n}$ represents the outward normal. The integration is extended over the surface S normal to the direction of power flow. The expression for P depends on the surface over which the integration is performed and, in general, will differ from the circuit theory definition of VI. The impedance according to the field theory is defined by the relation

$$Z = \frac{\left|\int_{r=0}^{a} E_r \, dr\right|^2}{\mathrm{Re}\int_S \mathbf{E}\times\mathbf{H}.\mathbf{n}\,ds} \qquad \text{.....(282)}$$

It may be pointed out that Z as given by the above relation is in general a function of r and hence is not always unique.

As Z depends on the energy flow and the direction in which the integration $\int \mathbf{E}.ds$ is performed, it is usual to define a set of impedances, such as transverse (Z_t) or longitudinal (Z_l) depending on the direction in which the impedance is measured. A set of other impedances can also be defined in the following way. The surface impedance Z_s is defined as the ratio of $\mathbf{n}\times\mathbf{E}$ to $\mathbf{n}\times\mathbf{H}$ but it is understood that the tangential components of the field vectors are at right angles to each other. The intrinsic impedance ζ of a homogeneous isotropic medium having permeability μ and permittivity ε and conductivity σ for plane waves of angular frequency ω is defined as $\zeta = \omega\mu/k$, where $k^2 = \omega^2\mu\varepsilon + j\omega\mu\sigma$. Considering the propagation to be in the z-direction, the longitudinal impedance is defined as

$$Z_l = \frac{\left|\int_{z=0}^{\lambda_g/2} E_z \, dz\right|^2}{\mathrm{Re}\int_S \mathbf{E}\times\mathbf{H}.\mathbf{n}\,ds} \qquad \text{.....(283)}$$

The longitudinal voltage V_l has been defined along the direction of propagation as the line integral of the longitudinal component of $\mathbf{E}$ (E_z) within the limits of $z = 0$, taken arbitrarily as a reference at any point along the guide to $z = \lambda_g/2$, where λg is the guide wavelength. The calculation of V_l in a simple waveguide is straightforward. In a composite waveguide, the longitudinal impedances at the interface between any two media have to be matched in order that $E_{\tan}$ and $H_{\tan}$ may be continuous across the boundary.

17. Wave Impedance

Schelkunoff's[155] impedance concept leads to the definition of the impedance matrix in cartesian coordinate system as follows:

$$|\eta| = \begin{bmatrix} \frac{E_x}{H_x} & \frac{E_x}{H_y} & -\frac{E_x}{H_z} \\ -\frac{E_y}{H_x} & \frac{E_y}{H_y} & \frac{E_y}{H_z} \\ \frac{E_z}{H_x} & -\frac{E_z}{H_y} & \frac{E_z}{H_z} \end{bmatrix} \qquad \text{.....(284)}$$

But the impedance is not a dyadic, as it does not transform to another coordinate system in the manner prescribed for the dyadic. However, in many cases of guided transmission, the ratio of the electric field to the magnetic field, which are perpendicular to each other and to the direction of transmission of power, is fundamental and is known as the wave impedance η. This definition has enabled a better understanding of some electromagnetic phenomena such as the reflection of electromagnetic waves at a discontinuity in a waveguide, representation of complicated waveguide junctions by equivalent circuits, matching of waveguides, etc., and has helped to improve considerably the measurement technique at microwave frequencies.

The definition of wave impedance $\eta_{ij} = E_i/H_j$, where i, j refer to some coordinate of space that is being considered, is quite consistent with the circuit

theory definition of characteristic impedance $Z = V/I$, because the field theory represented by Maxwell's equations is simply circuit theory applied to volume elements. Each volume element may be regarded as composed of inductance, capacitance and resistance. Each individual volume element may also be considered as coupled to its neighbouring volume element. It is by applying circuit theory to all the volume elements that we arrive at the field theory. This coordination of circuit and field theories has permitted the construction of three-dimensional networks capable of reproducing some elementary features of wave propagation in a medium.

For convenience of reference, the expressions for different impedances are collected together.

Wave impedance

$$\eta_{ij} = E_i/H_j$$

Intrinsic impedance

$$\zeta = \frac{\omega\mu}{[\omega^2\mu\varepsilon + j\omega\mu\sigma]^{\frac{1}{2}}}$$

Surface impedance

$$Z_S = E_{\tan}/H_{\tan}$$

Longitudinal impedance

$$Z_l = \frac{\left|\int_{z=0}^{\lambda_g/2} E_z \, dz\right|^2}{\mathrm{Re}\left[\int_S \mathbf{E}\times\mathbf{H}.\mathbf{n}\, ds\right]}$$

Transverse impedance

$$Z_t = \frac{\left|\int_{r=0}^{a} E_r \, dr\right|^2}{\mathrm{Re}\left[\int_S \mathbf{E}\times\mathbf{H}.\mathbf{n}\, ds\right]} \qquad \text{.....(285)}$$

17.1. *Wave Impedance and Orthogonality of Fields*

The wave impedance of a plane wave travelling along the z-direction in an unbounded medium of permeability μ, permittivity ε and conductivity σ is defined by the relation

$$\eta_{xy} = \frac{E_x}{H_y} = \sqrt{\frac{j\omega\mu}{\sigma + j\omega\varepsilon}} \qquad \text{.....(286)}$$

which is equal to the intrinsic impedance ζ of the medium. It is easy to show that the wave impedance

$$\eta_{yx} = \frac{E_y}{H_x} = -\frac{\gamma}{j\omega\mu} = -\eta_{xy} = -\zeta \qquad \text{.....(287)}$$

where

$$\gamma = \sqrt{j\omega\mu\sigma - \omega^2\mu\varepsilon}$$

The negative sign before ζ is only due to the choice of the positive direction of the coordinate axes and represents no new significant fact as is evident from the z-component of the Poynting vector

$$\begin{aligned} S_z &= \tfrac{1}{2}(\mathbf{E}\times\mathbf{H}^*)_z \\ &= \tfrac{1}{2}(\eta_{xy}H_yH_y^* - \eta_{yx}H_xH_x^*) \\ &= \tfrac{1}{2}\eta_{xy}(|H_x|^2 + |H_y|^2) \\ &= \tfrac{1}{2}\eta_{xy}|\mathbf{H}|^2 \end{aligned} \qquad \text{.....(288)}$$

Since $\eta_{xy} = -\eta_{yx}$, we have

$$\frac{E_x}{H_y} = -\frac{E_y}{H_x} \qquad \text{.....(289)}$$

which yields the relation

$$E_xH_x + E_yH_y = 0 \qquad \text{.....(290)}$$

This relation implies orthogonality between the electric field $\mathbf{E}$ and magnetic field $\mathbf{H}$ vectors, which is inherent in the definition of a plane wave. The impedance η_{xy} or η_{yx} as defined above is independent of position in the cross-section in which it is measured and is therefore unique. It may therefore be stated that the existence of a unique wave impedance along a direction implies the orthogonality of electric and magnetic fields in the plane perpendicular to the direction and vice versa.

17.2. *Wave Impedances of Guided Waves*

For H and E waves, the wave impedances are respectively

$$\eta_H = \frac{j\omega\mu}{\gamma}, \qquad \eta_E = \frac{\gamma}{j\omega\varepsilon} \qquad \text{.....(291)}$$

where the electric and magnetic fields satisfy the orthogonality relation. But such a wave impedance does not necessarily exist in the case of multimode transmission. Let us consider a combination of two pure H waves denoted by subscripts 1 and 2. Let η_1 and η_2 represent the wave impedances for the two modes

$$\begin{aligned} \mathbf{H}_1 &= H_{1x}\mathbf{i} + H_{1y}\mathbf{j} + H_{1z}\mathbf{k} \\ \mathbf{H}_2 &= H_{2x}\mathbf{i} + H_{2y}\mathbf{j} + H_{2z}\mathbf{k} \\ \mathbf{E}_1 &= \eta_1 H_{1y}\mathbf{i} - \eta_1 H_{1x}\mathbf{j} \\ \mathbf{E}_2 &= \eta_2 H_{2y}\mathbf{i} - \eta_2 H_{2x}\mathbf{j} \end{aligned} \qquad \text{.....(292)}$$

For the combination of two waves

$$\begin{aligned} \mathbf{H} &= \mathbf{H}_1 + \mathbf{H}_2 \\ \mathbf{E} &= \mathbf{E}_1 + \mathbf{E}_2 \end{aligned} \qquad \text{.....(293)}$$

The condition for the existence of a unique wave impedance is

$$(\eta_2 - \eta_1)(H_{2x}H_{1y} - H_{1x}H_{2y}) = 0 \qquad \text{.....(294)}$$

which is, in general, not satisfied. Hence, a unique wave impedance in general cannot be defined in the case of a combination of H waves. But if $\eta_1 = \eta_2$, the above relation is satisfied. A similar conclusion holds good in the case of a combination of two pure E waves.

In the case of a combination of a single H wave and a single E wave, the following expressions can be written

$$\mathbf{H}_h = H_{hx}\mathbf{i} + H_{hy}\mathbf{j} + H_{hz}\mathbf{k}$$
$$\mathbf{H}_e = H_{ex}\mathbf{i} + H_{ey}\mathbf{j}$$
$$\mathbf{E}_h = \eta_h H_{hy}\mathbf{i} - \eta_h H_{hx}\mathbf{j}$$
$$\mathbf{E}_e = \eta_e H_{ey}\mathbf{i} - \eta_e H_{ek}\mathbf{j}$$
$$\mathbf{H} = \mathbf{H}_h + \mathbf{H}_e$$
$$\mathbf{E} = \mathbf{E}_h + \mathbf{E}_e \qquad \text{.....(295)}$$

The condition for the existence of a unique wave impedance is

$$(\eta_h - \eta_e)(H_{hx}H_{ey} - H_{ex}H_{hy}) = 0 \qquad \text{.....(296)}$$

which is, in general, not satisfied. Hence a unique wave impedance cannot be defined in general for a HE or EH wave.

It may therefore be concluded that while the impedance concept has its domain of utility, it is rather limited. It has been pointed out by Waldron[85] that for a non-HSP-guide†, the wave impedances $\eta_{r\theta} = E_r/H_\theta$ and $\eta_{\theta r} = -E_\theta/H_r$ are not equal and both $\eta_{r\theta}$ and $\eta_{\theta r}$ are function of the radial coordinate r. This is also true for inhomogeneous guides,[160] such as a simple waveguide with two media when $E_z \neq 0$, $H_z \neq 0$ for EH modes. In this case it is obvious that $\eta_{\theta r} \neq \eta_{r\theta}$ and both the impedances are complicated functions of position in the waveguide. It has also been pointed out by Waldron[81] that a similar difficulty as regards the concept of unique wave impedance arises even with HSP-guide if it is not straight. It has therefore been concluded that wave impedance is a useful concept in waveguide problems only in the case of a straight HSP-guide. The concept of wave impedance has been used by several investigators[32,57,73,156–160] in the solution of different problems.

17.3. *Wave Impedance for E and H Waves in a Dielectric-filled Waveguide*

Figure 66 shows the equivalent circuit of a guide partially filled with dielectric. The plane of discontinuity is perpendicular to the axis of the guide. In such a case, the power flow down the guide is

$$P_z = \frac{\mathrm{Re}(\eta)}{2}\int |H_t|^2\,\mathrm{d}s \qquad \text{.....(297)}$$

where the tangential component H_t must satisfy the boundary condition at the interface of the two dielectric media. But η changes continuously and this gives rise to a reflected wave at the interface. The wave impedances for E and H waves reduce to the values as given below for a lossless guide

$$\eta_H = \frac{\lambda_g}{\lambda}\sqrt{\frac{\mu}{\varepsilon}} \quad \text{and} \quad \eta_E = \frac{\lambda}{\lambda_g}\sqrt{\frac{\mu}{\varepsilon}} \qquad \text{.....(298)}$$

where λ is the wavelength of the TEM wave in the medium and λ_g is the guide wavelength. The relative wave impedances for the two waves in terms of the free space wavelength λ_0 and the cut-off wavelength λ_c are

$$\frac{\eta_H^{(2)}}{\eta_H^{(1)}} = \sqrt{\frac{k_{e1} - (\lambda_0/\lambda_c)^2}{k_{e2} - (\lambda_0/\lambda_c)^2}} = Z_H \qquad \text{.....(299)}$$

and

$$\frac{\eta_E^{(2)}}{\eta_E^{(1)}} = \frac{k_{e1}}{k_{e2}}\sqrt{\frac{k_{e2} - (\lambda_0/\lambda_c)^2}{k_{e1} - (\lambda_0/\lambda_c)^2}} = Z_E \qquad \text{...(300)}$$

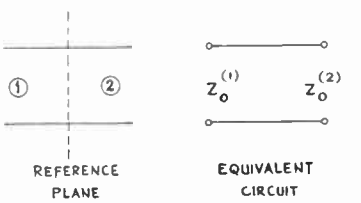

Fig. 66. Equivalent circuit of a guide partially filled with dielectric.

If $k_{e2} > k_{e1}$, then the relative **H** mode impedance (Z_H) decreases monotonically as k_{e2} increases. Whereas the relative E-mode impedance (Z_E) increases with k_{e2}, passes through a maximum when $k_{e2} = 2(\lambda_0/\lambda_c)^2$ and then decreases. The maximum value of Z_E is given by

$$Z_{E(\max)} = \frac{k_{e1}}{2(\lambda_0/\lambda_c)}\frac{1}{\sqrt{k_{e1} - (\lambda_0/\lambda_c)^2}} \qquad \text{.....(301)}$$

For sufficiently large values of λ_0/λ_c, there are two values of k_{e2} as follows that make $Z_E = 1$, namely

$$k_{e2} = k_{e1} \quad \text{and} \quad k_{e2} = \frac{1}{\left(\frac{\lambda_c}{\lambda_0}\right)^2 - \frac{1}{k_{e1}}} \qquad \text{...(302)}$$

The second value of k_{e2} corresponds to Brewster's angle for plane waves. The variation of Z_E and Z_H with k_{e2} when $k_{e1} = 1$ and $(\lambda_0/\lambda_c)^2 = 0{\cdot}8$ is shown in Fig. 67. In the case of a lossy material k_e is complex and the wave impedance for the two modes are[98]

† HSP-guide means a homogeneous simple perfect guide which consists of a single boundary surface, to one side of which is a conductor having $\sigma = \infty$ and to the other side a single uniform lossless medium having scalar properties. In other words, a guide is said to be HSP when all the media present in it are isotropic and lossless and when all the electromagnetic energy contained in the electromagnetic wave is propagated in a single uniform medium. This type of waveguide is an ideal one and may not be realized in practice. As in a conventional hollow metal waveguide, the conductivity of the metallic wall is very high and the loss tangent of air is very low, the metal tube waveguide for all practical purposes may be considered as a fair approximation to a HSP-guide.

$$\eta_H = \frac{\omega\mu}{\beta + \dfrac{\omega^4\mu^2\varepsilon''^2}{4\beta^3}}\left(1+\mathrm{j}\frac{\omega\mu\varepsilon''}{2\beta^2}\right) = \frac{\mathrm{j}\omega\mu}{\alpha+\mathrm{j}\beta} \qquad \text{.....(303)}$$

$$\eta_E = \frac{\alpha+\mathrm{j}\beta}{\mathrm{j}\omega k_e} = \frac{\beta}{\omega\varepsilon' + \omega\dfrac{\varepsilon''^2}{\varepsilon'}}\left[1+\frac{\omega^2\mu\varepsilon''^2}{2\beta^2\varepsilon'} - \mathrm{j}\left(\frac{\omega^2\varepsilon''\mu}{2\beta^2} - \frac{\varepsilon''}{\varepsilon'}\right)\right] \qquad (304)$$

It is noted that for H waves, the presence of loss makes η_H slightly inductive but for E waves, the reactive part is either positive or negative depending on ω. Near cut-off η_E is capacitive, and at higher frequencies it becomes inductive.

17.4. *Impedance of a Circular Cylindrical Guide with Two Coaxial Dielectrics*

The average transmitted power through the system (Fig. 21) in the z-direction is

$$P_z = \tfrac{1}{2}\int_{\theta=0}^{2\pi}\int_{r=0}^{r_1}(E_{r1}H_{\theta1} - E_{\theta1}H_{r1})r\,\mathrm{d}\theta\,\mathrm{d}r + \tfrac{1}{2}\int_{\theta=0}^{2\pi}\int_{r=r_1}^{r_2}(E_{r2}H_{\theta2} - E_{\theta2}H_{r2})r\,\mathrm{d}\theta\,\mathrm{d}r \qquad (305)$$

The power flows P_z^h, P_z^e, P_z^{he} for the H, E, and HE waves have been calculated[83-4.161] by using appropriate field components and using the following relations

$$\mathscr{F}_1(kr) = \frac{\partial Z_1(kr)}{\partial(kr)} - Z_1(kr)\log(kr)$$

$$\mathscr{F}_2(kr) = \frac{\partial Z_2(kr)}{\partial(kr)} - Z_2(kr)\log(kr)$$

$$Z_1(kr) = A_1 J_1(kr) + A_2 Y_1(kr)$$

$$Z_2(kr) = A_1 J_2(kr) + A_2 Y_2(kr) \qquad \text{.....(306)}$$

The expressions for P_z^h, P_z^e and P_z^{he} are as follows

$$P_z^h = \tfrac{1}{2}\pi A^2\frac{\mathrm{j}\omega\mu_0\gamma}{k^2}\mathrm{F}^h(kr_1, kr_2)$$

$$P_z^e = \tfrac{1}{2}\pi B^2\frac{\mathrm{j}\omega\gamma}{k^2}\mathrm{F}^e(kr_1, kr_2)$$

$$P_z^{he} = \tfrac{1}{2}\pi B^2\mathrm{F}^{he}(kr_1, kr_2) \qquad \text{.....(307)}$$

where

$$\mathrm{F}^h(kr_1, kr_2) = \left[\frac{2}{k^2}\left(\frac{kr_1}{2}\{J_2(kr_1)\mathscr{F}_1(kr_1) - J_1(kr_1)\mathscr{F}_2(kr_1)\} + \tfrac{1}{2}J_1^2(kr_1)\right) + \{\tfrac{1}{2}r_1^2(J_0(kr_1) + J_1^2(kr_1))\} + \frac{1}{k^2}\{J_0^2(kr_1) - 1\} + \frac{2}{k^2}\left\{\frac{kr_2}{2}(Z_2(kr_2)\mathscr{F}_1(kr_2) - Z_1(kr_2)\mathscr{F}_2(kr_2)) + \tfrac{1}{2}Z_1^2(kr_2) - \frac{kr_1}{2}(Z_2(kr_1)\mathscr{F}_1(kr_1) - Z_1(kr_1)\mathscr{F}_2(kr_1)) - \tfrac{1}{2}Z_1^2(kr_1)\right\} + \tfrac{1}{2}\{r_2^2(Z_0^2(kr_2) + Z_1^2(kr_2)) - r_1^2(Z_0^2(kr_1) + Z_1^2(kr_1))\} + \frac{1}{k^2}\{Z_0^2(kr_2) - Z_0^2(kr_1)\}\right] \qquad \text{...(308)}$$

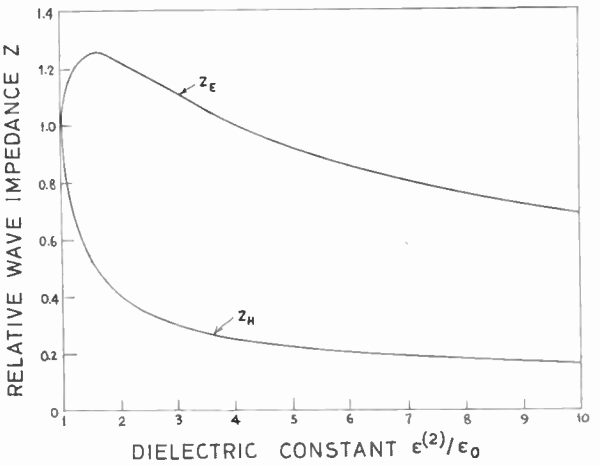

Fig. 67. Relative wave impedence for E and H waves as a function of dielectric constant. (Ref. 98.)

Similarly, F^e and F^{he} are expressed in terms of the functions Z's and $\mathscr{F}$'s. In calculating P_z^{he}, the excitation constant A has been absorbed in B by using the boundary conditions $E_{\theta2} = 0$ at $r = r_2$ which yields

$$A = -B\frac{\gamma}{\mathrm{j}\omega\mu_0 kr_2}\mathrm{f}(kr_2)\tan\theta \qquad \text{.....(309)}$$

The transverse voltage between the axis and the inner wall of the guide for the H_1 mode is calculated by using appropriate field components in the following equation

$$V_t^h = \int_0^{r_1} E_{r1}\,\mathrm{d}r + \int_{r_1}^{r_2} E_{r2}\,\mathrm{d}r$$

which yields $V_t^h = \dfrac{\mathrm{j}\omega\mu_1}{k}A\sin\theta\, g_1^h(kr_1, kr_2)$ .....(310)

where

$$g_1^h = \frac{\pi}{2}r_1\left\{J_0(kr_1)\left(\frac{2}{\pi} - \mathscr{H}_1(kr_1) + \mathscr{H}_0(kr_1)J_1(kr_1) - \frac{J_1(kr_1)}{k} + \frac{\pi}{2}r_2\left\{Z_0(kr_2)\left(\frac{2}{\pi} - \mathscr{H}_1(kr_2)\right) + \mathscr{H}_0(kr_2)Z_1(kr_2)\right\} - \frac{Z_1(kr_2)}{k} - \frac{\pi}{2}r_1\left\{Z_0(kr_1)\left(\frac{2}{\pi} - \mathscr{H}_1(kr_1)\right) + \mathscr{H}_0(kr_1) - Z_1(kr_1)\right\} + \frac{Z_1(kr_1)}{k}\right. \qquad \text{...(311)}$$

In deriving the above relation for V_t^h, the following relations for the Struve functions $\mathscr{H}$'s and the gamma function Γ have been used

$$\mathscr{H}_{\nu-1}(z)-\mathscr{H}_{\nu+1}(z)=2\mathscr{H}'_{\nu}(z)-\frac{(\frac{1}{2}z)^{\nu}}{\sqrt{\pi}\Gamma(\nu+\frac{3}{2})}$$

$$\mathscr{H}_{-1}=\frac{2}{\pi}-\mathscr{H}_1$$

$$\Gamma(\nu+\tfrac{3}{2})=\Gamma(\tfrac{3}{2})=\frac{\sqrt{\pi}}{2} \quad \text{when } \nu=0$$

$$\Gamma(\nu+\tfrac{1}{2})=\Gamma(-\tfrac{1}{2})=-2\sqrt{\pi} \quad \text{.....(312)}$$

Similarly, the transverse voltages for the E_1 and HE_1 waves are

$$V_t^e=-\frac{\gamma}{k^2}B\cos\theta\, g_1^e(kr_1,kr_2)$$

$$V_t^{he}=-\frac{\gamma}{k^2r_2}B\tan\theta\sin\theta\, f(kr_2)g_1^h(kr_1,kr_2)-$$

$$-\frac{\gamma}{k^2}B\cos\theta\, g_1^e(kr_1,kr_2) \quad \text{...(313)}$$

where

$$g_1^e(kr_1,kr_2)=[J_1(kr_1)+Z_1(kr_2)-Z_1(kr_1)] \quad \text{...(314)}$$

The longitudinal voltages for the E_1 and HE_1 modes are

$$V_l^{e,(he)}=B\cos\theta\frac{\lambda_g}{2}Z_1(kr_2) \quad \text{.....(315)}$$

For the H_1 mode $E_z=0$, hence $V_l^h=0$. So, the transverse and longitudinal impedances for the three modes are

$$Z_t^h=\frac{j\omega\mu_0\sin^2\theta}{\pi\gamma}\frac{g^h}{F^h}$$

$$Z_t^e=\frac{\gamma\cos^2\theta}{j\pi\omega k^2}\frac{g^e}{F^e}$$

$$Z_t^{he}=\frac{\gamma^2}{\pi k^4}\frac{g^{he}}{F^{he}}$$

$$Z_l^h=0$$

$$Z_l^e=\frac{k^2\lambda_g^2\cos^2\theta}{4\pi j\omega\gamma}\frac{1}{F^e}$$

$$Z_l^{he}=\frac{\lambda_g^2\cos^2\theta\, J_1^2(kr_1)}{4\pi F^{he}} \quad \text{.....(316)}$$

where the functions

$$F^h=F(kr_1,kr_2)$$

$$F^e=F(kr_1,kr_2;\varepsilon_1,\varepsilon_2)$$

$$F^{he}=G(kr_1,kr_2;\varepsilon_1,\varepsilon_2) \quad \text{.....(317)}$$

17.5. *Impedance of a Coaxial Waveguide Containing Two Different Dielectrics*

The characteristic impedance is of practical significance for the symmetrical modes as only in these cases are the field components invariant with θ. By applying Maxwell's equations in their integral form over appropriate paths and surfaces of integration (Fig. 39), the line integral of the radial electric field component E_r between the two conductors is found. This when divided by the current in the inner conductor, yields the following result[21] for the characteristic impedance for the principal mode E_{00} when $\varepsilon_1 > \varepsilon_2$.

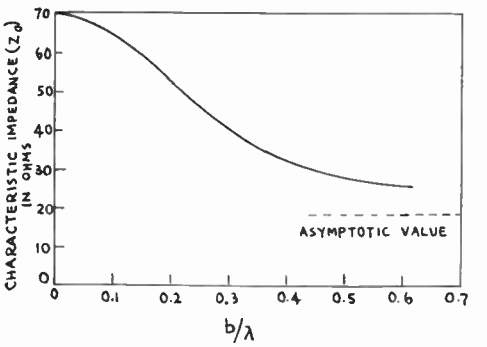

Fig. 68. Variation of characteristic impedance for the E_{00} mode with respect to b/λ, $\epsilon_1 = 2{\cdot}5$, $\epsilon_2 = 1{\cdot}0$, $a/b = 0{\cdot}5$, $c/b = 2{\cdot}0$. (Ref. 21.)

$$Z_0=\left(\frac{\eta_0}{4\varepsilon_1}\right)\left(\frac{\lambda}{\lambda_g}\right)\left(1-\frac{k_1^2}{k_2^2}\right)\times$$

$$\times\left[J_0\left(k_1\frac{a}{b}\right)Y_0(k_1)-J_0(k_1)Y_0\left(k_1\frac{a}{b}\right)\right] \quad \text{(318}$$

At zero frequency, $b/\lambda = 0$ and the above expression for Z_0 reduces to

$$Z_0=\frac{\eta_0}{2\pi}\left[\left(\ln\frac{c}{a}\right)\left(\frac{1}{\varepsilon_1}\ln\frac{b}{a}+\frac{1}{\varepsilon_2}\ln\frac{c}{b}\right)\right]^{\ddagger} \quad \text{...(319)}$$

At infinite frequency, the expression (318) for Z_0 reduces to

$$Z_0=\frac{\eta_0}{2\pi k_1\sqrt{\varepsilon_1}}\frac{J_0\left(\frac{a}{b}k_1\right)}{J_1(k_1)} \quad \text{.....(320)}$$

where k_1 is the solution of the following equation

$$J_1(k_1)Y_0\left(\frac{a}{b}k_1\right)-J_0\left(\frac{a}{b}k_1\right)Y_1(k_1)=0 \quad \text{...(321)}$$

The inductance (L) and capacitance (C) per unit length at zero frequency are respectively given by the following relations:

$$L=\frac{\mu_0}{2\pi}\ln\frac{c}{a} \quad \text{.....(322)}$$

$$C=\frac{2\pi\varepsilon_0}{\frac{1}{\varepsilon_1}\ln\frac{c}{a}+\frac{1}{\varepsilon_2}\ln\frac{c}{b}} \quad \text{.....(323)}$$

The characteristic impedance variation with respect to b/λ for E_{00} mode is shown in Fig. 68, where $\varepsilon_1 = 2{\cdot}5$, $\varepsilon_2 = 1{\cdot}0$, $a/b = 0{\cdot}5$, $c/b = 2{\cdot}0$. The values of Z_0 at zero and high frequencies are respectively (318)

$$Z_0 \text{ (zero frequency)} = 69{\cdot}53 \text{ ohms}$$

and $$Z_0 \text{ (high frequency)} = 18{\cdot}84 \text{ ohms}$$

18. Conclusion

An attempt has been made to include in this review as much available information as possible. The subject is a recent and fast developing one and as such it is felt that much remains to be done. The study of impedance characteristics of composite waveguides is complicated and there is much scope for further work in this aspect of the problem. It is hoped that the investigations by different authors will lead to some original ideas. Before we conclude, it may be mentioned that one of the most significant contributions that has emerged out of the investigations on dielectric in waveguides is the idea of the existence of backward waves in such structures.

19. Acknowledgment

The authors express their grateful thanks to the many authors and publishers who have kindly given permission for material which has appeared in different journals and reports to be used in this review. The sources of information and illustrations have been recorded in each case.

20. References and Bibliography

1. O. J. Lodge, "On the theory of lightning conductors", *Phil. Mag.*, **26**, pp. 217–30, August, 1888.
2. O. J. Lodge and J. L. Howard, "On electric radiation and its concentration by lenses", *Phil. Mag.*, **28**, pp. 48–65, July, 1889.
3. J. J. Thomson, "Recent Researches in Electricity and Magnetism", Sect. 300. (Oxford, 1893).
4. Lord Rayleigh, "On the passage of electric waves through tubes, the vibrations of dielectric cylinders," *Phil. Mag.*, **43**, No. 261, pp. 125–32, 1897.
5. A. Sommerfeld, "Über die fortpflanzung elektrodynamischer Wellen langs eines Drahten", *Ann. Phys.*, **67**, No. 2, pp. 233–90, 1899.
6. D. Hondros and P. Debye, "Elektromagnetische Wellen an dielektrischen Drahten", *Ann. Phys.*, **32**, No. 8, pp. 465–76, 1910.
7. W. L. Barrow, "Transmission of electromagnetic waves in hollow tubes of metal", *Proc. Inst. Radio Engrs*, No. 10, pp. 1298–1328, 1936.
8. G. C. Southworth, "Hyperfrequency waveguides—general consideration and experimental results", *Bell. Syst. Tech. J.*, **15**, No. 2, pp. 284–309, 1936.
9. J. R. Carson, S. P. Mead and S. A. Schelkunoff, "Hyperfrequency waveguides—mathematical theory", *Bell. Syst. Tech. J.*, **15**, No. 2, pp. 310–33, 1936.
10. L. J. Chu and W. L. Barrow, "Electromagnetic waves in hollow metal tubes of rectangular cross-section", *Proc. I.R.E.*, **26**, No. 12, pp. 1520–55, 1938.
11. F. E. Borgnis and C. H. Papas, "Electromagnetic waveguides and resonators," "Handbuch der Physik", Vol. 16, pp. 285–422, Edited by S. Flugge, (Springer Verlag, Berlin, 1958).
12. F. Harms, "Elektromagnetische Wellen an einem Draht mit isolierender zylindrischer Hülle", *Ann. Phys.*, **23**, No. 6, pp. 44–60, 1907.
13. L. Pincherle, "Electromagnetic waves in metal tubes filled longitudinally with two dielectrics", *Phys. Rev.*, **66**, No. 5 and 6, pp. 118–30, 1944.
14. S. Frankel, "TM mode in circular waveguides with two coaxial dielectrics", *J. Appl. Phys.*, **18**, No. 7, pp. 650–5, 1947.
15. A. M. Woodward, "Transmission in waveguides cross-section partly of solid dielectric", *Wireless Engineer*, **24**, No. 286, pp. 192–6, 1947.
16. G. G. Bruck and E. R. Wicher, "Slow transverse magnetic waves in cylindrical guides", *J. Appl. Phys.*, **18**, No. 8, pp. 766–9, 1947.
17. R. D. Teasdale and T. J. Higgins, "Electromagnetic waves in circular waveguides containing two coaxial media," *Proc. Natl Electronics Conf.*, **5**, pp. 427–41, 1949.
18. A. Banos, D. S. Saxon and H. Gruen, "Propagation characteristics in a coaxial structure with two dielectrics", *J. Appl. Phys.*, **22**, No. 2, pp. 117–23, 1951.
19. J. V. Bladel and T. J. Higgins, "Cut-off frequency in two dielectric layered rectangular waveguides", *J. Appl. Phys.*, **22**, No. 3, pp. 329–34, 1951.
20. R. D. Teasdale and G. N. Crawford, "Cut-off frequency for circular waveguides containing two coaxial dielectrics", *Proc. N.E.C.*, **8**, pp. 296–300, 1952.
21. R. E. Beam and D. A. Dobson, "Duo-dielectric coaxial waveguide", *Proc. N.E.C.*, **8**, pp. 301–12, 1952.
22. Ll. G. Chambers, "Compilation of propagation constants of an inhomogeneously filled waveguide," *Brit. J. Appl. Phys.*, **3**, pp. 19–21, 1952.
23. R. B. Adler, "Waves on inhomogeneous cylindrical structures," *Proc. I.R.E.*, **40**, No. 3, pp. 339–48, 1952.
24. S. K. Chatterjee, "Propagation of microwaves through a cylindrical metallic guide filled coaxially with two different dielectrics, Part I", *J. Indian Inst. Sci.*, **35**, No. 1, pp. 1–16, 1953.
25. S. K. Chatterjee, "Propagation of microwaves through a cylindrical metallic guide, filled coaxially with two different dielectrics, Part II", *J. Indian Inst. Sci.*, **35**, No. 3, pp. 103–17, 1953.
26. S. K. Chatterjee, "Propagation of microwaves through cylindrical metallic guide filled coaxially with two different dielectrics, Part III", *J. Indian Inst. Sci.*, **35**, No. 4, pp. 149–69, 1953.
27. J. A. Kostriza, "Composite dielectric coaxial line", *Electrical Communication*, **30**, No. 2, pp. 155–64, 1953.
28. F. J. Tischer, "Microwellenleitung mit geringen Verlusten", *Arch. Elekt. Übertragung.*, **7**, pp. 592–6, 1953.
29. S. K. Chatterjee, "Propagation of microwaves through a cylindrical metallic guide filled coaxially with two different dielectrics, Part IV," *J. Indian Inst. Sci.*, **36**, No. 1, pp. 1–13, 1954.

30. S. K. Chatterjee "Propagation of microwaves through a cylindrical metallic guide filled coaxially with two different dielectrics, Part V", *J. Indian Inst. Sci.*, **36**, No. 2, pp. 48–58, 1954.

31. Ll. G. Chambers, "An approximate method for the calculation of propagation constants for inhomogeneously filled waveguides", *Quart. J. Mech. Appl. Maths.*, **7**, pt. 3, pp. 299–316, 1954.

32. A. E. Karbowiak, "Theory of composite guides: stratified guides for surface waves", *Proc. Instn Elect. Engrs*, **101**, Part III, pp. 238–42, 1954.

33. S. K. Chatterjee, "Some investigations at microwave frequencies", *J. Inst. Telecomm. Engrs*, **2**, No. 2, pp. 67–86, 1956.

34. R. A. Moore and R. E. Beam, "A duo-dielectric parallel-plane waveguide", *Proc. N.E.C.*, **12**, pp. 689–705, 1956.

35. F. J. Tischer, "The H-guide, a waveguide for microwaves", *I.R.E. Conv. Rec.*, pt. 5, pp. 44–7, 1956.

36. C. M. Angulo, "Discontinuities in a rectangular waveguide partially filled with dielectric", *Trans. I.R.E.*, **MTT-5**, No. 1, pp. 68–74, 1957.

37. F. J. Tischer, "Properties of the H-guide at microwaves and millimeter waves", *Wescon Conv. Rec.*, Part 1, pp. 4–12, 1958.

38. Ll. G. Chambers, "The propagation of constant longitudinal magnetic waves in dielectric filled waveguides", *Quart. J. Mech. Appl. Maths*, **11**, Pt. 2, pp. 244–52, 1958.

39. M. Cohn, "Parallel plane waveguide partially filled with a dielectric", *Proc. I.R.E.*, **46**, No. 12, pp. 1952–3, 1958.

40. P. H. Vartanian, N. P. Ayres and A. L. Helgesson, "Propagation in dielectric slab loaded rectangular waveguide", *Trans. I.R.E.*, **MTT-6**, No. 1, pp. 215–22, 1958.

41. M. Cohn, "Propagation in a dielectric loaded parallel plane waveguide", *Trans. I.R.E.*, **MTT-7**, No. 2, pp. 202–8, 1959.

42. M. Cohn, "Attenuation of the HE mode in the H-guide", *Trans. I.R.E.*, **MTT-7**, No. 4, pp. 478–80, 1959.

43. J. H. Collins and P. Daly, "Calculations for guided electromagnetic waves using finite-difference methods", *J. Electronics Control.*, **14**, No. 4, pp. 361–80, 1963.

44. S. P. Morgan, "Theory of curved circular waveguide containing an inhomogeneous dielectric", *Bell. Syst. Tech. J.*, **36**, pp. 1209–51, 1957.

45. H. G. Unger, "Circular electric wave transmission in a dielectric coated waveguide", *Bell. Syst. Tech. J.*, **36**, pp. 1253–78, 1957.

46. H. M. Wachouski and R. E. Beam, "Shielded dielectric rod waveguides", Final Report on investigations of multimode propagation in waveguides and microwave optics, Microwave Laboratory, North Western University, U.S.A., 1950.

47. A. N. Didenko and L. N. Bezmaternykh, "Contribution to the design of rectangular waveguides loaded with dielectric diaphragms", *Radio Engineering and Electronic Physics*, No. 10, pp. 1491–7, 1961.

48. V. V. Nikolskiy and V. G. Sukhov, "On the Ritz method for hollow systems with an isotropic media", *Radio Engineering and Electronic Physics*, No. 10, pp. 1497–1504, 1961.

49. J. P. Kotik, "Propagation of H modes in annular waveguide with dielectric sheath and metal braid", *Radio Engineering and Electronic Physics*, No. 12, pp. 1796–1802, 1961.

50. E. M. Guttsayt, "Types of waves in an H-junction metal dielectric waveguide", *Radio Engineering and Electronic Physics*, No. 2, pp. 288–97, 1962.

51. V. I. Bespalov and M. A. Miller, "Electromagnetic waves in rectangular channels with a dielectric", *Trudy Gor'kovsk Univ.* (*Radio Fizika*), **30**, p. 61, 1956.

52. L. N. Bezmaternykh, "Some electrodynamic characteristics of a rectangular waveguide loaded by dielectric diaphragms", *Radio Engineering and Electronic Physics*, No. 6, pp. 934–9, 1962.

53. W. Janssen, "Bestimmung Nodenun Wandlunn in rund Hohlleiter mit unregelmässigem dielektrischeg Belag", *Arch. Elekt. Übertragung* **15**, pp. 525–36, 1961.

54. Ll. G. Chambers, "Propagation in waveguides filled longitudinally with two or more dielectrics", *Brit. J. Appl. Phys.*, **4**, No. 2, pp. 39–45, 1953.

55. H. Bucholz, "Der Hohlleiter von kreisformigen Querschnitt mit geschnitenem dielektrischen Einsatz", *Ann. Phys.*, **43**, No. 5, pp. 313–68, 1943.

56. S. K. Chatterjee, "Propagation of microwaves through an imperfectly conducting cylindrical guide filled with an imperfect dielectric", *J. Indian Inst. Sci.*, **37**, No. 1, pp. 1–9, 1955.

57. A. E. Karbowiak, "Theory of imperfect waveguides—the effect of wall impedance", *Proc. I.E.E.*, **102B**, pp. 698–708, 1955.

58. V. M. Papadopoulos, "Propagation of electromagnetic waves in cylindrical waveguides with imperfectly conducting walls", *Quart. J. Mech. Appl. Maths*, **7**, pt. 3, pp. 326–34, 1954.

59. B. Z. Katsenelenbaum, "The effect of a dielectric film on the attenuation of H waves in a straight nearly circular waveguide", *Radiotekhnika i Elektronika*, **3**, pp. 38–45, 1958.

60. H. G. Unger, "Random imperfections in waveguides", *Arch. Elekt. Übertragung* **15**, No. 9, pp. 393–401, 1961.

61. H. L. Kreife and H. G. Unger, "Imperfections in lined waveguide", *Bell Syst. Tech. J.*, **41**, No. 5, pp. 1589–1619, 1962.

62. H. Unger, "Round waveguide with lossy lining", Proc. Symposium on Millimeter Waves, New York, 1959.

63. J. K. Sinha and J. Brown, "A new cavity resonator method for measuring permittivity" (Appendix), *Proc. I.E.E.*, **107B**, pp. 522–30, 1960.

64. P. N. Robson, "A variational integral for propagation coefficient of a cylindrical waveguide with imperfectly conducting walls", *Proc. I.R.E.E.*, **110**, No. 5, pp. 859–64, 1963.

65. H. E. Rowe and W. D. Warters, "Transmission in multimode waveguide with random imperfections", *Bell. Syst. Tech. J.*, **41**, pp. 1031–70, 1962.

66. V. V. Malin, "The influence of a semiconductor film on the attenuation in a waveguide of circular cross-section", *Radiotekhnika i Elektronika*, **1**, p. 34, 1956.

67. V. V. Shevchenko, "A waveguide with wall impedance as a surface compensator", *Radio Engineering and Electronic Physics*, No. 7, pp. 1034–9, 1962.

68. R. A. Waldron, "Electromagnetic wave propagation in cylindrical waveguides containing gyromagnetic media—Part 1", *J. Brit.I.R.E.*, **18**, No. 9, pp. 597–612, 1958.

69. R. A. Waldron, "Electromagnetic wave propagation in cylindrical waveguides containing gyromagnetic media—Part 2", *J. Brit.I.R.E.*, **18**, No. 10, pp. 677–90, 1958.

70. R. A. Waldron, "Electromagnetic wave propagation in cylindrical waveguides containing gyromagnetic media—Part 3", *J. Brit.I.R.E.*, **18**, No. 11, pp. 733–46, 1958.

71. P. J. B. Clarricoats and R. A. Waldron, "Nonperiodic slow and backward wave structures", *J. Electronics and Control*, **8**, pp. 455–8, 1960.

72. P. J. B. Clarricoats, "Backward waves in waveguide containing dielectric", *Proc. I.E.E.*, **108**, Pt. C, pp. 496–501, 1961.

73. P. J. B. Clarricoats, "Circular waveguide backward wave structure", *Proc. I.E.E.*, **110**, No. 2, pp. 261–70, 1963.

74. J. Brown, "Backward waves in homogeneous waveguide", *J. Instn Telecomm. Engrs*, **9**, No. 2, pp. 140–51, 1963.

75. R. A. Waldron, "Properties of inhomogeneous cylindrical waveguides in the neighbourhood of cut-off", *J. Brit.I.R.E.*, **25**, No. 6, pp. 547–55, 1963.

76. K. J. Button, "Theory of non-reciprocal ferrite phase-shifters in dielectric loaded coaxial line", *J. Appl. Phys.*, **29**, pp. 998–1000, 1958.

77. B. J. Duncan, L. Swern and K. Tomiyasu, "Microwave magnetic fields in dielectric-loaded coaxial line", *Proc. I.R.E.*, **46**, pp. 500–2, 1958.

78. B. C. De Loach, "Radial line coaxial filters in the microwave region", *Trans. I.R.E.*, **MTT-11**, pp. 50–55, 1963.

79. D. J. Angelakos, "A coaxial line filled with two non-concentric dielectrics", *Trans. I.R.E.* **MTT-2**, pp. 39–44, 1954.

80. B. J. Duncan, L. Swern, K. Tomiyasu and J. Hannwackers, "Design considerations for broad-band ferrite coaxial line isolators", *Proc. I.R.E.*, **45**, pp. 483–90, 1957.

81. R. A. Waldron, "The theory of waveguides and cavities, Parts 1 and 2", *Electronic Technology*, **38**, Nos 3 and 4, pp. 98–104, 140–7, 1961.

82. S. K. Chatterjee and (Mrs) R. Chatterjee, "Impedance of a cylindrical waveguide with dielectric", *J. Indian Inst. Sci.*, Golden Jubilee Research Volume, pp. 398–410, 1959.

83. S. K. Chatterjee and (Mrs) R. Chatterjee, "Impedance of a composite waveguide, Pt. 1", *J. Instn Engrs (India)*, **62**, No. 1, Pt. ET-1, pp. 6–14, 1961.

84. S. K. Chatterjee and (Mrs.) R. Chatterjee, "Impedance of a composite waveguide, Pt. 2", *J. Instn Engrs (India)*, **62**, No. 1, Pt. ET-1, pp. 14–20, 1961.

85. R. A. Waldron, "Features of cylindrical waveguides containing gyromagnetic media", *J. Brit.I.R.E.*, **20**, No. 9, pp. 695–706, 1960.

86. F. E. Goodwin and G. E. Moss, "Broad band impedance matching into dielectric-filled waveguides", *Trans. I.R.E.*, **MTT-11**, pp. 36–39, 1963.

87. J. A. Stratton, "Electromagnetic Theory", (Mcgraw-Hill, New York, 1941).

88. A. Nisbet, "Hertzian electromagnetic potentials and associated gauge transformation", *Proc. Roy. Soc.*, A, **231**, No. 1185, pp. 250–63, 1955.

89. A. E. Karbowiak, "Some comments on the classification of waveguide modes", *Proc. I.E.E.*, **107B**, pp. 85–93, 1960.

90. E. Ledinegg, "Uber die allgemeinste Lösung der Maxwellschen Gleichungen", *Ann. Phys.* (v), **41**, pp. 537–66, 1942.

91. Parry Moon and D. E. Spencer, "Field Theory Handbook" (Springer Verlag, Berlin, 1961).

92. R. A. Waldron, "A helical coordinate system and its applications in electromagnetic theory", *Quart. J. Mech. Appl. Maths*, **11**, pp. 438–61, 1958.

93. H. R. L. Lamont, "Waveguides", (Methuen, London, 1947).

94. J. V. Bladel, "Field expandability in normal modes for a multilayered rectangular or circular waveguide", *J. Franklin Inst.*, **253**, No. 4, pp. 313–21, 1952.

95. R. F. Harrington, "Time Varying Electromagnetic Fields", (McGraw-Hill, New York, 1961).

96. A. D. Bresler and N. Marcuvitz, "Operator Methods in Electromagnetic Theory" Part I, Polytech. Inst. Brooklyn Res. Rep., R-495-56, May 1956; Part II, Polytech. Inst. Brooklyn Res. Rep. R.565–57, March 1957.

96a. A. D. Bresler, G. H. Joshi and N. Marcuvitz, "Orthogonality properties for modes in passive and active uniform waveguides", *J. Appl. Phys.*, **29**, No. 5, pp. 794–9, 1958.

97. N. Marcuvitz, "Waveguide Handbook", Radiation Lab. Series, Vol. 10, (McGraw-Hill, New York, 1951).

98. C. G. Montgomery, "Principles of Microwave Circuits", Radiation Lab. Series, Vol. 8, (McGraw-Hill, New York, 1948); N. H. Frank, R. L. Report, No. T-9, 1942.

99. J. Schwinger, "Discontinuities in waveguides" M.I.T. Notes on Lectures. Unpublished, edited by D. S. Saxon, 1940–45.

100. P. M. Morse and H. Fesbach, "Methods of Theoretical Physics", Pt. II, Chapter 9, (McGraw-Hill, New York, 1953).

101. H. Fesbach and A. M. Clogston, "Perturbations of boundary conditions", *Phys. Rev.*, **59**, pp. 189–94, 1941.

102. H. Fesbach, "On the perturbation of boundary conditions", *Phys. Rev.*, **65**, pp. 307–18, 1944.

103. E. C. Titchmarsh, "Eigenfunction Expansions Associated with Second Order Differential Equations", Pt. II, (Clarendon Press, Oxford, 1958).

104. H. A. Bethe and J. Schwinger, "Perturbation Theory for Cavities", N.D.R.C. Rep., DI-117, 4th March, 1943.

105. A. Cunliffe and L. E. S. Mathias, "Some perturbation effects in cavity resonators", *J. I.E.E.*, **97**, Pt. III, pp. 367–76, 1950.

106. S. K. Chatterjee, "Microwave cavity resonators—some perturbation effects and their applications", *J. Brit.I.R.E.* **13**, No. 10, pp. 475–84, 1953.

107. R. A. Waldron, "Perturbation theory of resonant cavities", *Proc. I.E.E.*, **107C**, pp. 272–4, 1960.

108. Y. Hayashi, "Perturbation theory of electromagnetic fields in anisotropic inhomogeneous media", *Proc. Japanese Acad.*, **36**, No. 9, pp. 547–9, 1960.

109. C. Lanczos, "The Variational Principle of Mechanics", (University of Toronto Press, 1957).

110. S. H. Gould, "Variational Methods for Eigenvalue Problems", (University of Toronto Press, 1957).

111. C. Fox, "An Introduction to the Calculus of Variations", (Oxford University Press, 1950).

112. F. B. Hildebrand, "Methods of Applied Mathematics", (Prentice-Hall, New York, 1954).

113. E. L. Ince, "Ordinary Differential Equations", Chapter XI, (Dover, New York, 1944).

114. V. H. Rumsey, "Reaction concept in electromagnetic theory", *Phys. Rev.*, **94**, No. 6, pp. 1483–91, 1954.

115. G. H. Shortley and R. Weller, "The numerical solution of Laplace's equation", *J. Appl. Phys.*, **9**, pp. 334–48, 1938.

116. G. E. Forsythe, "Difference methods on a digital computer for Laplacian boundary value and eigenvalue problems", *Commun. Pure Appl. Math.*, **9**, pp. 425–34, 1956.

117. G. E. Forsythe and W. R. Wasow, "Finite Difference Methods for Partial Differential Equations", (Wiley, New York, 1959).

118. M. Cohn, "Parallel Plane Waveguide Partially Filled with a Dielectric", The Johns Hopkins University Radiation Lab., Baltimore, Md., Tech. Rep. No. AF.56, Nov. 1958.

119. A. D. Berk, "Variational principle for electromagnetic resonators and waveguides", *Trans. I.R.E.*, **AP-4**, No. 2, pp. 104–11, 1956.

120. R. E. Collin and R. M. Vaillancourt, "Application of Rayleigh-Ritz method to dielectric steps in waveguides", *Trans. I.R.E.*, **MTT-5**, No. 3, pp. 177–84, 1957.

121. N. Marcuvitz, "Field representation in spherically stratified region", New York University Res. Rep. No. En.-29, 1951.

122. R. E. Collin and J. Brown, "The calculation of the equivalent circuit of an axially unsymmetrical waveguide junction", *Proc. I.E.E.*, **103C**, pp. 121–8, 1956.

123. W. R. Smyth, "Static and Dynamic Electricity", pp. 67–8, (McGraw-Hill, New York, 1950).

124. P. J. B. Clarricoats, "Propagation along unbounded and bounded dielectric rods, Part 1", *Proc. I.E.E.*, **108**, Pt. C, No. 13, pp. 170–6, 1961.

125. P. J. B. Clarricoats, "Propagation along unbounded and bounded dielectric rods, Part 2", *Proc. I.E.E.*, **108**, Pt. C, pp. 177–86, 1961.

126. E. F. F. Gillespie, "Power flow and negative wave impedance in the dielectric rod waveguide", *Proc. I.E.E.*, **107**, Pt. C, pp. 198–201, 1960.

127. P. J. B. Clarricoats and D. E. Chambers, "Backward wave propagation on non-periodic waveguide structures", Proc. U.R.S.I. Symposium on Electromagnetic Theory and Antennas, Copenhagen, June, 1962.

128. J. Thelen, "Über das Backward wave-band im metallischen Hohlleiter der mit längsmagnetisierten Plasma gefüllt ist", *Zeitschrift für Angewandte Physik*, **13**, pp. 268–75, 1961.

128a. A. W. Trivelpiece and R. W. Gould, "Space charge waves in cylindrical plasma columns", *J. Appl. Phys.*, **30**, pp. 1784–93, 1959.

128b. A. W. Trivelpiece, A. Ignatius and P. C. Holscher, "Backward waves in longitudinally magnetised ferrite rods", *J. Appl. Phys.*, **32**, pp. 259–67, 1961.

128c. G. H. B. Thompson, "Propagation in ferrite filled circular waveguides", *Proc. I.E.E.*, **109B**, Supplement No. 21, pp. 81–9, 1962; "Backward waves in ferrites", Proc. U.R.S.I., Symposium on Electromagnetic Theory and Antennas, Copenhagen, June, 1962.

128d. P. J. B. Clarricoats and D. E. Chambers, "Some properties of ferrite filled circular waveguides", *Proc. I.E.E.*, **109B**, Supplement No. 21, pp. 71–4, 1962.

129. R. A. Waldron, "Properties of ferrite loaded cylindrical waveguide in the neighbourhood of cut-off", *Proc. I.E.E.* **109B**, pp. 90–4, Jan. 1962.

130. D. Fleri and G. Hanley, "Non-reciprocity of dielectric loaded TEM mode transmission lines", *Trans. I.R.E.*, **MTT-7**, pp. 23–7, 1959.

131. M. Sucher and H. J. Carlin, "Coaxial line non-reciprocal phase shifters", *J. Appl. Phys.*, **28**, pp. 921–2, 1957.

132. D. J. Sullivan and D. A. Parker, "Stepped transformers for partially filled transmission lines", *Trans. I.R.E.*, **MTT-8**, pp. 212–7, 1960.

133. F. R. Morganthaler and D. L. Fye, "Yttrium garnet u.h.f. isolator", *Proc. I.R.E.*, **45**, pp. 1551–2, 1957.

134. R. Mangiaracuia and B. J. Duncan, "Non-reciprocal ferrite devices in TEM mode transmission lines", Presented at the annual P.G. M.T.T. meeting, New York, May 9–10, 1957.

135. B. Lax, K. J. Button and L. M. Roth, "Ferrite phase shifters in rectangular waveguide", *J. Appl. Phys.*, **25**, pp. 1413–21, 1954.

136. M. L. Kales, N. H. Chait and N. G. Sakiotis, "A non-reciprocal microwave component", *J. Appl. Phys.*, **23**, pp. 816–7, 1953.

137. J. H. Rowen, "Ferrites in microwave applications", *Bell Syst. Tech. J.*, **32**, pp. 1333–69, 1953.

138. A. G. Fox, S. E. Miller and M. T. Weiss, "Behaviour and application of ferrites in the microwave region", *Bell Syst. Tech. J.*, **34**, pp. 5–103, 1955.

139. H. Seidel, "Ferrite slabs in transverse electric mode waveguide", *J. Appl. Phys.*, **28**, pp. 218–26, 1957.

140. R. E. Beam, M. M. Astrahan, W. C. Jakes, H. G. Wachowski and W. L. Firestone, "Dielectric tube waveguides", Final Rep. U.S. Army contract, No. W36–39, Sc 38240, Microwave Lab. Northwestern Univ., Evanston, Illinois, Nov. 30, 1950.

141. R. E. Collin, "Field Theory of Guided Waves", Chapter 5, (McGraw-Hill, New York, 1960).

142. W. S. Burnside and A. W. Panton, "Theory of Equations", (Longmans, Green, London, 1924).

143. K. Kurokawa, "Electromagnetic waves in waveguides with wall impedance", *Trans. I.R.E.*, **MTT-10**, pp. 314–20, 1962.

144. K. Kurokawa, "The effect of wall losses on the propagation constant of waveguides", *J. Elect. Commun. Engrs, Japan*, **39**, pp. 794–800, 1956.

145. J. C. Slater, "Microwave Electronics", p. 49 (Van Nostrand, New York, N.Y., 1950).

146. A. Lavik and H. G. Unger, "Ruckwärtswellen in homogenen Wellenleitern", *Arch. Elekt. Übertragung*, **18**, Pt. 1, pp. 35–42, 1964.

147. A. Lavik and H. G. Unger, "Der Rechteckhohlleiter mit rechteckgem Stoffeinsatz" *Arch. Elekt. Ubertragung*, **18**, Pt. 1, pp. 25–34, 1964.

148. H. Suhl and L. R. Walker, "Topics in guided wave propagation through gyromagnetic media, Part III", *Bell Syst. Tech. J.*, **33**, pp. 1133–94, 1954.

149. G. G. Macfarlane, "Quasi-stationary field theory and its application to diaphragms and junctions in transmission lines and waveguides", *J.I.E.E.*, **93**, Pt. III, pp. 703–19, 1946.

150. J. W. Miles, "The equivalent circuit for a plane discontinuity in a cylindrical guide", *Proc. I.R.E.*, **34**, pp. 728–42, 1946.

151. N. Marcuvitz and J. Schwinger, "On the representation of the electric and magnetic fields produced by currents and discontinuities in waveguides", *J. Appl. Phys.*, **22**, pp. 806–19, 1951

152. P. Debye, "Polar Molecules", (Dover, New York, 1945).

153. H. Frohlich, "Shape of collision broadened spectral lines", *Nature*, **157**, No. 3989, p. 478, 1946.

154. J. H. Van Vleck and V. F. Weisskopf, "On the shape of collision broadened lines", *Rev. Mod. Phys.*, **17**, No. 2–3, pp. 227–36, 1945.

155. S. A. Schelkunoff, "The impedance concept and its application to problems of reflection, refraction, shielding and power absorption", *Bell Syst. Tech. J.*, **17**, pp. 17–48, 1938.

156. H. G. Booker, "The elements of wave propation using the impedance concept", *J.I.E.E.*, **94**, Part III, pp. 171–202, 1947.

157. Huang Hung-chia and Ch'ien Ching-jen, "The concept of impedance perturbation as applied to imperfect waveguides", *Scientia Sinica*, **12**, No. 9, pp. 1285–309, 1963.

158. Huang Hung-Chia, "General theory of non-conventional waveguides for long distance transmission", *Scientia Sinica*, **11**, No. 6, pp. 761–84, 1962.

159. A. E. Karbowiak, "The concept of heterogeneous surface impedance and its application to cylindrical cavity resonators", *Proc. I.E.E.*, **105**, Pt. C, No. 7, pp. 1–12, 1958.

160. R. A. Waldron, "Theory of helical waveguide of rectangular cross-section", *J. Brit.I.R.E.*, **17**, No. 10, pp. 577–92, 1957.

161. R. A. Waldron, "Ferrites: An Introduction for Microwave Engineers" (Van Nostrand, New York and London, 1961).

162. P. J. B. Clarricoats, "Microwave Ferrites" (Chapman & Hall, London, 1961).

163. R. A. Waldron, "Properties of inhomogeneous cylindrical waveguides in the neighbourhood of cut-off", *The Radio and Electronic Engineer*, **25**, No. 6, pp. 547–55, 1963.

164. R. A. Waldron, "Theory and potential applications of backward waves in non-periodic inhomogeneous waveguides", *Proc. I.E.E.*, **111**, No. 10, pp. 1659–67, 1964.

165. A. Lavik and H. G. Unger, "Rückwartswellen in homogenen Wellenleitern", *Arch. Elekt. Übertragung*, **18**, p. 35, 1964.

21. Appendix 1

Brief Review of the Theory of Dielectrics

When an alternating electric field **E** of angular frequency ω is applied to a dielectric, polarization vector **P** will depend on ω and be out of phase with **E**. This phase difference δ, given by the relation $\delta = \arctan(\varepsilon''/\varepsilon')$ and called the loss angle of the dielectric, gives rise to heat dissipation in the dielectric which is proportional to ω and $\tan\delta$. The frequency dependence of **P** and polarizability α lead to the frequency dependence of the complex dielectric constant $k_e^* = \varepsilon'/\varepsilon_0 - j\varepsilon''/\varepsilon_0$. The polarizability α depends on ω in two ways. When ω approaches the natural frequency of rotation of the molecule ω_0, anomalous dispersion occurs. But generally ω_0 lies in the infrared region, though in some cases its influence may reach into the centimetre wave region. It may therefore seem that α is frequency independent when ω lies in the microwave range. But the rotation of the electric moment is frequency dependent. Assuming that the rotation of the permanent dipoles is hindered by a viscous force and that the dipoles have a single resonant angular frequency ω_0 related to the relaxation time τ as $\omega_0 = 1/\tau$ and on the basis of the Clausius-Mosotti internal field, Debye[152] arrived at the frequency dependence of the real and the imaginary parts ε' and ε'' of the permittivity ε and hence of k_e^* as follows

$$\varepsilon' = \varepsilon_\infty + \frac{\varepsilon_s - \varepsilon_\infty}{1+\omega^2\tau^2} \qquad \text{.....(324)}$$

$$\varepsilon'' \simeq \frac{(\varepsilon_s - \varepsilon_\infty)\omega\tau}{1+\omega^2\tau^2} \qquad \text{.....(325)}$$

The above theory neglects the interaction forces between dipoles. The relations (324) and (325) hold good in the case of gases, dilute solutions of polar substances and cubic crystals but fail in the case of solids. Debye[152] extended his theory on the basis of rotating dipoles possessing a distribution $f(\tau)$ of relaxation time and obtained

$$\varepsilon' \propto \int \frac{f(\tau)}{1+\omega^2\tau^2}\,d\tau \qquad \text{.....(326)}$$

$$\varepsilon'' \propto \int \frac{\omega(\tau)f(\tau)}{1+\omega^2\tau^2}\,d\tau \qquad \text{.....(327)}$$

In solids there is usually a discrete number of equilibrium directions for a dipole so that the transition from one direction to another is discontinuous. When a dielectric is placed in an alternating electric field, the oscillation of the dipoles of angular frequency ω_0 gives rise to a loss as given by the relation

$$\tan\delta = \frac{(\varepsilon_s - \varepsilon_\infty)\omega\tau}{(\varepsilon_s + \varepsilon_\infty\omega^2\tau^2)} \qquad \text{.....(328)}$$

This is not of the Debye type but arises due to the width of the resonance absorption when $\omega \to \omega_0$. In this case the loss angle δ as derived by Frohlich[153] is

$$\tan\delta = \frac{\Delta\varepsilon'}{2\varepsilon_s}\left\{\frac{\omega\tau}{1+(\omega+\omega_0)^2\tau^2} + \frac{\omega\tau}{1+(\omega-\omega_0)^2\tau^2}\right\} \qquad (329)$$

provided $\Delta\varepsilon'$, the contribution of the oscillating dipoles to ε_s, is very small so that $\Delta\varepsilon' < \varepsilon_s$. The relation (329) which was also derived independently by Van Vleck and Weisskopf[154] becomes identical with the corresponding Debye relation if $\omega \gg \omega_0$. So a solid is expected to have two maxima for $\tan\delta$, one a long-wave one which is of the Debye type and is connected with the transition of dipoles between the equilibrium directions, and the other a short-wave maximum of the Frohlich type.

The same information about the loss in a dielectric may also be conveyed by other parameters such as the index of absorption $\kappa = \alpha/\beta$ which enables the propagation constant $\gamma = \alpha + j\beta$ of the wave to be expressed in terms of the complex index of refraction n^* as

$$\gamma = j\frac{2\pi}{\lambda_0}n(1-j\kappa) = j\frac{2\pi}{\lambda_0}n^* \qquad \text{.....(330)}$$

The other important parameter is the intrinsic

impedance $Z_0 = (\mu/\varepsilon)^{\frac{1}{2}}$ which when expressed as $Z_0 = |Z_0| \exp(j\zeta)$ gives the phase relation between **E** and **H** vectors, where the phase factor ζ is given by the relation

$$\tan 2\zeta = \frac{\varepsilon''\mu' - \varepsilon'\mu''}{\varepsilon'\mu' + \varepsilon''\mu''} \qquad \text{.....(331)}$$

If the magnetic loss is negligible ($\mu'' = 0$), the above equation reduces to

$$\tan 2\zeta = \tan\delta = \frac{2\kappa}{1-\kappa^2} \qquad \text{.....(332)}$$

or

$$\zeta = \arctan\kappa$$

22. Appendix 2

Exact Expression for the Attenuation Constant

Assuming $\bar{\mu} \neq 1$, Clarricoats[125] formula for α is

$$\bar{\mu}''\left[(\bar{\varepsilon}+\bar{\Lambda}^2\bar{\beta}^2)T_1 + 2\bar{\Lambda}\bar{\varepsilon}\bar{\beta} + \left(\frac{\lambda_0}{2\pi}\right)^2\bar{\Lambda}^2k^4T_5\right] + \bar{\varepsilon}''\left\{[\bar{\beta}^2+(\bar{\Lambda}\bar{\mu})^2]T_1 + 2\bar{\Lambda}\bar{\mu}\bar{\beta} + \left(\frac{\lambda_0}{2\pi}\right)^2 k^4T_5\right\}$$

$$(\bar{\varepsilon}-\bar{\varepsilon}_1)\left\{\left(\frac{2\pi r_1}{\lambda_0}\right)^2(\bar{\varepsilon}\bar{\mu}-\bar{\beta}^2)^2 + [\bar{\beta}+\bar{\mu}\bar{\Lambda}\mathrm{F}(kr_1)]^2 + \frac{\varepsilon}{\varepsilon_1}[\bar{\beta}\mathrm{F}(kr_1)+\bar{\mu}\bar{\Lambda}]^2\right\} +$$

$$+(\bar{\mu}-\bar{\mu}_1)\left\{\bar{\Lambda}^2\left(\frac{2\pi r_1}{\lambda_0}\right)^2(\bar{\varepsilon}\bar{\mu}-\bar{\beta}^2)^2 + [\bar{\beta}\bar{\Lambda}+\bar{\varepsilon}\mathrm{F}(kr_1)]^2 + \frac{\mu}{\mu_1}[\bar{\varepsilon}+\bar{\beta}\bar{\Lambda}\mathrm{F}(kr_1)]^2\right\}$$

where $\mathrm{F}(x) = x\mathrm{J}_1'(x)/\mathrm{J}_1(x)$

The attenuation constant in terms of the magnetic and dielectric loss is expressed as

$$\alpha = \frac{2\pi}{\lambda_0}(\bar{\mu}''\mathrm{F}_M + \varepsilon''\mathrm{F}_D) \times 8{\cdot}686 \text{ dB per unit length}$$

Manuscript first received by the Institution on 16th January 1963, in revised form on 30th December 1963, and in final form on 17th December 1964. (Paper No. 1000/3.)

STANDARD FREQUENCY TRANSMISSIONS

(Communication from the National Physical Laboratory)

Deviations, in parts in 10^{10}, from nominal frequency for **November 1965**

November 1965	GBR 16 kc/s 24-hour mean centred on 0300 U.T.	MSF 60 kc/s 1430–1530 U.T.	Droitwich 200 kc/s 24-hour mean centred on 0300 U.T.	November 1965	GBR 16 kc/s 24-hour mean centred on 0300 U.T.	MSF 60 kc/s 1430–1530 U.T.	Droitwich 200 kc/s 24-hour mean centred on 3303 U.T.
1	—	− 151·0	—	16	− 150·6	− 149·2	+ 0·4
2	− 150 4	− 150·5	− 0 5	17	− 149·5	− 150·4	+ 1·0
3	—	− 149·7	+ 0·3	18	− 150·1	− 150·7	+ 0·5
4	—	− 150·4	+ 0·5	19	− 150·5	− 151 2	− 0·1
5	—	− 150·5	+ 0·5	20	− 151·0	− 150 5	− 0·4
6	− 150·4	− 150·1	+ 0·8	21	− 150·6	− 150·7	− 0·2
7	—	—	+ 0·1	22	− 150·3	− 150 4	0
8	− 150·9	− 151·4	− 0·6	23	− 150·0	− 150·0	+ 0·6
9	− 150·8	− 150 8	− 1·0	24	− 150·0	− 150 5	+ 0·2
10	− 151·5	− 151·2	− 1·5	25	− 150·4	− 151 3	− 1·8
11	− 150 0	− 150·0	− 1·5	26	− 150·4	− 151·2	− 3·9
12	− 149·6	− 149·9	− 1·4	27	− 150·2	− 151·1	+ 0·8
13	− 149·6	− 149·5	− 1·0	28	− 150·3	− 150·3	+ 0·6
14	− 148·7	− 147·8	− 0·3	29	− 150·5	− 150·4	+ 0·5
15	− 148·7	− 149·7	+ 0·4	30	− 150·2	− 150·3	+ 0·8

Nominal frequency corresponds to a value of 9 192 631 770 c/s for the caesium F,m (4,0)–F,m (3,0) transition at zero field.

Notes:—(1) *The Bureau International de l'Heure has announced that the fractional frequency offset to be adopted in 1966 is:—* $-300^{11}\ 10^{-10}$.

Accordingly the frequencies of all the MSF transmissions will be adjusted to the new value of offset at 0000 U.T. on the 1st January, 1966.

(2) *Following the recent increase in the stability of the Droitwich 200 kc/s transmission the accuracy of the daily calibration has now been increased to 1 part in 10^{11}. The result for each day is a mean value obtained by integrating the phase of the received carrier over a 24 hour period centred on 0300 U.T. The hour-to-hour variations in frequency do not usually exceed ±5 parts in 10^{11} relative to the 24 hour value.*

U.D.C.681.851

A Groove Feed and Depth Control System for Gramophone Disk Cutting Equipment

By

H. LINDSKOV HANSEN†

Presented at a meeting of the Electro-Acoustics Group in London on 19th May, 1965.

Summary: The efficiency of various groove control systems and the complexity of the equipment required are evaluated. Systems for monaural and sterophonic disks are described which derive the feed and groove depth at any point of the groove from the signal amplitudes within ±1 disk revolution.

1. Introduction

The ideal groove control system must maintain the distance from any turn of the groove to the following turn just large enough to provide sufficient space for the signal amplitudes and it must also keep the groove just wide enough to guide the play-back needle safely even at the narrowest points of the groove.

A control system allowing an amplitude peak from one groove turn to fill in the space left by the coinciding amplitude peaks of the preceeding turn would come quite close to this ideal. However, it is shown in Appendix 1 that it would be necessary to keep the turntable speed variations an order of magnitude smaller than the value specified even for the most advanced cutting lathes, if the location of an amplitude peak, relative to a coinciding one, is to be predicted with the necessary accuracy. It might be possible to overcome this difficulty, but the equipment necessary would be so complicated that its use would not be justified by the gain in efficiency.

A control system maintaining constant distance from the envelope curve of the amplitudes of one groove turn to the envelope curve of the coinciding amplitudes of the next turn can be realized with good approximation, but it requires rather complex equipment.[1] Consider the simple case shown in Fig. 1,

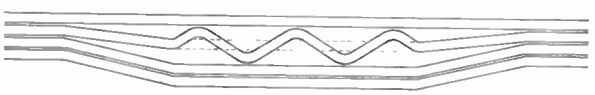

Fig. 1. Passage of lateral modulation. The feed is different in the intervals 'before', 'during' and 'after' the modulation.

where the modulation is constant over a fraction of a revolution following a revolution with an unmodulated groove. The groove spacing must first be increased by the signal amplitude above the value when cutting a uniform spiral of unmodulated groove during the small fraction of a revolution from change of feed to the first amplitude, then while the modulation is constant the feed must again be the same as for the unmodulated groove; when the last amplitude has been recorded the feed must be reduced bringing the groove distance back to that of the unmodulated groove. And this must be done during a small fraction of a revolution. Very big feed variations are necessary —the feed may even become negative and the variation is a rather complicated function of the amplitudes. Furthermore, similar changes of feed must take place during the next revolution to bring the groove around the modulated passage, and so on with all the following revolutions. This makes a synchronized 'memory' device necessary.

With the control system described in this paper, the feed at an interval of constant modulation, as shown in Fig. 2, is increased so far in advance that sufficient

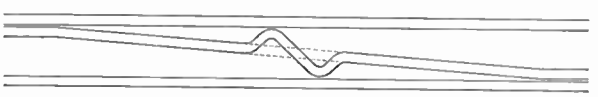

Fig. 2. Passage of lateral modulation. The feed in the interval 'during' the modulation is equal to the feed in the intervals 'before' and 'after' the modulation.

groove spacing is obtained, using the same feed as that necessary to give sufficient groove spacing if the modulation were kept constant for more than one revolution. This feed is maintained while the amplitudes are recorded and for so long after that the following groove turn will be cut at a safe distance without further change of the feed.[2]

The intervals of increased feed before and after a modulated passage will in no case be longer than one revolution. The increase of feed is thus proportional to the maximum amplitude present within ± 1 revolution. This can be achieved with relatively simple components and experience from equipment built on this principle has shown that the cases where better efficiency would be of advantage are very rare.

† Ortofon A/S, Copenhagen, Denmark.

2. Groove Control in Lateral Recording

The amplitudes of a laterally modulated groove are symmetrical about the axis of the groove, with good approximation. The increase in groove spacing necessary when the beginning of a long passage of constant modulation is recorded is therefore half that necessary at the following revolutions. The increased groove spacing at the increased modulation is the result of an increased constant feed of the cutter head applied over one revolution. To obtain half the increase in groove spacing at the same feed it must be applied for half a revolution. Consequently the feed must be increased in proportion to the increase of the amplitudes half a revolution before the first increased amplitude is to be recorded. Similarly, at the point where the amplitudes decrease, the distance to the next following turn can only be reduced by half of the total reduction. The feed can therefore not be reduced until half a revolution after the last of the larger amplitudes has been recorded.

Figure 3 shows schematically the recorded surface of a disk, transformed into an unfolded cylinder. The groove starts at the upper left corner and ends at the lower right corner. The black lines represent the narrowest permissible 'land' between two turns of the groove, the hatched stripes represent the groove width. The shaded areas represent the unutilized parts of the record. From A to P the amplitudes are a_1. At P they are increased to a_2 and at Q they are reduced to a_3. From A to E the feed, indicated by the slope of the hatched stripes, is $l+g+2a_1$, from E to L it is $l+g+2a_2$, and from L to M it is $l+g+2a_3$.

At P the groove distance to the point of the groove cut one revolution earlier is obtained by applying the feed $l+g+2a_1$, during the first half and the feed $l+g+2a_2$ during the second half of the revolution. This gives $l+g+a_1+a_2$, i.e. exactly the groove distance necessary at this point. At Q, the distance to the following turn must be $l+g+a_2+a_3$ and this distance is obtained by applying the feed $l+g+2a_2$ during the first half, and the feed $l+g+2a_3$ during the second half of the revolution following immediately after Q.

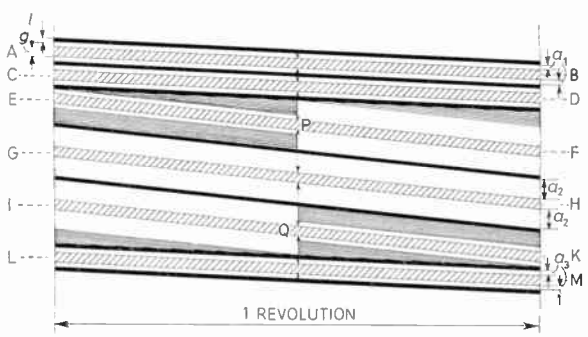

Fig. 3. 'Unfolded cylinder' groove diagram. Symmetrical amplitudes varying in magnitude.

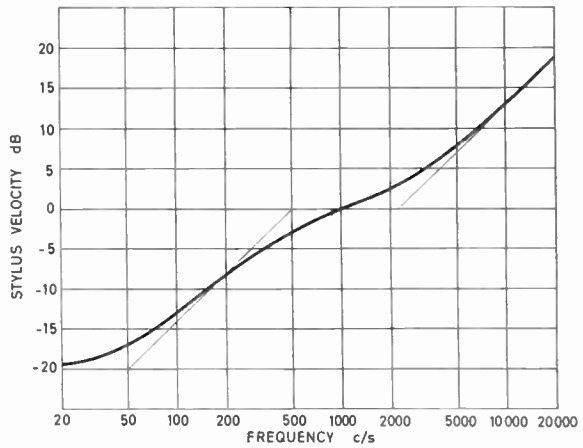

(a) Stylus velocity.

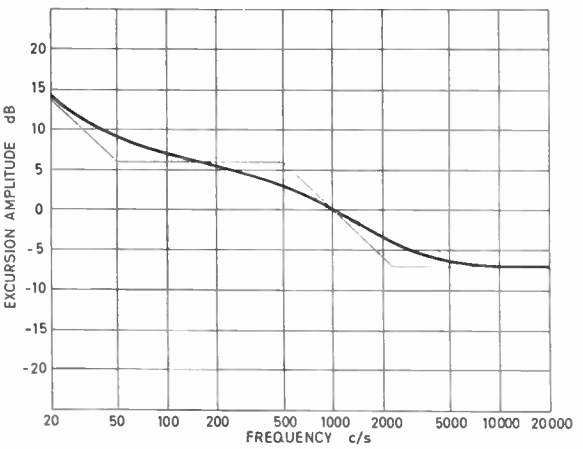

(b) Excursion amplitude.

Fig. 4. Recording characteristics.

In lateral recording l and g are independent of the modulation. Disregarding the time differences the feed equation for lateral recording is therefore

$$f = f_0 + 2a \qquad \text{.....(1)}$$

and the corresponding feed control voltage is

$$V_f = V_0 + V_a \qquad \text{.....(2)}$$

The amplitude-dependent voltage V_a must be derived and applied at a time corresponding to half a revolution before the corresponding amplitude is recorded. In practical disk cutting, the modulation is transferred from tape to disk, and V_a can therefore be derived from the output of a pre-play-back head reading the tape modulation at the appropriate distance in advance of the play-back head of the modulation channel.

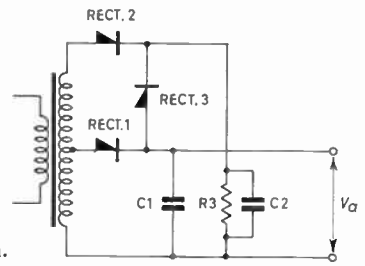

(a) Circuit diagram.

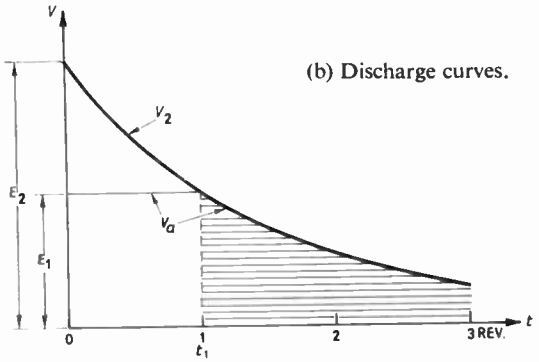

(b) Discharge curves.

Fig. 5. Timing circuit with delayed discharge.

The distance from the play-back head to the pre-play-back head will be:

$$d_p = \tfrac{1}{2}.60\,\frac{\text{tape velocity (cm/s)}}{\text{disk velocity (rev/min)}}\ \text{cm} \qquad .....(3)$$

As V_a must be proportional to the amplitudes recorded on the disk the output from the pre-play-back head must be equalized according to the excursion amplitude recording characteristic of the modulation channel. The disk recording characteristic normally gives the stylus velocity vs. frequency as in Fig. 4(a). Figure 4(b) shows the corresponding excursion amplitude characteristic.

The final step in the derivation of V_a is the rectification and the introduction of delay of the decay. When the input voltage to the rectifier and delay circuit is decreasing the output voltage must remain constant for a length of time corresponding to one disk revolution and then decrease rapidly to the value determined by the input voltage now present. A modified version of the time circuit with delayed discharge[3] meets these requirements.

The principle of this circuit is explained with reference to the circuit diagram (Fig. 5(a)) and the discharge curves (Fig. 5(b)). C_1 is charged via rectifier 1 to the voltage E_1, and C_2 is charged via rectifier 2 to E_2. Suppose that the input voltage disappears at $t = 0$, then the voltage across C_2 will decrease according to:

$$V_2 = E_2.\exp\left(-\frac{t}{RC}\right) \qquad .....(4)$$

while the voltage across C_1 (the output voltage V_a), will remain practically constant until $t = t_1$ where $V_2 = V_a$. Rectifier 3 will then become conductive and V_a will start decreasing according to

$$V_a = E_1 \exp\left[-\frac{t-t_1}{R(C_1+C_2)}\right] \qquad .....(5)$$

t_1 is a constant determined by the circuit elements. The required delay can thus be achieved but the subsequent decay of V_a is not very rapid. The ideal is that V_a should drop instantly to 0 at t_1. The shaded area on Fig. 5(b) represents a part of the available disk surface left unutilized because of the slow decay of V_a. (See Appendix 2.)

For this reason the original circuit was modified as shown in Fig. 6(a). V_a and V_2 are applied to the control grids of a differential amplifier stage which has the coil of a polarized relay connected from anode to anode. When the relay contact is closed, the resistor R_2 is connected in parallel to C_2. Using the potentiometer, the differential stage can be adjusted to open

(a) Circuit diagram.

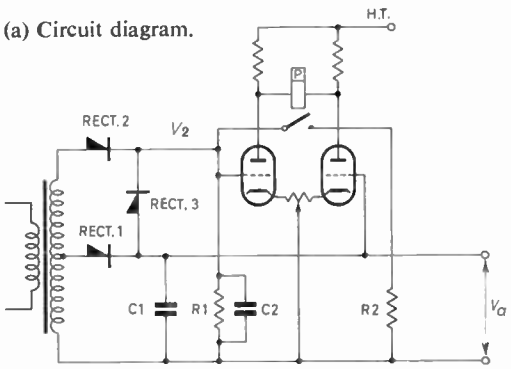

(b) Discharge curves.

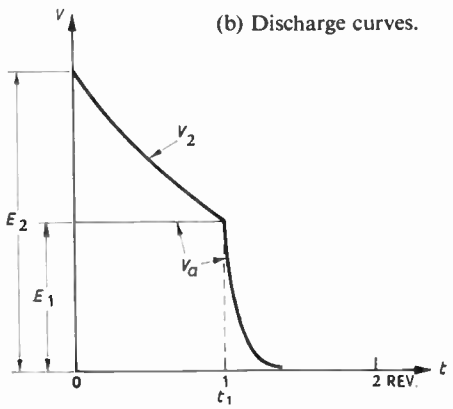

Fig. 6. Timing circuit with delayed rapid discharge.

the relay contact when $V_2 > V_a$ and close the relay contact when $V_2 \leqq V_a$. Figure 6(b) is a typical discharge curve of this circuit. The relay contact closes at $t = t_1$. The decay of V_a can be made as rapid as required in practice, as R_2 can be chosen independently of the other circuit elements.

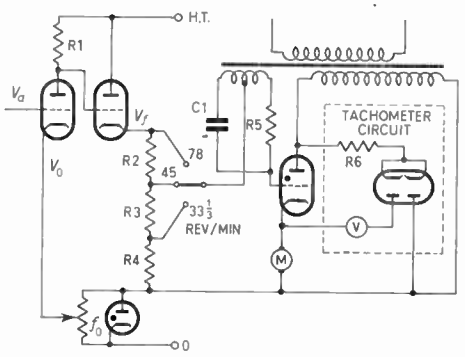

Fig. 7. Motor control circuit.

Having described the derivation of the amplitude-dependent component V_a of the feed control voltage V_f, the feed screw drive translating V_f to cutter carriage velocity will be briefly described.

The cutter carriage velocity must be proportional to the speed of rotation of the disk and the feed. At 33⅓ rev/min the slowest feed used is 50 μm per revolution corresponding to 20 revolutions per millimetre cutter head travel or 20 lines per millimetre. At 78 rev/min a feed as high as 300 μm corresponding to 3·3 lines per millimetre is used. This gives a ratio of highest to lowest cutter carriage velocity of 14/1. A thyratron controlled d.c. shunt motor drives the cutter carriage feed screw via a belt transmission. A simplified diagram of the motor control circuit is shown in Fig. 7. The speed of the motor is proportional to the motor control voltage from approximately 75 rev/min up to 1200 rev/min.

A tachometer circuit is associated with the motor control circuit. In the intervals where the thyratron is not fired the motor is running idle and the e.m.f. generated by the motor can be measured across the armature. The double diode connects the meter in parallel to the armature in the idle interval where the thyratron anode voltage is negative. The meter scale is calibrated in ' lines per inch'.

The amplitude-dependent component of the feed control voltage is applied to the control grid of a d.c. amplifier stage, and the component V_0, applied as cathode bias voltage to the same stage, is manually selected at the potentiometer f_0 according to the groove width and the minimum land required on the disk to be recorded. The feed control voltage V_f is equal to the motor control voltage at 78 rev/min. At the voltage divider terminating the d.c. amplifier, the voltage V_f is reduced by the factors 45/78 and 33/78 to give the correct motor control voltage at 45 and 33⅓ rev/min respectively.

Figure 8 is a block diagram of the groove control system for lateral recording. The groove control channel and the related elements of the modulation channel are shown.

3. Groove Control in Vertical Recording

In contemporary recording technique, vertical recording is of interest, because it can be considered as a special case of stereophonic recording. The groove control in vertical recording is here dealt with separately because it makes the presentation of the principles easier.

With reference to Fig. 9, the groove distance d between two vertically modulated turns must be

$$d = l + g_{av} + 2a \qquad \text{.....(6)}$$

where g_{av} is the average groove width determined by

$$g_{av} = g_{min} + 2a \qquad \text{.....(7)}$$

(g_{min} is the groove width just necessary to guide the play-back needle safely.)

When the groove is unmodulated the groove width can be reduced to g_{min}, and the groove distance to

$$d_0 = l + g_{min} \qquad \text{.....(8)}$$

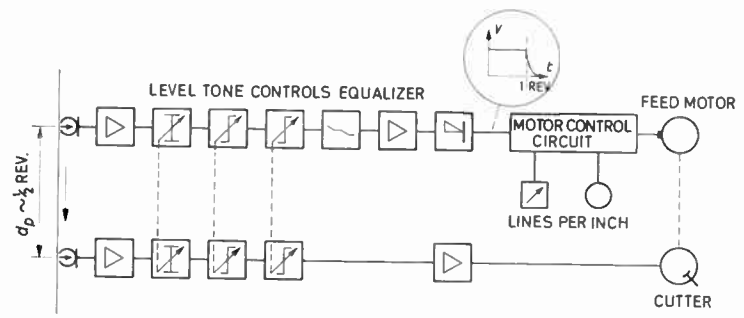

Fig. 8. Block diagram of 'lateral' groove control system.

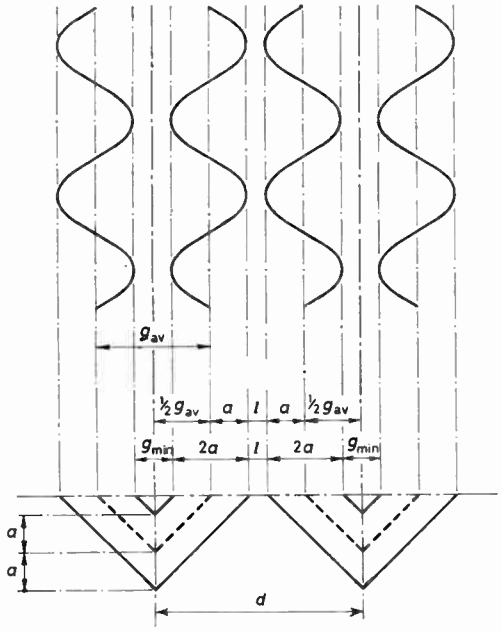

Fig. 9. Vertical amplitudes.

Substituting for g_{av} in equation (6) by equation (7) gives

$$d = l + g_{min} + 4a \qquad \text{.....(9)}$$

Comparing equation (6) with equation (9) it is found that the amplitude dependent part of the groove distance is doubled by introducing a variation of the average groove width proportional to the amplitudes.

As the amplitudes are strictly symmetrical about the axis of the groove, the feed control voltage is derived in the same way as in lateral recording. During the half revolutions preceeding and following a passage of increased modulation the groove spacing increases and decreases gradually leaving unutilized areas of the disk surface. The groove width can therefore increase and decrease gradually in these intervals, as shown on Fig. 10. The changes in groove width are effected by an electromechanical transducer driven by a d.c. amplifier requiring a control voltage proportional to the change in groove width. The reaction time of the transducer is short as compared to the time of half a revolution. This makes it possible to derive the feed control voltage and the groove width control voltage from the same pre-play-back head, provided that the groove width control voltage rises gradually during half a revolution after an increase in modulation has been detected by the pre-play-back head and starts falling back half a revolution after a decrease of modulation has been detected. A timing circuit with a delay of discharge corresponding to half a revolution is used followed by an RC circuit as shown in Fig. 11. An RC circuit is not ideal, as it will make the control voltage rise exponentially, whereas the increase in groove distance is linear. It could be expected that this would cause the groove width to increase much more than the groove distance at the beginning, but in Appendix 3 it is proved that

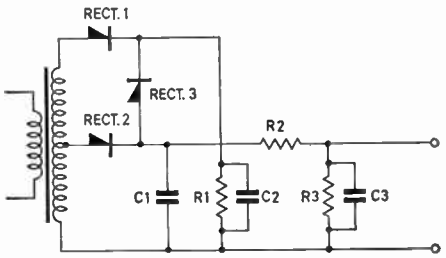

Fig. 11. Timing circuit and delay circuit for groove width control. (Rapid discharge arrangement omitted.)

the excess increase in groove width is negligible if the time-constant of the RC circuit

$$\text{i.e. } R_2R_3/(R_2+R_3)\,.\,C_3$$

allows the control voltage to rise to 90% of its maximum value during half a revolution.

The cutter suspension and the electromechanical transducer are shown in Fig. 12.

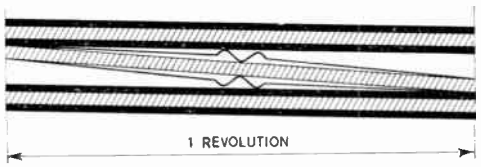

Fig. 10. Groove width and groove distance variations at a passage of vertical modulation.

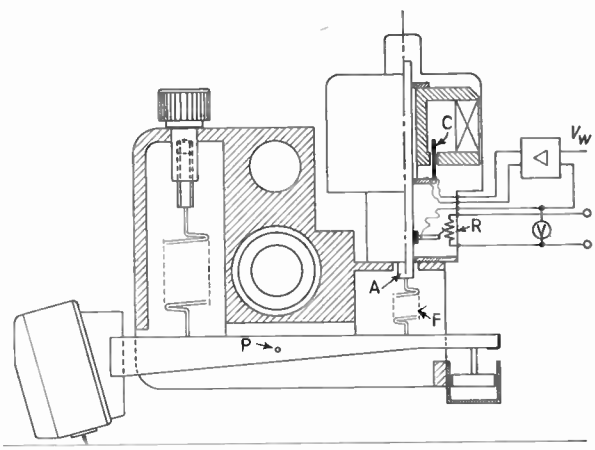

Fig. 12. Cutter carriage and groove width transducer.

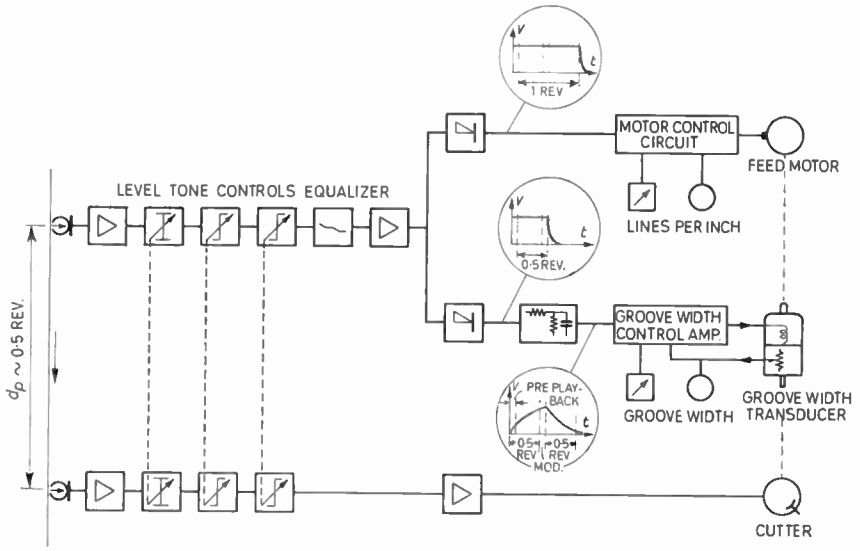

Fig. 13. Block diagram of 'vertical' groove control system.

The transducer consists of the vertically moveable shaft A carrying the coil C located in a magnetic field, and the slider of the potentiometer R. A current through the coil will make the shaft move upwards until the force acting upon the coil is in equilibrium with the tension of the spring F. The tension of F tends to lift the rear part of the cutter arm pivoted at P and force the cutting stylus deeper into the lacquer. The groove depth, and thereby the groove width, will increase until the increase in cutting force on the stylus tip balances the tension of the spring F. The force on the stylus tip is proportional to the groove width from approximately 40 μm up to 150 μm. In this range a vertical movement of the shaft will cause a proportional change in groove width. A constant voltage is applied across the potentiometer R and a voltmeter connected to the slider indicates the groove width variations effected by the transducer. The current passed through the transducer coil is supplied by a d.c. amplifier controlled by the groove width voltage and the voltage from the transducer potentiometer slider applied as feed-back. Figure 13 is a block diagram of the groove control system for vertical recording.

4. Groove Control in Stereophonic Recording

The lateral and the vertical control systems described above can be combined to form a groove control system for stereophonic recording. Figure 14 is a block diagram of this system, referred to as the M-S system. A matrix converts the A and B signals from the pre-play-back-head to lateral and vertical signals. From the two signals obtained, feed control voltages are derived and the two voltages are added at the input of the motor control circuit. From the vertical signal also the groove width control voltage is derived.[4]

If pure lateral or pure vertical amplitudes are to be recorded, the relationship between the two matrix input signals is $A = B$ and $A = (-B)$ respectively. $A = B$ results in 'lateral' output from the matrix, $A = (-B)$ in 'vertical' output. The feed control voltages derived from the two matrix outputs therefore correspond to the groove distance required for each of the two modes of modulation.

When only one of the stereo channels is modulated the amplitudes are recorded at an angle of 45 deg to the vertical, and the signal will be present only at one of the matrix inputs. The lateral matrix output is then equal to the vertical, and the lateral component of the recorded amplitude is equal to the vertical component. But the feed control voltages derived from the matrix outputs will each correspond to the groove distance required by the two amplitude components as if they occurred separately, and by adding the two voltages the groove distance determined will be that required if the two components had modulated both groove walls.

As the original amplitudes modulate only one groove wall the groove distance, with respect to the original axis of the groove, is correct only at the modulated side of the groove, as shown in Fig. 15. This gives correct groove distance at the beginning of a passage of modulation of the groove wall nearest to the rim of the disk, and at the end of a passage of modulation of the groove wall nearest to the centre of the disk. At the constant single channel modulation, one-third of the amplitude dependent groove spacing is left unutilized.

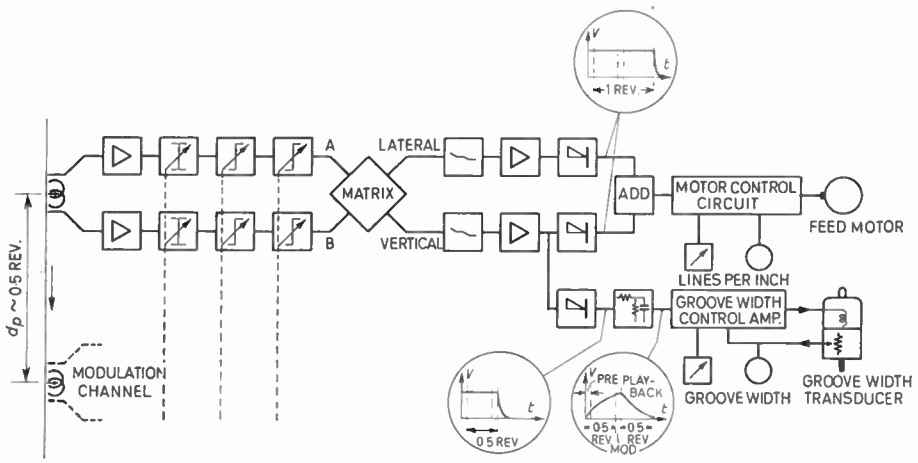

Fig. 14. Block diagram of 'MS' groove control system.

This demonstrates clearly that the groove spacing in stereophonic recording cannot be controlled efficiently from a single pre-play-back head placed at a distance corresponding to half a revolution. This distance is correct only if the modulation is symmetrical about the axis of the groove.

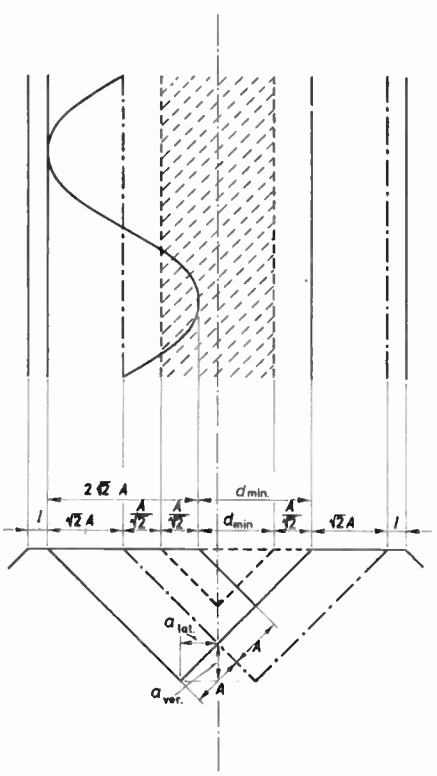

Fig. 15. Single channel amplitudes.

The groove distance is determined by 'MS' control.

In single channel modulation, as in Fig. 15, only the increase in average groove width is symmetrical about the axis. Therefore, only the groove spacing variations corresponding to the variation of the average groove width can be controlled as for symmetrical modulation.

Apart from this component of the groove control the amplitudes of either side of the groove can be considered independent.

Figure 16(i) then shows the situation at a passage of constant A-channel modulation. The amplitudes are recorded on the groove wall nearest to the centre of the disk. When the first amplitude is recorded no increase in groove distance is necessary, but the feed must be increased at this point to provide sufficient groove spacing for the following turn and this feed must be maintained over a complete revolution after the end of the passage to provide sufficient groove spacing also at the last amplitude. In this case the feed must be derived from the A-modulation channel, and a timing-circuit with a delay of discharge corresponding to one revolution must be employed.

Figure 16(ii) shows the situation at a similar passage of B-channel modulation. The amplitudes are recorded on the groove wall nearest to the rim of the disk. To obtain sufficient groove spacing at the first amplitude, the feed for constant modulation must be set a complete revolution in advance, but it can be reduced as soon as the last amplitude has been recorded. The feed in this case must be derived from a pre-play-back head reading the B-track of the tape at a distance corresponding to one revolution in advance, and a timing circuit with a delay of discharge corresponding to one revolution must also be employed.

If A-channel modulation coincides with B-channel modulation in the following turn, as shown in Fig.

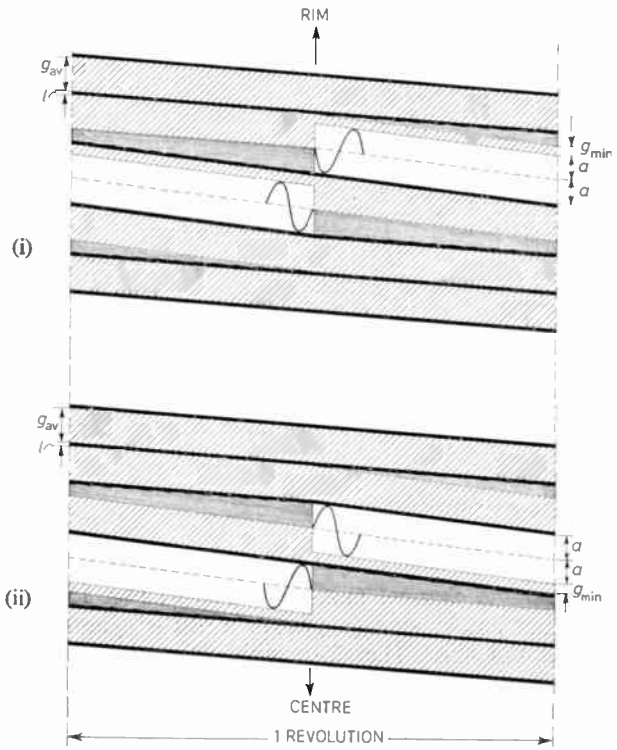

Fig. 16. Groove distance variations at single channel modulation determined by 'ABS' control.

(i) A-channel modulation.

(ii) B-channel modulation.

17(i), the feed must be increased in accordance with the sum of the amplitudes of the two modes of modulation. This sum could be obtained by deriving the control voltages independently, and then adding the output of the two timing circuits. But due to the fact that the feed for A and B modulation, coinciding as in Fig. 17(i), are determined simultaneously, it is possible to make the system still more efficient. The envelope voltages of the modulation of the two control channels are derived and added, and the sum of the two is then applied to a common timing circuit giving a discharge delay. If the two modulation peaks do not fully coincide as in Fig. 17(ii) the groove spacing determined in this process is still sufficient, but considerably less than it would have been if the two control voltages had been derived independently. The groove spacing would then have been the same as in the case of Fig. 17(i).

A block diagram of a groove control system based on this principle is shown in Fig. 18. This system is referred to as the 'ABS' system.

As mentioned already, the pre-play-back head of the groove width control channel is placed at a distance corresponding to half a revolution. The signal from this head is the difference of the A and the B modulation. This corresponds to the vertical component of the amplitude to be recorded.

The d.c. amplifier following the feed control timing circuit of this channel is similar to the first stage of the motor control circuit, and the output voltages of these two similar stages are added, forming the final feed control voltage.

The manual groove width control and the corresponding manual feed control attached to the d.c. amplifier are ganged. By means of the manual feed control attached to the motor control circuit, the land between the grooves is selected.

5. Combined Stereophonic and Monaural Equipment

Finally, the combined adaptation of the groove control systems to a 'tape to disk transferring equipment' will be briefly described.

Figure 19 is a block diagram of this equipment. It is designed to replay tapes at $7\frac{1}{2}$, 15 and 30 in/s, and record disks at $33\frac{1}{3}$, 45 and 78 rev/min. Stereophonic as well as monaural disks are recorded at $33\frac{1}{3}$ and 45 rev/min; at 78 rev/min, only monaural disks are recorded.

If the 'ABS' control system were to be used with all 9 combinations of tape and disk speed, 12 pre-play-

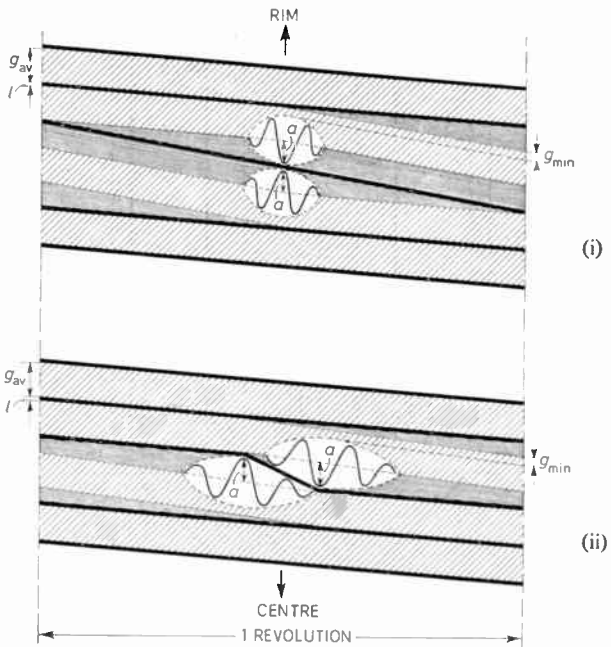

Fig. 17. Groove distance variations at single channel modulation peaks determined by 'ABS' control.

(i) A and B modulation peaks coinciding.

(ii) A and B modulation peaks 'just not' coinciding.

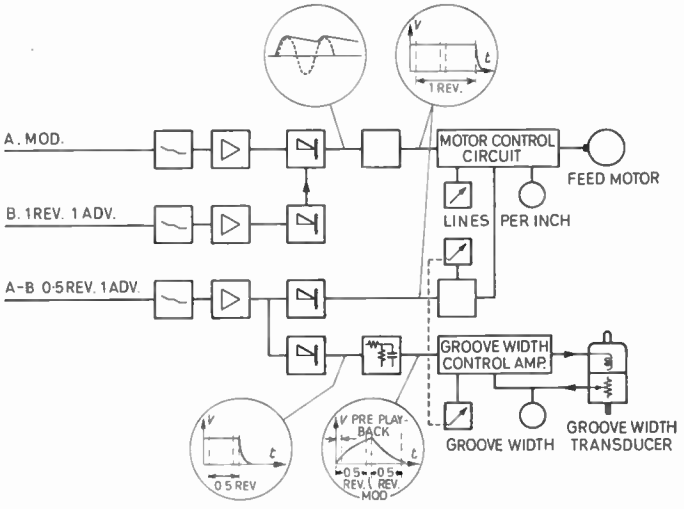

Fig. 18. Block diagram of 'ABS' groove control system.

back positions would be required and the longest distance between the heads on the tape deck would be 137·2 cm. By employing MS control at 30 in/s tape speed and ABS control at 7½ and 15 in/s the number of pre-play-back positions has been reduced to 9 and the longest distance between the heads to 68·6 cm.

This number of pre-play-back positions is covered by two heads mounted on trolleys. The heads are shifted from one position to another by a tackle arrangement which maintains a 2/1 ratio between the distance from each of the pre-play-back heads to the play-back head. This solution was chosen instead of a multitude of heads or a system of tape loops, because it gives the smoothest tape transport and it can easily be automatized. The shortest head distance corresponding to half a revolution at 78 rev/min and 7½ in/s was difficult to achieve in this way. But at 78 rev/min only monaural disks are recorded. The head next to the play-back head is therefore placed at a distance corresponding to one revolution for this combination, and the A and B components of the ABS control system are used as a lateral control system.

This type of groove control is correct because lateral modulation can be considered a special case of stereophonic modulation. But it was desired also to cut monaural disks directly from stereophonic tapes. A matrix is therefore inserted in the modulation channels whenever monaural disks are to be recorded, and the lateral control system is employed at the four important combinations: 7½, 15 in/s—33⅓, 45 rev/min.

The four outputs of the pre-play-back heads must be selected, combined and directed in accordance with the type of groove control in use. This is done at as early a stage as possible in order to reduce the number of sections of the ganged controls for level, tone control and balance as well as the number of tape equalizers and line level amplifiers. Four straight, low level amplifiers bring the pre-play-back head outputs to exactly the same level and the four outputs are then selected, combined by two matrices and directed to the two pre-play-back channels, one for the groove width control and one for the B signal for ABS control as well as for the A + B signal for M, S and lateral control. Only the balance cannot be controlled after combining the signals. The balance control pre-play-back sections are therefore inserted between the low level amplifiers and the matrices.

In accordance with the disk speed and the tape speed selected and the type of modulation to be recorded (stereophonic or monaural), all changes in the groove control equipment are effected automatically. The pre-play-back heads move in position and their outputs are selected, the delay of discharge of the timing circuits change, and the cutter carriage velocity is changed.

6. Conclusions

It is very difficult to obtain an exact measure for the effectiveness of a groove spacing control system. The playing time which it is possible to record varies so widely with the contents of the programme to be recorded, that only very broad generalizations can be made. When symphonic music is recorded the playing time, as compared with that obtained without groove control, can normally be extended by 50% in monaural recording and by 100% in stereophonic recording. Naturally, experienced operators can achieve very good results by manual control but this often

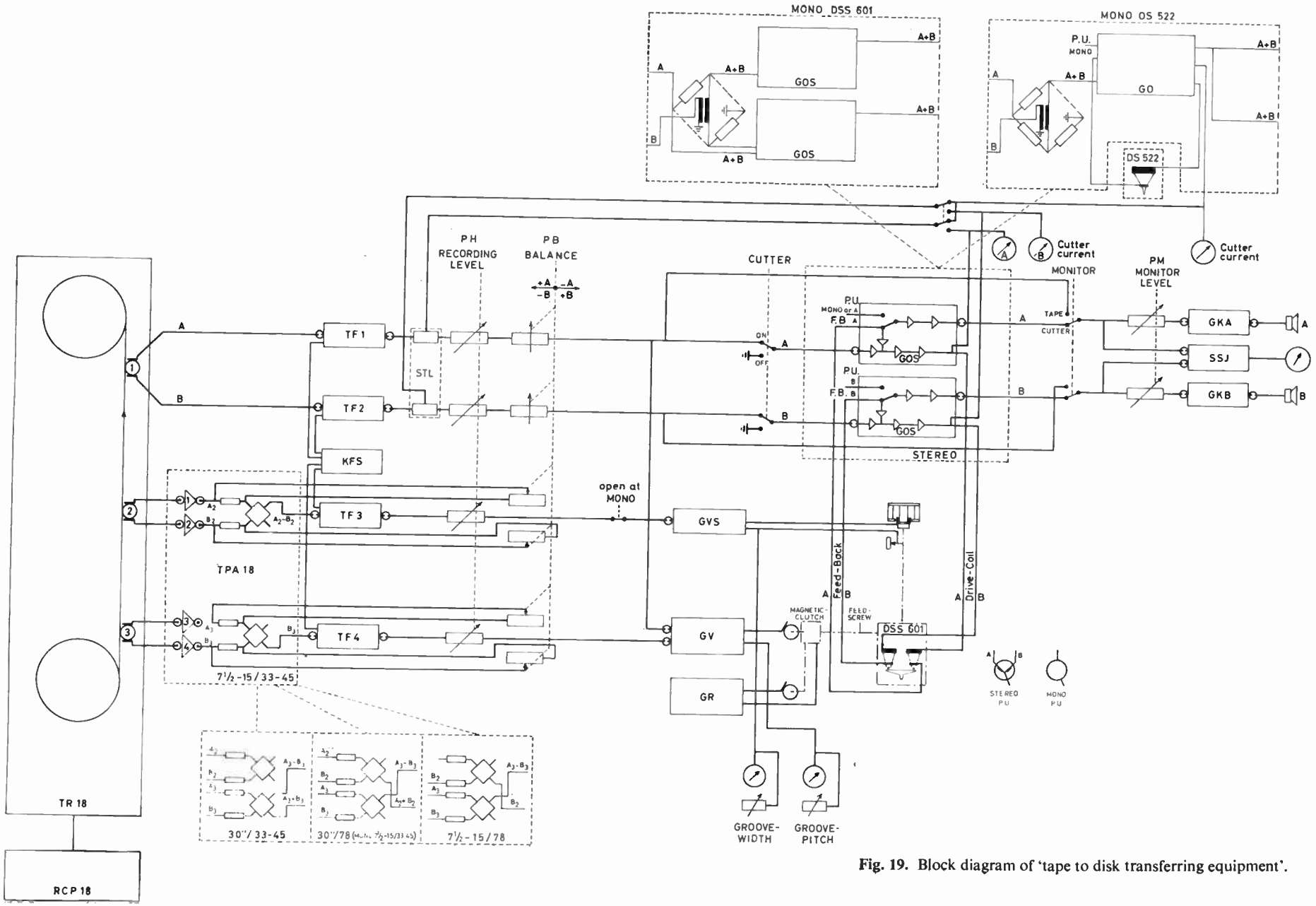

Fig. 19. Block diagram of 'tape to disk transferring equipment'.

requires a complete rehearsal and human errors may still occur. An automatic groove spacing control system helps to avoid both, and also thereby adds considerably to the productivity of disk cutting equipment.

7. Acknowledgments

The author thanks the Directors of Ortofon A/S and Fonofilm Industri A/S for their permission to publish this paper, and the Director V. Anneberg for constant encouragement and constructive criticism during its preparation. The inspiring guidance of the late Dr. F. Schlegel during the development of the equipment described is gratefully acknowledged.

8. References

1. German patent no. 966210. "Verfahren zur Aufzeichnung einer Tonschrift mit Steuerung des Abstandes zwischen benachbarten Tonspuren". Inventor: Eduard Rhein, Hamburg.
2. German patent no. 962120. "Verfahren zum Schneiden von Tonträgern". Inventor: Dr. Ing. Friedrich Bergtold, Dachau.
3. Danish patent no. 55822. "Fremgangsmåde og apparat til nedskrivning af lyd". Inventor: Ingeniør Dr. phil. Karl Hermann Franz Schlegel.
4. Gunther Lützkendorf and Günter Kiess, "Schneidtechnik bei Stereo-Schallplatten", *Radio Mentor*, **24**, p. 683, October 1958.

9. Appendix 1

The tolerances claimed for speed variations ('wow') of professional disk cutting lathes are normally $\pm 0{\cdot}05\%$. In the extreme case this would be + or $-0{\cdot}05\%$ during an entire revolution. An amplitude predicted to coincide with an amplitude recorded at the beginning of that revolution would be recorded at a distance $0{\cdot}05\%$ of the length of a groove turn from the predicted position.

The deviation would be

$$d = 0{\cdot}05 \times 10^{-2} \pi D \text{ cm}$$

where D is the diameter of the groove turn in cm.

The groove velocity is

$$V = \frac{\text{rev/min}}{60} . \pi D \text{ cm/s}$$

For stylus velocity v and the land measured in the direction of a radius l_r, the land measured in the direction of the groove axis is

$$l_a = \frac{l_r}{v} . v = \frac{l_r}{V} . \frac{\text{rev/min}}{60} . \pi D$$

For $v = 15$ cm/s; $l_r = 10$ µm and $33\frac{1}{3}$ rev/min

$$l_a = 0{\cdot}37 \times 10^{-4} \pi D \text{ cm}$$

and l_a is the biggest permissible deviation.

10. Appendix 2

The advantage of the rapid discharge of the timing circuit with delayed discharge can be evaluated by calculating the time, in disk revolutions, which the rapid discharge should be held back for the same area to arise as that determined by the decay function $V = E_1 \exp[-t/RC(C_1 + C_2)]$ in the interval $t_1 \lesssim t \lesssim \infty$, i.e. the shaded area in Fig. 5(b).

C_1 can be chosen to be small compared to C_2. Then

$$V = E_2 . \exp(-t/RC)$$

and the area

$$A = E_2 \int_{t_1}^{\infty} \exp(-t/RC)\, dt$$

$$= E_2 RC \exp(-t/RC)$$

From

$$V = E_1 = E_2 . \exp(-t/RC) \text{ at } t = t_1$$

follows

$$\exp\left(-\frac{t_1}{RC}\right) = \frac{E_1}{E_2} \quad \text{and} \quad \frac{t_1}{RC} = \ln \frac{E_2}{E_1}$$

Then

$$A = \frac{E_1 . t_1}{\ln \dfrac{E_2}{E_1}}$$

A is small if the ratio E_2/E_1 is large, but the modulation must decrease by more than that ratio to start the decay of V at all. Therefore E_2/E_1 should not be chosen higher than 2.

The unit of time is disk revolutions and the delay of discharge is one revolution.

Therefore, $\frac{E_2}{E_1} = 2$ and $t_1 = 1$

which gives

$$A = \frac{E_1}{\ln 2} = 1{\cdot}44\, E_1$$

The same area would arise if V was maintained at the value E_1 for 1·44 revolutions longer than necessary and then rapidly reduced to 0.

11. Appendix 3

The voltage V_c across a capacitance C charged via a resistance R to the voltage V applied at the time $t = 0$

is

$$V_c = V[(1 - \exp(-t/RC)]$$

If the groove width is increased by y_w to one side of the groove, and y_w rises proportional to V_c from 0 at $t = 0$ to K_1 at $t = \infty$

then

$$y_w = K_1[(1 - \exp(-t/RC)]$$

and if the groove distance is increased by y_d proportional to t from 0 at $t = 0$ to K_2 at $t = 1$, then

$$y_d = K_2 t$$

The increase in groove width exceeds the increase in groove distance by Δ_y if

$$\Delta y = y_w - y_d \text{ is positive}$$

and maximum value of the excess, Δy_{max}, is found at

$$\Delta y' = 0$$

$$\Delta y = K_1[1-\exp(-t/RC)]-K_2 t$$

$$\Delta y' = K_1 \frac{1}{RC} . \exp(-t/RC)-K_2$$

If

$$y' = 0 \text{ at } t = t_{\Delta y\,max}$$

then

$$\exp\left(-\frac{t_{\Delta y\,max}}{RC}\right) = \frac{K_2}{K_1} . RC$$

and

$$t_{\Delta y\,max} = RC \ln\left(\frac{K_1}{K_2} . \frac{1}{RC}\right)$$

Hence

$$\Delta y\ max = K_1\left(1 - \frac{K_2}{K_1} . RC\right) - K_2 RC \ln \frac{K_1}{K_2 . RC}$$

$$\Delta y\ max = K_1\left[1 - \frac{K_2}{K_1} . RC\left(1 + \ln \frac{K_1}{K_2 . RC}\right)\right]$$

From $y_w = 0{\cdot}9\ K_1$ at $t = 1$ follows

$$RC = \frac{1}{2{\cdot}3}$$

and as y_w at $t = 1$ will be equal to the vertical amplitude a_v

$$a_v = 0{\cdot}9\ K_1$$

At vertical modulation K_2 will be equal to the maximum increase in groove width plus the vertical amplitude

Hence

$$K_2 = K_1 + a_v = 1{\cdot}9\ K_1$$

If the maximum recorded stylus velocity, v_{max}, is 15 cm/s and the cross-over frequency of the recording characteristic is 500 c/s the maximum amplitude will be:

$$a_{max} = \frac{v_{max}}{w} = \frac{15}{2\pi \times 500} = 4{\cdot}8 \times 10^{-3} = 48\mu m$$

In this case

$$K_1 = 53{\cdot}5\mu m$$

and

$$y_{max} = 0{\cdot}63\mu m$$

The land between the grooves is reduced by this value. Compared to 10 μm which is the minimum land selected for unmodulated grooves, this figure is negligible.

In the ABS control system the groove distance is increased only by the increase in groove width to one side of the groove, in advance of a passage of A-channel modulation.

In this case $K_2 = K_1$.

The maximum value of vertical component of single channel amplitudes is half the value of maximum vertical amplitudes.

Therefore

$$a_{v\,max} = 24\mu m$$

and

$$K_1 = 26{\cdot}75\mu m$$

This gives

$$\Delta y_{max} = 5{\cdot}3\mu m$$

This value is permissible. Only if 10 μm land is selected and the maximum level is exceeded by 5 dB will the land be reduced to 0 in this case.

Manuscript received by the Institution on 19th May 1965 (Paper No. 1013/EA24.)

U.D.C. 621.315.592.9 : 621.373

The Mechanism and Device Applications of High Field Instabilities in Gallium Arsenide

By

J. S. HEEKS, B.Sc., Ph.D.,†

A. D. WOODE (*Graduate*)†

AND

C. P. SANDBANK, B.Sc., D.I.C.†

Reprinted from the Proceedings of the Joint I.E.R.E.-I.E.E. Symposium on "Microwave Applications of Semiconductors" held in London from 30th June to 2nd July 1965.

Summary: The paper reviews the present understanding of the behaviour of high field instabilities in GaAs and discusses the device prospects in the light of work carried out to obtain a phenomenological model for the Gunn effect.

The moving high field domain, which forms in n-type GaAs when the applied field of several thousand volts per cm exceeds a sharply-defined threshold value, has been studied over a wide range of drift paths, but particularly in long samples. For applied voltages below the threshold value a novel technique of triggered operation has been used whereby just one cycle of operation is produced. A model for domain formation which has been derived from the results is characterized by two well-defined field values. The ohmic current flowing in the material when a domain is present is associated with the lower field value. The transient current in the period between the decay of one domain and the creation of the next is associated with the higher field level. An important consequence of the model is that it suggests a direct proportionality between the voltage appearing across the domain at a given bias field and the length of the sample. This conclusion has been confirmed by measurements on samples in the range 0·025 in to 0·10 in where domain amplitudes from 60 V to 300 V respectively have been observed. The results are in agreement with Ridley's theoretical prediction of domain formation arising from a voltage controlled bulk negative resistance.

The implication of the model on the use of the device for power generation and modulation at microwave frequencies are discussed and the results of experiments studying the change of the main parameters under varying ambient conditions are given.

1. Introduction

Undoubtedly the most interesting and potentially useful advance in the art of bulk effect microwave generation has been the work on n-type gallium arsenide and indium phosphide recently reported by J. B. Gunn.[1] Current instabilities were observed in these materials at fields of a few thousand volts per centimetre. The effect occurred at a sharply defined threshold field and in short samples (< 0·025 cm) driven from a constant voltage source appeared as a coherent oscillation in the microwave region. In subsequent experiments[2] he demonstrated that the phenomenon was associated with a spatially sharp voltage step of about 50 V in amplitude which appeared to move through the material with the saturation velocity of the carriers. The phenomenological explanation given by Gunn is illustrated schematically in Fig. 1(a) and accounts for the observed correlation of oscillation frequency and threshold voltage with specimen length, and also the

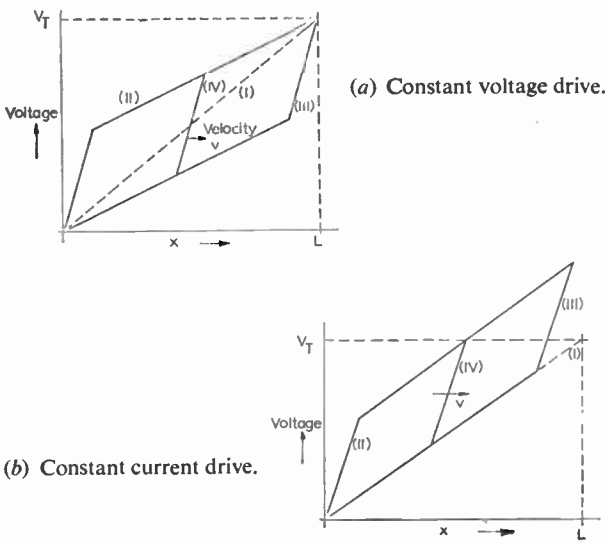

Fig. 1. Voltage distribution across sample at various instants in the oscillatory cycle; (I) at time $t = 0$, (II) at end of build-up of shock wave, (III) when shock wave reaches anode, and (IV) at intermediate time in cycle.

† Standard Telecommunication Laboratories, Harlow, Essex.

non-sinusoidal character of the lower frequency oscillations. Further, by assuming the amplitude of the voltage step to be a constant of the material, he suggested that the change in the field at the cathode resulting from the step formation will become less as the drive tends to constant current. He points out that a significant reduction in the cathode field is required to inhibit the random generation of further voltage steps and thus explains incoherence in long specimens or short specimens in constant current circuits (Fig. 1(b)). No satisfactory explanation for the origin of the voltage step was given although a number of possible mechanisms were considered and rejected.

Initial investigations in these laboratories using short samples of GaAs gave general confirmation of the results reported by Gunn but correlation of frequency and threshold voltage with specimen length was poor. Often for the same sample a marked difference in these parameters occurred when the current was reversed. The results could be explained in terms of a 'virtual' cathode in the body of the material from which the voltage steps were launched. Presumably this was due to material inhomogeneity or geometrical irregularities. A more significant difference, however, was that coherent current waveforms were obtained in circuits which approximated to constant current drive. This is not inconsistent with the model to be described in this paper.

A clear picture of the voltage step (or high field domain†) properties has emerged from studies of longer samples in the range 0·025 in to 0·10 in (0·063 cm to 0·025 cm). Practical difficulties such as obtaining the necessary precise geometries of small samples and the limiting resolution of the measuring equipment are avoided. Further, as the quality of the devices can be easily assessed by the shape of the current waveforms we can be sure of obtaining meaningful results from the various experiments. The results can be extrapolated to the behaviour of devices at microwave frequencies where detailed experimental analysis of the instability is not possible.

2. Experiments with Fields Above and Below Threshold

2.1. *Principles of the Experiments*

Gunn has pointed out that his proposed explanation of the oscillator driven from a constant voltage source implies that the high field domain can continue to propagate, once formed, in spite of the consequent reduction in field (to below the threshold level E_T) in the main bulk of the material. It was of interest to know what reduction in applied field would still sustain the domain, and, more important, how its amplitude and velocity varied with field in the sub-threshold region. This technique can be realized by biasing the device at various levels below the threshold field and triggering just one cycle of operation by exceeding E_T for a short interval of time. A number of factors indicate that the experiment should be performed on long samples. For example, a practical width of trigger pulse would be in the nanosecond region, and ideally this should be a small fraction of the cycle period. Other advantages of working with long samples include greater accuracy in the measurement of time and length, the elimination at the low repetition rates of the effects of chance resonance circuits associated with the sample mount, and finally the relative ease with which voltage probe measurements can be made along the surface of the device. The latter measurements provide confirmation of current measurements and do establish that the shock wave moves across the whole length of the specimen.

Measurements at fields higher than the threshold level are easily performed by simply overdriving the device.

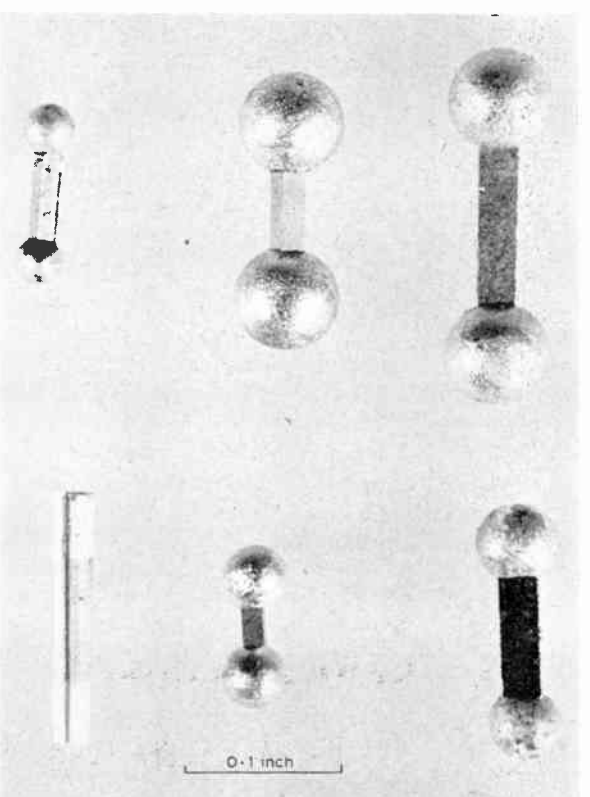

Fig. 2. Long GaAs samples.

† We shall anticipate our results, which identify the voltage step with the high field domain of the Ridley model, and refer henceforth to the latter nomenclature.

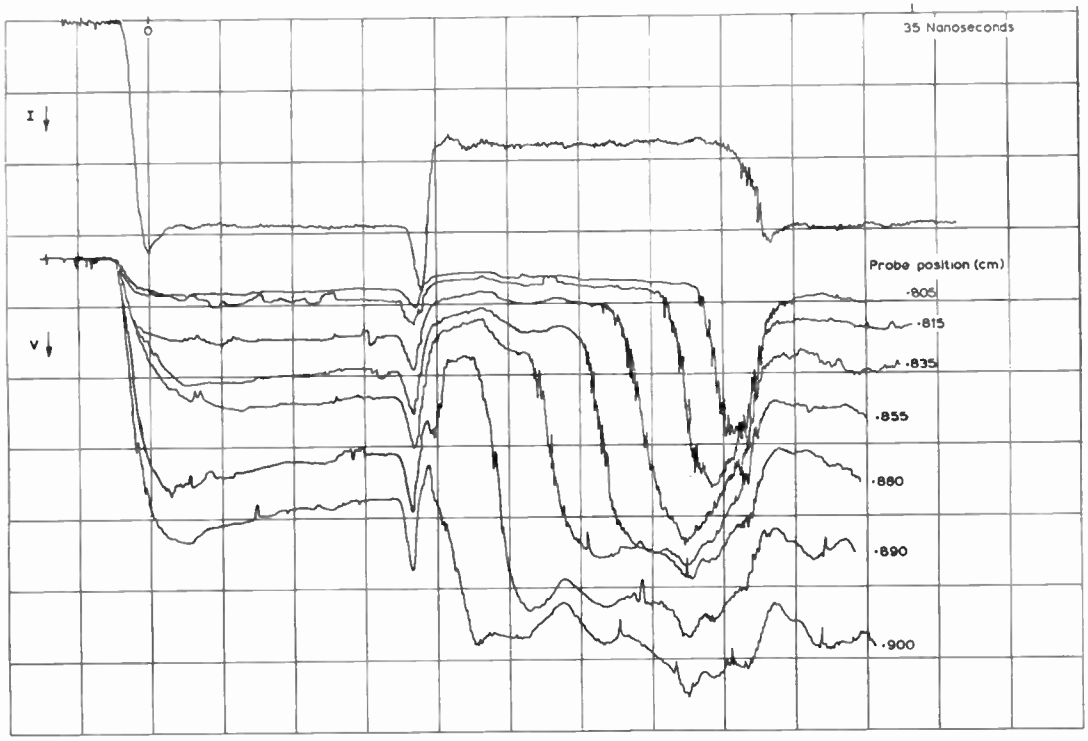

Fig. 3. Current (upper trace) and voltage (lower traces) versus time for 0·05 in sample in triggered mode of operation.

2.2. *Sample Preparation and Experimental Arrangement*

Samples were prepared from GaAs of 3·5 ohm cm resistivity, $2{\cdot}4 \times 10^{14}$ carriers/cm^3, and mobility 6700 cm^2/s by cutting to the required dimensions with a diamond wheel. After thorough cleaning, the material was lightly etched in 60% H_2SO_4, 30% H_2O_2. Tin dots were alloyed to the ends of the bars by heating to 400°C for a few minutes in a hydrogen atmosphere. A jig of high purity graphite with a dumb-bell-shaped groove held the tin dots in the correct position against the GaAs during the alloying process. Subsequent experience of the devices as Gunn oscillators indicated that a final careful lapping and etching of the sides of the sample to remove work damage was not necessary. Long samples of various sizes are illustrated in Fig. 2.

All measurements were made in a resistive circuit, the sample being mounted axially in a 50-ohm line, the centre conductor of which had a spring-loaded section in order to accommodate the various sizes. A current-monitoring 1-ohm disk resistor was placed within 0·1 in (0·25 cm) of the sample and a 10-dB pad was included in the line to the sampling oscilloscope to cut out ringing. Due to the high power dissipation, pulsed operation was necessary. Pulses of up to 700 V were obtained from a mercury switch delay line generator provided with an external high voltage charging supply. The specially shaped waveform required for the triggered mode of operation was achieved by placing a 2 in (5·1 cm) section of low impedance line near the beginning of the generator pulse forming line. The actual shape of the voltage pulse is closely similar to the current waveform just below threshold shown in Fig. 4 (curve 1) as the voltage-current characteristic of the device is nearly ohmic up to the threshold bias.

Where it has been of interest to study the voltage distribution along the sample, a very simple surface probe has been useful. It consisted of a short 0·005 in (0·013 cm) diameter wire which was tinned at the end making contact with the GaAs. The other end was attached to a small 500-ohm resistor which in turn was connected to a 50-ohm disk resistor across the input probe of the sampling oscilloscope. The purpose of the 500-ohm resistor was to increase the resistance in the path from the probe to earth. The whole arrangement was built on to a micromanipulator which enabled the probe to be moved accurately along the sample.

2.3. *Results and Discussions*

Triggered one-cycle operation in a sample 0·05 in (0·13 cm) long is illustrated in Fig. 3. The upper trace shows the current waveform (negative) and the lower traces the voltage versus time at various positions

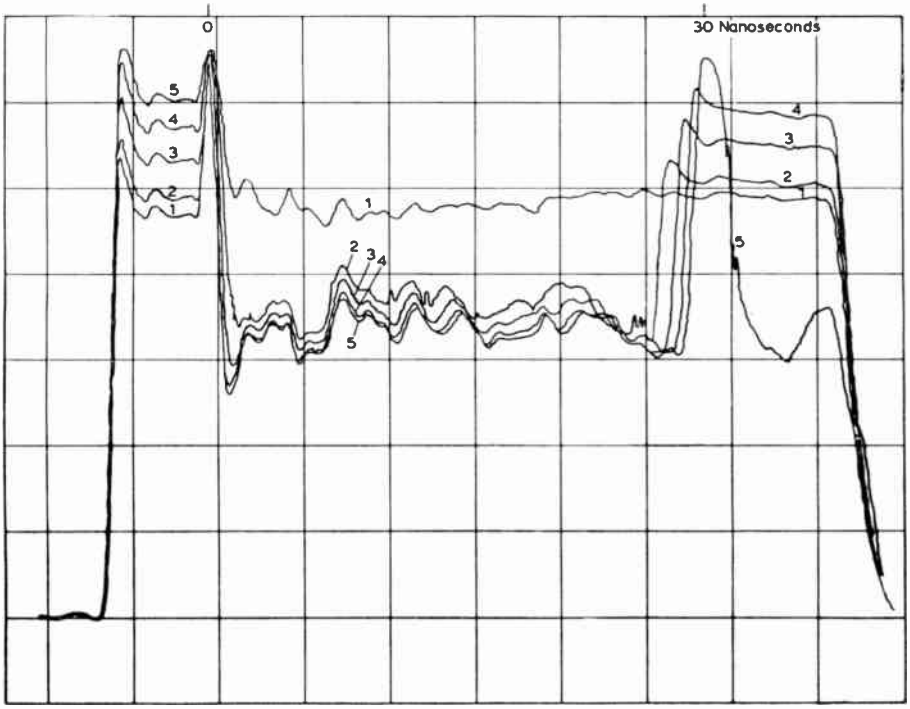

Fig. 4. Effect of increasing the drive towards threshold with triggered one-cycle operation.

along the device. These recorder tracings demonstrate unambiguously that the high voltage domain initiated by the trigger pulse moves through the material at constant amplitude taking 15 ns to traverse from cathode to anode. It is apparent from a comparison of the current and voltage rise-times that resolution of the voltage plots is limited by the probe system and the domain width could be narrower than indicated.

The effect on the current waveform of increasing the applied field towards the threshold value is shown in Fig. 4. In this case the sample is 0·1 in (0·25 cm) long and the transit time about 30 ns.† Waveforms 1 and 2 correspond respectively to peak trigger voltages just below and above threshold. With further increase in drive voltage the average value of the reduced current decreases slightly and there is a corresponding increase in the transit time, both parameters, however, tending asymptotically to fixed values as threshold bias is approached. Clearly, the amplitude of the high field domain increases with bias voltage and tends to a one-to-one correspondance as the applied voltage increases. These results have been confirmed with voltage probe experiments. The triggering of a second domain at an apparently lower threshold than the first (see curve 5 of Fig. 4) is not at present fully understood.

For the experiments with applied voltages greater than the threshold level a normal 100-ns rectangular pulse was used. In general, there was a rapid loss in current waveform coherence as the drive was increased above threshold but in one sample it was possible to overdrive by 50%. Current and voltage waveforms for this sample are shown in Fig. 5. It will be observed that the current waveform changes very little with overdrive although there is still a detectable fall in the plateau current and an increase in the period of oscillation. A slight increase in the height and a narrowing in width of the current spike is also noted. The relative constancy of the plateau current for bias voltages greater than the threshold value has been anticipated from the results of the triggered mode of operation. Some of the samples had resistances as low as 50 ohms and hence the drive could no longer be regarded as constant voltage. Once a domain was triggered the voltage across the device increased and at the higher drive levels exceeded the threshold voltage during the transit time of the domain.

† Because of the inconsistency of the GaAs material it is difficult to obtain many samples which behave identically unless very large numbers are made. Thus different samples have been chosen which best illustrate the various points discussed, i.e. the very constant value of the reduced current in Fig. 3 implies homogeneous material and is suitable for studies on the constancy of domain form. Similarly, the long period and rapid recovery obtained in Fig. 4 gives a sensitive indication of the small changes in domain velocity.

The main features of these results can be described by the idealized graphical constructions of the voltage distributions which are shown in Fig. 6. Evidently, for a particular material, two characteristic values of the electric field can be identified, the upper one being the threshold for spontaneous and cyclic production of domains and the lower value (typically $E_T/2$) above which a domain will be sustained if suitably triggered. The lower field defines the ohmic current in the material while a domain is in transit and the higher field the peak transient current during the interval between the decay of one domain and the generation of the next. The model implies that in the overdriven condition, high field domains are simultaneously present at both the anode and cathode during this transient condition.

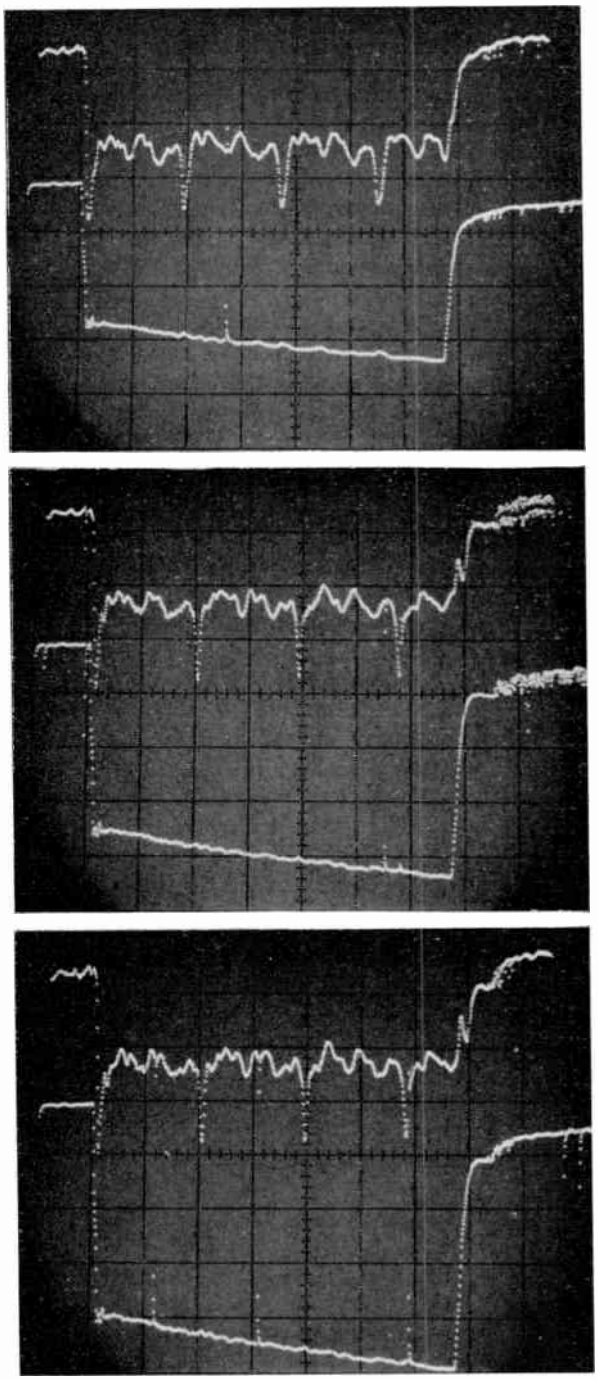

Fig. 5. Coherent current waveforms (upper traces) with increasing applied voltages (lower traces). Time scale 15 ns/cm, current and voltage scales 1 A/cm and 200 V/cm respectively. Note that the voltage waveform is distorted by the measuring set-up.

Voltage versus current plots on an X–Y recorder together with the known zero field mobility of the material enabled the carrier velocity to be precisely estimated for any value of field up to the threshold level. The observed domain velocity was in good agreement with the calculated carrier velocity at the lower characteristic field.

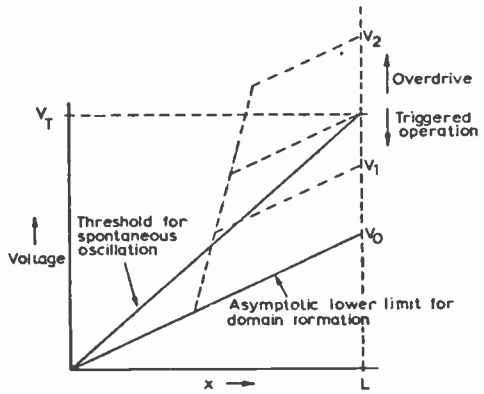

Fig. 6. Construction of the voltage distribution for an arbitrary position of the high field domain and applied voltages above and below threshold.

An important consequence of the model indicated in Fig. 6 is that not only are threshold voltage and oscillation period proportional to the sample length but also the voltage across the high field domain for a given applied field. Measurements on over twenty samples in the length range 0·025 in to 0·10 in (0·065 cm–0·25 cm) have proved this conclusion to be justified and domain amplitudes of over 300 V have been obtained with the longest samples at threshold bias. Plots of threshold voltage, domain transit time, and domain voltage at threshold bias, versus sample length are given in Fig. 7. The mean threshold field and domain velocity are 2400 V/cm and 8×10^6 cm/s respectively.

In a recent note Kroemer[3] has pointed out that most of the known properties of the Gunn effect can be explained by assuming that the basic interaction phenomenon results in a drift velocity or current versus electric field characteristic with a

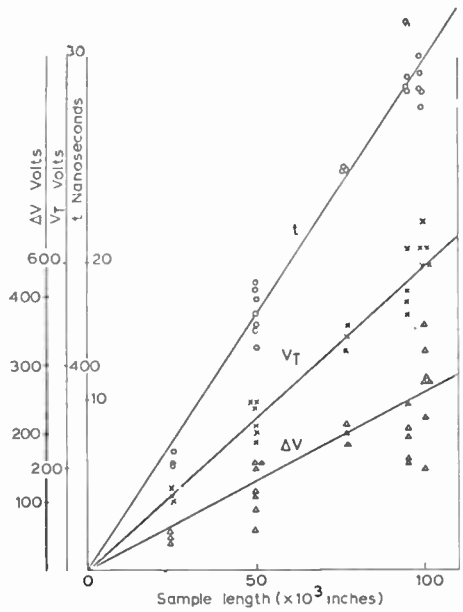

Fig. 7. Domain transit time (t), amplitude (ΔV) and threshold voltage (V_T) versus sample length.

region of negative differential conductivity. Such a characteristic is shown in Fig. 8. Ridley[4] has demonstrated by theoretical arguments based on thermodynamic considerations that such a bulk characteristic will result in two domains of high and low field (E_2 and E_1) being formed when the material is biased anywhere in the negative conduction region. These domains move with the carrier drift velocity. The width of the high field domain can very simply be shown to be given by the expression

$$x = \frac{E_{\text{applied}} - E_1}{E_2 - E_1} L \qquad \text{.....(1)}$$

Clearly our results for long samples are consistent with Ridley's model and suggest identifying I_T and I_{min} with currents at the peak and valley of Fig. 8.† An interesting feature of the model is that the high field domain supports more voltage by increasing in width rather than increasing in field intensity. (This has been implied in Fig. 6.) Unfortunately our present probe arrangement does not have sufficient resolving power to detect this change in width. Operation in the triggered mode ($E_T > E_{\text{applied}} > E_1$), the proportionality of domain voltage to specimen length, at a given bias, and the unchanging oscillator current waveform on overdriving, all follow naturally from the Ridley model. Other implications concerning d.c. to a.c. conversion efficiency and waveform coherence are discussed in the next section.

† Since writing this paper the authors have carried out further experiments which, although they do not invalidate these arguments, show that the above model is only applicable to a first approximation.

Of the basic mechanisms for the Gunn effect which have been suggested (for an excellent review of these see reference 1) only two are without serious objection. The first of these involves coupling of the drifting electrons to optical phonons in a manner analogous to the process occurring in piezo-electric materials whereby electrons transfer energy to the acoustic phonons. However, simple calculations[1,5] indicate that the threshold velocity in GaAs is lower than that predicted for this type of interaction. The other process is based on a suggestion of Ridley and Watkins[6] that in suitable materials electrons becoming 'hot' in an electric field can transfer from a low energy sub-band to a higher one in which the effective mass is greater and the mobility lower. Hilsum[7] did, in fact, predict a negative resistance arising from this mechanism in GaAs at a field of 3000 V/cm. The measurements reported in Section 4 are not inconsistent with the latter theory.

3. Practical Implications of the Model

Although the study of high field instabilities such as the Gunn effect is still very new, it is useful to review the device application potential in the light of our present understanding of the phenomena.

Undoubtedly, the most promising application of the device is the solid-state microwave generator. Operating in a pulse mode Bell Laboratories[8] have reported peak r.f. power of 1·8 W at 5 Gc/s and Lincoln Laboratories[9] 2·5 W at 3 Gc/s with a d.c. to r.f. conversion efficiency of 7%. Three laboratories[8,9,10] have reported c.w. operation, Bell Laboratories obtaining 15 mW at 4 Gc/s with a conversion efficiency of 3%. Their technique has been to use a material of high resistivity to cut down the threshold power dissipation. It is also possible to reduce the power dissipation in devices using lower resistivity GaAs by having a small cross-section for the drift path. These devices have the operative region mechanically supported to ensure ruggedness.

3.1. *Frequency Range*

Among the basic device limitations which are of interest the two most important are probably the

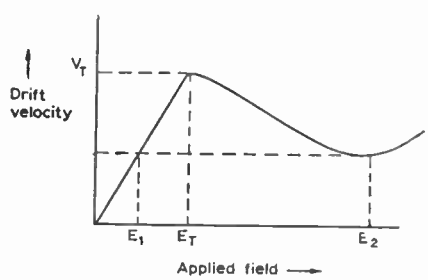

Fig. 8. Electron drift velocity (or current) versus field plot showing negative differential conductivity.

efficiency and the upper frequency limit. In connection with the latter point Kroemer[3] has indicated that Ridley's simple model must be modified to take into account the finite thickness of the domain walls. These walls are composed of the space charge necessary to support the field discontinuity and on the positive side charge density at complete depletion is limited by the ionized donor density. Taking the criterion that the length of the sample must be at least longer than the positively charged domain wall for domain formation Kroemer concludes that the product of the net donor density and sample length must be a few times greater than 10^{10} cm^{-2}. This relation gives a lower limit to sample length and hence an upper limit to the frequency for material of a given doping level. For the range of carrier concentrations which have been used so far in Gunn oscillators this limitation is comparable with those imposed by the practical limitations of device fabrication technology. Frequencies as high as 7 Gc/s with sample thickness of 30 microns have been achieved at the time of writing.[7]

3.2. *Efficiency*

The effective resistance of a device and an approximate idea of the theoretical efficiency can be obtained directly from the simple Ridley model. From the experimental data it is possible to assign values to the more important parameters of the curve of Fig. 8. For our material the ratio I_{max}/I_{min} is typically equal to 2. As the characteristic below E_T is reasonably ohmic this sets a value to E_1 of $E_T/2$. Also from the voltage probe measurements at the surface of the sample one can assign a maximum value to the ratio (domain width/sample length) of 0·1 at the threshold field. (The measurement of the domain width is known to be limited by the resolution of the probe system. If one takes the current rise-time at domain decay to be a measure of its width the ratio would be about 0·03.) Thus substituting in equation (1) for an applied field of E_T and $E_1 = E_T/2$ one obtains $E_2 = 5{\cdot}5E_T$. Defining an average negative resistance as the reciprocal of the slope between points on the voltage-current characteristic at V_T and V_2 (i.e. E_2L) its value can be deduced in the above case to be |negative resistance| = 9 × (positive resistance of the sample).

Ridley has assumed, by analogy to the tunnel diode analysis, that for stability, in this case domain formation, the circuit resistance must be less than the negative resistance. In our measurements on long samples the lowest sample resistance was 50 ohms and the total circuit resistance 51 ohms and so the above criterion was always well satisfied. However, in a practical circuit for generating r.f. power it is necessary to consider the optimum bias and load resistance required for maximum efficiency. As the device operates by switching current in the load between the fixed upper and lower values it is clear that increasing the drive to the circuit will not improve efficiency (see Fig. 5). However, the efficiency should improve as the load resistance is increased until the limiting condition is reached when the load resistance approaches the device negative resistance. A simple calculation of efficiency for a circuit consisting of a constant voltage source and a load resistance equal to nine times the ohmic resistance of the device and assuming a sine wave output varying between I_T and $I_T/2$ gives a value of about 4·5%. It has been assumed that the model developed for long samples is applicable also to short samples and that the 'spikey' waveform becomes more sinusoidal without loss of amplitude. There is some experimental evidence to support these assumptions. The characteristic long sample current waveform has been obtained[11] down to 0·01 in (0·025 cm) and the sine waves observed with shorter samples often have peak to valley ratios of 2 : 1. The low value of the theoretical efficiency compared to some measured values which have been reported, suggests that higher current peak to valley ratios have been obtained or that operation in a reactive circuit may result in better performance.

3.3. *Modulation and Tuning*

The results of the experiments with the triggered mode of operation show that the device need not be limited to use as a fixed frequency oscillator. With the sample biased just below the threshold for self oscillation, an input signal superimposed on the bias will produce a domain every time the threshold is exceeded. Thus, in a sense, Fig. 4 may be regarded as the output from the device operating as a pulse amplifier with the energy for the power gain coming from the applied d.c. bias. Although the shape of the input pulse is clearly not reproduced, its position in time (e.g. for p.p.m.) is accurately maintained at the output, provided that the repetition interval is longer than the transit time of the instability. Further in short samples where the output approaches a sine wave, a sinusoidal input at a frequency near, but lower than, the self-oscillating frequency should appear as a sine wave of increased amplitude. One can thus envisage the device being used as a generator for frequency-modulated signals operating at a centre frequency a few percent below the self-oscillating frequency.

The above argument can be applied to the realization of a tuned microwave generator if a conventionally tuned low-power active circuit can be used as a local oscillator to trigger the device. However, the sensitivity of the element to slight changes of field at

the threshold level suggests that there might in fact be an interaction between the Gunn effect mechanism and a passive resonant circuit which could have the effect of triggering instabilities at the voltage peaks associated with the ringing of the circuit. There is some experimental evidence of frequency pulling[12] and improved coherence when the device is operated in resonant circuits. A third way in which tuning may perhaps be achieved is deliberately to create an inhomogeneous device so that a 'virtual' cathode is produced whose position may be varied by external means.[13]

At the time of writing trigger pulses have only been added directly to the bias circuit. However, from our conclusions on the mechanism of operation, there is no reason why the triggering operation should not be achieved with a third electrode. For example, the voltage across the device when fed from a constant current source could be altered from below to above threshold by applying a potential to an isolated gate electrode such as in a metal-oxide-semiconductor transistor.

3.4. *Waveform Coherence*

Some comments are in order on one of the most puzzling features of the Gunn effect, namely, the tendency to incoherence in the current waveform. Although we have used the term coherence in describing waveforms of the type shown in Fig. 5, there is always an increasing loss of sharpness with increasing numbers of cycles. This deterioration is accentuated as the total circuit resistance is raised from a value where it is comparable to the specimen resistance (but still significantly less than the estimated negative resistance of the sample). Similarly, a progressive deterioration in coherence is obtained by increasing the drive above threshold under constant voltage conditions and in the limit reversible current 'break away' often results. As both these operations involve an increase in the amplitude of the high field domain, and are independent of sample length (in the range 0·025 in to 0·1 in; 0·065–0·25 cm), they are suggestive of an upper limit to the ratio of domain width to sample length. The problem of waveform incoherence is being investigated in greater detail at the present time. The origin seems to be associated with imperfections in the material but the effects of these may well be reduced by operating in resonant circuits.

4. Effects of Cooling and Illumination

4.1. *General Principles*

The previous series of experiments involved only variation of the bias field and have given a description of the factors governing domain formation. The object of the investigations involving the temperature dependence and the response to illumination was to study the effect of variation in ambient conditions and also to gain some insight into the primary mechanism which is responsible for the negative resistance characteristic. Cooling GaAs generally results in a reduction in the carrier concentration and an increase in carrier mobility together with a lowering of the lattice temperature. Any, or all three, of these parameters could influence the Gunn effect and ideally one would aim at changing each one independently of the other two, or at least vary any two of them independently and infer the influence of the third from the temperature experiment. Illumination of the cooled material produces mainly changes in the carrier concentration either by creating hole-electron pairs at short wavelengths or by emptying traps at longer wavelengths. However, it is difficult to conceive of experiments for altering the mobility or lattice temperature independently of each other. Thus, although it has not been possible to isolate the individual contributions from the changing mobility and lattice temperature to the variation in the properties of the high field domain, the results obtained will provide useful data for the operating range of devices based on the effect and also for testing any detailed mathematical treatment of the basic interaction.

4.2. *Temperature Dependence*

The specimens were cooled by placing the mount in liquid nitrogen contained in an expanded polythene trough. Temperatures between 77°K and 300°K were obtained by allowing the system, which was well insulated, to warm up slowly. The actual sample temperature was measured using a chromel-alumel thermo-couple made of 0·005 in (0·013 cm) wire held on the side of the GaAs with a piece of wax. Experiments in the range from room temperature to 200°K were also carried out in a petrol bath cooled with solid CO_2. It is interesting to note that petrol was the only commonly available liquid of low freezing point which did not degrade the electrical performance of the device. Methyl alcohol, for example, completely destroyed the characteristic domain formation although the current saturation level was unaltered. This phenomenon must be associated with the dielectric properties of the liquids.

Preliminary cooling experiments showed that in most specimens the quality (i.e. shape) of the current waveform got progressively worse as the temperature was lowered although nearly all continued to oscillate coherently in liquid nitrogen. The degree of trapping out also varied widely but in the few devices in which the waveform was still reasonable at 77°K the trapping out was slight. In some 0·8 ohm cm material that had been used to make quite good short oscillators but from which it proved impossible to make long

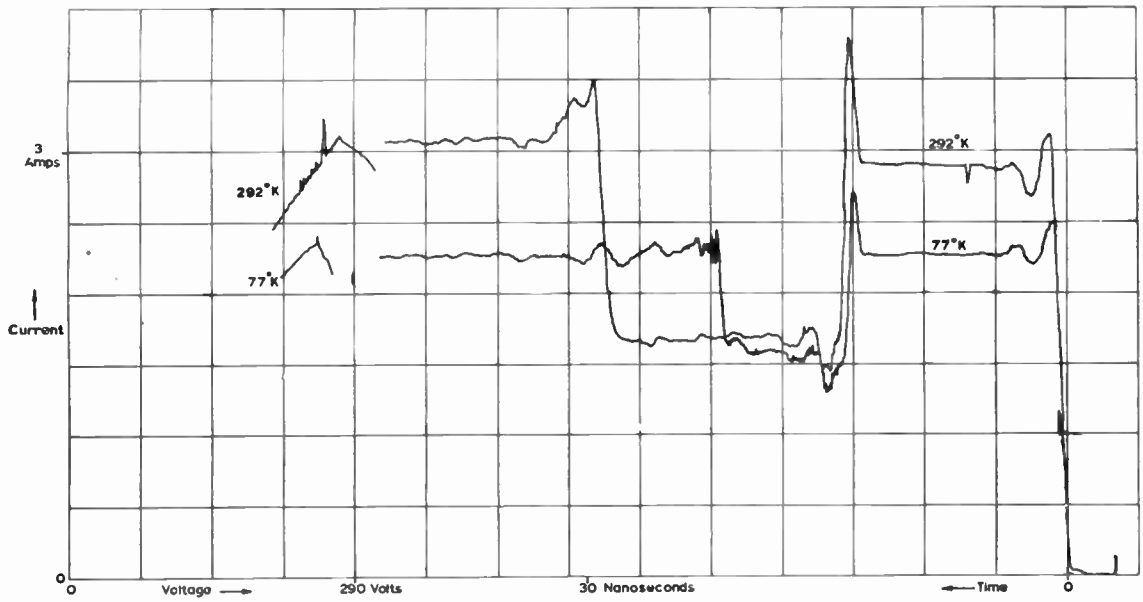

Fig. 9. Current waveform (right) for triggered one-cycle operation at 292°K and 77°K. Voltage versus current (left).

samples, the current dropped by a few orders of magnitude on cooling to 77°K. No oscillations were observed at the low currents and even the current saturation disappeared. It is our experience that materials which produce the best Gunn oscillators have shallow donor levels.

Detailed experiments were carried out on one of our best samples over the temperature range 77°K to 350°K. In order to facilitate accurate measurements the current waveforms were recorded on an X–Y plotter whose vertical and horizontal scales could be accurately calibrated. Figure 9 illustrates the room temperature and 77°K waveforms of a 0·05 in (0·15 cm) sample. In this case the triggered single pulse mode of operation was being used. Between each current observation the final portion of the voltage–current plot was recorded so that the threshold voltage and current could be monitored. The results of one experimental run are summarized in Figs. 10 to 12.

Of the six parameters considered, four were measured directly, namely the threshold voltage and current, the ratio I_{max}/I_{min}, and the domain velocity. The remaining two, namely mobility and carrier concentration, were calculated from the other four parameters. The basis of these simple calculations is as follows: The reduced current in the presence of a high field domain can be represented by the relationship $I = CN\mu V$, where C is a constant, N the carrier concentration, μ the mobility and V the voltage dropped across the material external to the high field domain. Then at temperatures T_1 and T_2

$$I_1 = CN_1\mu_1 V_1 \quad \text{and} \quad t_1 = \frac{L}{\mu_1 V_1}$$
$$I_2 = CN_2\mu_2 V_2 \quad \text{and} \quad t_2 = \frac{L}{\mu_2 V_2} \qquad \text{.....(2)}$$

where t and L refer to the domain transit-time and sample length respectively. Thus

$$\frac{I_1}{I_2} = \frac{n_1}{n_2}\frac{t_2}{t_1} \qquad \text{.....(3)}$$

Hence the relative change in carrier concentration can be calculated from the values of the reduced currents and associated domain transit-times. Then knowing the relative carrier concentration at a given temperature the relative electron drift mobility can be calculated from the threshold current and voltage at this same temperature. The cumulative errors involved in the derivation of mobility probably account for the scatter of the observations. The general trend of the curve is however consistent with the accepted data on the temperature dependence of mobility in GaAs.

We believe that the largest source of experimental error in these investigations arises in the measurements of sample temperature since the thermo-couple junction is, of necessity, separated from the surface of the GaAs by a thin layer of wax. From temperature runs using three thermo-couples, one on the sample and the others close to the sample but on the centre conductor of the mount and in air, we concluded that temperature gradients could result in errors of up to 10°K over the temperature range 120°K to 200°K.

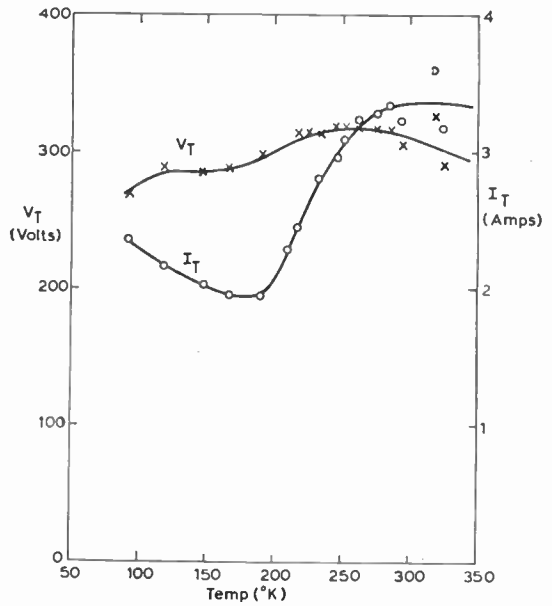

Fig. 10. Threshold voltage and current versus temperature.

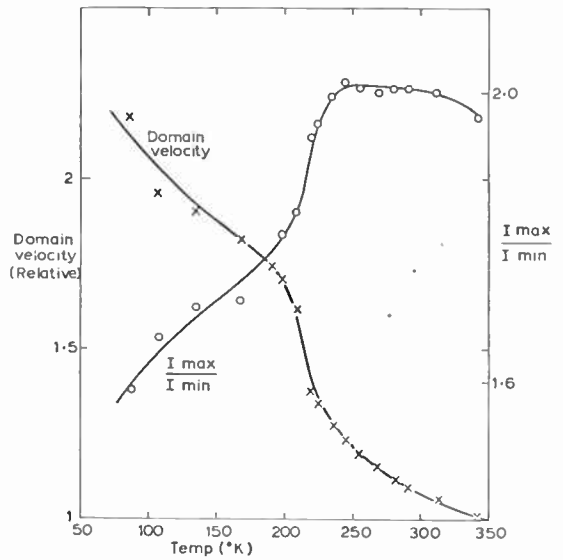

Fig. 11. Domain velocity and I_{max}/I_{min} versus temperature.

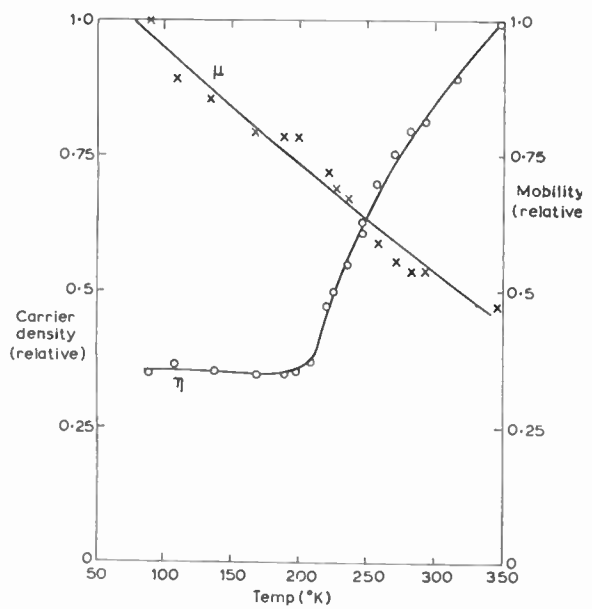

Fig. 12. Carrier density (η) and mobility (μ) versus temperature.

4.3. *Illumination*

The original object of this experiment was to restore the carrier concentration in a cooled sample, which had showed trapping out, by illumination with infra-red radiation. Light from a 12-V filament lamp was focused with a metal mirror through a thin slice of GaAs, used as a filter, and then on the cooled device. Barely discernible changes in the carrier concentration were observed using this technique, presumably due to a very short life-time of carriers lifted from the donor levels or deep traps. Thus it was necessary to use unfiltered light to vary the carrier concentration. The only additional experimental innovation was to use a light chopper having a 10% open segment to enable the heating and photoconductive effects to be separated.

When specimens were illuminated to produce changes in current comparable with those caused by cooling, the variation in the domain velocity and I_{max}/I_{min} was small. Thus we conclude that the basic mechanism responsible for the negative resistance characteristic is not very sensitive to the carrier concentration. This conclusion was also indicated by the fact that samples of the same nominal dimensions showed a variation in resistance, in some cases by almost an order of magnitude, and yet the threshold voltages and domain velocities were closely similar. As these samples were from the same crystal the observation suggests that carrier mobility is relatively constant and changes in resistivity arise from changes in the carrier concentration. McCumber and Chynoweth[5] have observed no variation in domain velocity for changes in carrier concentration of four orders of magnitude.

4.4. *Discussion*

The diagnostic experiments reported in this section give little positive indication of which one of the two proposed mechanisms for the Gunn effect (Sect. 2) is favoured although the observed increase in domain

velocity on cooling can be seen from a simple argument, to be consistent with the Ridley-Watkins-Hilsum model. Evidently, the electron temperature must be great enough for the transition into the upper sub-band and as the thermal energy of the carrier is lowered by cooling one would expect to have to provide more heating via the electron field. However, probably the best evidence to date in support of the transferred electron mechanism is that the Gunn effect is apparently restricted to materials with the required characteristic sub-band structure. Detailed theoretical treatments, which would indicate the effects of temperature change, are needed for each mechanism.

5. Conclusions

The study of the Gunn effect in long samples suggests a mechanism which is consistent with the simple Ridley model of domain formation arising from a bulk negative differential resistance. The most likely origin of the bulk negative resistance appears to be the Ridley-Watkins-Hilsum transferred electron mechanisms.

In order to consider in detail the factors limiting the maximum operating frequency, the thickness of the domain walls would have to be taken into account. However, from the present data it seems likely that devices can be operated at frequencies well above 10 Gc/s.

Operation in resonant circuits should improve efficiency, coherence, and provide some degree of tuning or compensation for variation of transit time with temperature. The transit time is not sensitive to changes in bias voltage.

The launching of single instabilities by triggering above the upper threshold shows that modulation and perhaps three terminal operation is possible.

6. References

1. J. B. Gunn, "Instabilities of current in III–V semiconductors", *I.B.M. J. Res. Dev.*, **8**, p. 141, April 1964.
2. J. B. Gunn, "Instabilities of current and of potential distribution in GaAs and InP", I.B.M. Research Paper RC 1216, June 1964.
3. H. Kroemer, "Theory of the Gunn effect", *Proc. Inst. Elect. Electronics Engrs*, **52**, p. 1736, December 1964.
4. B. K. Ridley, "Specific negative resistance in solids", *Proc. Phys. Soc.*, **82**, p. 954, 1963.
5. D. E. McCumber and A. G. Chynoweth, "Electrostatic instabilities in one-stream plasmas in semiconductors", *Phys. Rev. Letters*, **13**, p. 651, 30th November 1964.
6. B. K. Ridley and T. B. Watkins, "The possibility of negative resistance in semiconductors", *Proc. Phys. Soc.*, **78**, p. 293, 1961.
7. C. Hilsum, "Transferred electron amplifiers and oscillators", *Proc. Inst. Radio Engrs*, **50**, p. 185, February 1962.
8. B. W. Hakki and F. C. Irvin, "C.w. microwave oscillations in GaAs", *Proc. I.E.E.E.*, **53**, p. 80, January 1965.
9. T. M. Quist and A. G. Foyt, "S-band GaAs Gunn effect oscillators", *Proc. I.E.E.E.*, **53**, p. 303, March 1965.
10. N. Braslau, J. B. Gunn and J. L. Staples, "Continuous microwave oscillations of current in GaAs", *I.B.M. J. Res. Dev.*, **8**, p. 545, November 1964.
11. G. King, private communication.
12. B. W. Hakki, "C.w. microwave oscillations in GaAs", 1965 Intl Solid State Circuit Conference Digest, p. 44, February 1965.
13. R. Harcourt, J. Froom and C. P. Sandbank, "Acoustic amplification in semiconductors", Proceedings of Symposium on Microwave Applications of Semiconductors, London, June 1965, Paper No. 28. (To be reprinted in *The Radio and Electronic Engineer* **31**, 1966.)

Manuscript first received by the Institution on 15th April 1965. (Paper No. 1014.)

Radio Engineering Overseas . . .

The following abstracts are selected from Commonwealth, European and Asian journals received by the Institution's Library. Abstracts of papers published in American journals are not included because they are available in many other publications. Members who wish to consult any of the papers quoted should apply to the Librarian, giving full bibliographical details, i.e. title, author, journal and date of the paper required. All papers are in the language of the country of origin of the journal unless otherwise stated. Translations cannot be supplied.

TELEVISION NOISE REDUCTION

In this German paper, the authors describe a new method for eliminating from the television picture most of the shot noise added to a picture signal on a transmission path, in particular when the latter operates with frequency modulation. The method gives rise only to very low signal distortion with negligible effect on picture transmission. A requisite condition is pre-distortion of the signal before transmission.

Basically the method consists in splitting the signal into two channels having respectively high-pass and low-pass character, while reducing the amplitude of the shot noise by corresponding distortion of the characteristic of the signal coming from the channel having high-pass character.

The same method can be used for reduction of the shot-noise conversion in encoding and decoding colour signals, if a suitable crossover frequency of the two channels is chosen. A slight resolution loss must indeed be accepted for low-amplitude oscillations, but this does not make itself felt in the picture.

By the application of more than two channels it is possible to eliminate additional shot-noise introduced in the composite colour signal by the transmission path.

"On the possibility of improving the signal/noise ratio in frequency-modulated systems, particularly in a video signal magnetic recorder", W. Dillenburger and G. Krause, *Archiv der Elektrischen Ubertragung*, **18**, No. 9 pp. 537–43, September 1965.

LOW-DISTORTION FREQUENCY MODULATOR

Frequency modulators become simple devices if the frequency of the oscillator is controlled by the bias voltage for variable capacitance diodes. The disadvantage of such a circuit lies in the fact that for many applications the harmonic distortion of the demodulated low frequency signal is too high. The distortion can be reduced by pre-distortion of the low frequency signal before it is applied to the variable capacitance diodes.

The calculation of the parameters of non-linear amplifiers suitable for this purpose is shown in a German paper. The requirements for the distortion factor determine the conditions for the magnitude of the amplification factor and its tolerance, for the phase of the amplification factor and its permissible deviation, as well as for the band-width of the amplifier. Measurement results confirm the theory and show that such frequency modulators can be used for microwave link systems.

"A low-distortion frequency modulator with variable capacitance diodes and a logarithmic amplifier", A. Knoll, *Nachrichtentechnische Zeitschrift*, **18**, No. 8, pp. 455–463, August 1965.

MICROWAVE FEEDERS

During installation and operation a microwave feeder which can be coiled on a drum is subjected to mechanical stresses which could alter the mechanical dimensions and thus also the electrical transmission properties. For this reason the stresses caused by pull, external pressure, internal pressure, bending, and recoiling as well as the mechanical distortion caused by these stresses were investigated by a German engineer. Some of the resulting requirements are mutually conflicting and a compromise in the design of such lines is discussed.

"The mechanical properties of a microwave feeder which can be coiled on a drum and has a cross-section differing from a circle", G. Herberts, *Nachrichtentechnische Zeitschrift*, **18**, No. 11, pp. 637–42, November 1965.

SAMPLING OSCILLOSCOPE

A survey is given in this Dutch paper of the factors limiting the bandwidth of a sampling oscilloscope. The most important factor seems to be the resonance frequency of the sampling diode. With present-day components it is possible to build a sampling oscilloscope with a bandwidth of 50 Gc/s, but with an improvement in mechanical construction of the sampling diode a bandwidth of 100 Gc/s could be achieved.

Since the real bandwidth may be considerably smaller than the apparent bandwidth, it is possible to achieve an apparent noise factor of less than 1. An experimental input circuit is described having a bandwidth of 15 Gc/s or a transient response of 20 p/seconds. The apparent noise factor is 0·3.

"Possibilities of using a sampling oscilloscope for very fast aperiodic phenomena", A. v. d. Grijp, *Tijdschrift van het Nederlands Elektronica- en Radiogenootschap*, **30**, No. 2, pp. 59–70, 1965.

H.F. SURFACE WAVE AERIALS

Since 1960 research has been in progress at Rockbank, Victoria, by the University of Melbourne and the Australian Army, on surface wave aerials intended for high frequency radio communication. The design of an aerial of improved performance was believed to be a direct method by which propagation via the ionosphere could be enhanced during the prevailing period of depressed maximum usable frequencies which is associated with the minimum of sun-spot cycle.

The principles of operation, the practical design and the measured performance of the new array are discussed by the author of this paper.

"The low delta, high frequency array for radio communication and research", J. F. Ward, *Electrical Engineering Transactions of the Institution of Engineers*, Australia, **EE1**, No. 2, pp. 117–126, September 1965.

SUBJECT INDEX

Papers and major articles are denoted by printing the page numbers in bold type.

INDEX OF PERSONS

Names of authors of papers published in the volume are indicated by bold numerals for the page reference.
Authors of papers which are given in abstract form are denoted by A.
Contributors to discussion are indicated by D.
Biographical references are denoted by B.

INDEX OF ABSTRACTS

This index classifies under subject headings the abstracts published throughout the volume in "Radio Engineering Overseas".

JOURNALS FROM WHICH ABSTRACTS HAVE BEEN TAKEN DURING THE SECOND HALF OF 1965

Archiv der Elektrischen Ubertragung (Germany)
Canadian Journal of Physics.
E.B.U. Review (Switzerland)
Electrical Engineering Transactions of the Institution of Engineers (Australia)
Journal of the Institution of Engineers, Australia
N.E.C. Research and Development (Japan)
Nachrichtentechnische Zeitschrift (Germany)
L'Onde Electrique (France)
Slaboproudý Obzor (Czechoslovakia)
Tijdschrift van het Nederlands Elektronica- en Radiogenootschap
Transactions of Chalmers University of Technology, Gothenburg